

April 2020

Threshold Processes and Stream Temperature Distribution in a Small New England Headwater Stream Catchment.

mitchell isaacson

Follow this and additional works at: https://scholarworks.umass.edu/masters_theses_2



Part of the [Geology Commons](#)

Recommended Citation

isaacson, mitchell, "Threshold Processes and Stream Temperature Distribution in a Small New England Headwater Stream Catchment." (2020). *Masters Theses*. 879.
https://scholarworks.umass.edu/masters_theses_2/879

This Open Access Thesis is brought to you for free and open access by the Dissertations and Theses at ScholarWorks@UMass Amherst. It has been accepted for inclusion in Masters Theses by an authorized administrator of ScholarWorks@UMass Amherst. For more information, please contact scholarworks@library.umass.edu.

Threshold processes and stream temperature distribution in a small New England
headwater stream catchment

A Thesis Presented

By

MITCHELL R. ISAACSON

Submitted to the Graduate School of the
University of Massachusetts Amherst in partial fulfillment
of the requirements for the degree of

MASTER OF SCIENCE
FEBRUARY 2020
Department of Geosciences

Threshold processes and stream temperature distribution in a small New England
headwater stream catchment

A Thesis Presented

By

MITCHELL R. ISAACSON

Approved as to style and content by:

David F. Boutt, Chair

Christine E. Hatch, Member

Robert Newton, Member

Stephen J. Burns, Department Head
Department of Geosciences

DEDICATION

To the fish of the past and the fry of the future.

ACKNOWLEDGEMENTS

I thank my advisor, Dave for instilling in me a sense of the greater unknowns and mysteries of how our planet and the hydrologic cycle work. He has encouraged me to view science, and life, with a greater sense of curiosity and appreciation for the interconnection of things.

I also thank my committee advisors Christine and Bob, whom I both look up and am inspired by. Christine opened my eyes to an entirely new level of technological scientific investigation and Bob has been my model for multi-disciplinary geoscience investigation.

I thank Ben Letcher and the Conte Lab for sharing data and resources with me.

I thank Smith College and the MacLeish Field Station for allowing me to study such a wonderful location and to use their facilities.

I also would like to thank my wife Caroline, Wes, and Amy Hudson for their continued support and encouragement.

ABSTRACT

THRESHOLD PROCESSES AND STREAM TEMPERATURE DISTRIBUTION IN A SMALL NEW ENGLAND HEADWATER STREAM CATCHMENT.

FEBRUARY 2020

MITCHELL ISAACSON, B.S. UNIVERSITY OF WISCONSIN STEVENS POINT

M.S., UNIVERSITY OF MASSACHUSETTS AMHERST

Directed by: Dr. David F. Boutt

Rising air temperature and decreasing stream flow trends are predicted to result in corresponding increases in stream temperatures. As a result, the future of ectothermic stream fishes, which rely on seasonal and spatial distributions of stream temperature for growth and survival, could be in jeopardy. Fortunately, contradicting stream temperature trends in forested headwater catchments suggest that non-climatic variables, such as baseflow indices and catchment geologic structure, may have an important confounding influence on the future of stream temperature. Most significantly, the annual stability of groundwater temperature has long been recognized as an important buffer between air and stream temperature. The hyporheic zone has been the subject of an emerging focus of new research over the past decade and breakthroughs in our understanding in groundwater and surface water interactions have given rise to new conceptual frameworks in hydrology. Once such framework is the concept of threshold discharge in which inputs to streams are activated once critical metrics are met in antecedent moisture, rainfall intensity, and rising water tables in the riparian areas and topographical depressions.

This study investigates the extent to which threshold connectivity between soil saturation, groundwater, precipitation, and streamflow exist in a shallow bedrock/till-mantled headwater catchment, and how threshold characteristics may influence the fluid flux and temperature variability of the stream. This study uses stable water isotopes, fiber-optic distributed temperature sensing, and hydrometric analyses to observe the fluid and heat flux within the catchment. The results indicate that threshold discharge is an inherent property of the saturated soil conductivity curve which drives macropore and fractured-bedrock discharge into the stream. The sequential activation of flow in fractured storage reservoirs and soil can be observed in the isotopic, temperature, and conductivity measurements of the stream. Fiber-optic distributed temperature sensing (FO-DTS) produced the locations of both discrete seeps in areas with bedrock outcrops and thin overburden, and diffuse seeps where thicker alluvial deposits occurred. The net effect of threshold discharge events on seep locations was a reduction of the instream temperature variability and decrease in the persistence of thermal refugia, or seeps buffered from the main stream channel temperature.

TABLE OF CONTENTS

	Page
ACKNOWLEDGEMENTS	iv
ABSTRACT	v
LIST OF FIGURES	x
CHAPTER	
1. INTRODUCTION AND BACKGROUND	1
1.1 Heat Transport	3
1.2 Threshold Discharge	4
1.3 Expected Outcomes/Hypothesis	7
2. SITE DESCRIPTION	8
2.1 Vegetation	10
2.2 Soils.....	11
2.3 Surficial geology	11
2.4 Bedrock geology	15
2.6 Conceptual geologic model.....	16
2.7 Hydrogeologic characteristics of Glacial units	22
3.METHODS	24
3.1 Weather	26

3.2 Soil Moisture TDR field measurements	26
3.3 Saturated conductivity lab measurement	28
3.4 Groundwater	30
3.5 Streamflow	32
3.6 Stable water isotope tracers	33
3.7 Distributed Temperature Sensing	35
4. RESULTS AND DISCUSSION.....	39
4.1 Soil Moisture Thresholds.....	39
4.3 Stable Isotope tracers	49
4.4 DTS temperature distribution in JN.....	58
5. CONCLUSIONS	71
5.1 Study Limitations.....	72
5.2 Broader Impacts.....	73
APPENDICES.....	75
A. IDEALIZED STRUCTURAL GEOLOGY SECTION.....	76
B. CROSS SECTION OF THE UNQUOMONK BROOK VALLEY	77
C. DIAGRAM OF GROUNDWATER FLOW PATHS	78
D. SOIL WATER RETENTION CURVE.....	79
E. TABLE OF WATER ISOTOPE SAMPLE NAMES	80
F. SURFICIAL GEOLOGY OF JIMMY NOLAN BROOK	81

G. BEDROCK GEOLOGY OF WHATELY AREA	82
H. CORE LOG OF FRACTURED BEDROCK WELL MFS-1	83
I. CORE LOG OF TILL/BEDROCK WELL MFS-2	88
BIBLIOGRAPHY	90

LIST OF FIGURES

	Page
Figure 1. NRCS soil classification at the MacLeish Field Station, Whately MA.	11
Figure 2. Map of ERT transect and the surficial geology extending to Jimmy Nolan Brook.....	17
Figure 3. Cross section of ERT model and interpreted polygons with calculated mean resistivity and standard deviation. Vertical axis shown in depth in meters below ground surface.....	18
Figure 4. Interpolated resistivity values with well stratigraphy overlayed.	19
Figure 5. Conceptual Geologic Model of well site near Poplar hill road extending east.	22
Figure 6. Map of the Smith College MacLeish Field Station and Jimmy Nolan Brook catchment.	25
Figure 7. Baseflow separation for Jimmy Nolan Brook.	33
Figure 8. DTS downstream calibration coil with straight-line fit.....	37
Figure 9. DTS Upstream calibration coil in telescope well with straight-line fit.....	38
Figure 10. Saturated hydraulic conductivity curve results from Hyprop testing.....	40
Figure 11. Semi-log plot of the mean change in VWC over a 60 min interval for scaled values of VWC recorded in the soil moisture probes installed in the 'Field'	41
Figure 12. Semi-log plot of the mean change in VWC over a 60 min interval for scaled values of VWC recorded in the soil moisture probes installed in the 'Forest'	42
Figure 13. Table of VWC inflection points for scaled and measured (uncalibrated) values from TDR soil moisture probes and annotation points corresponding to Figure 11. and Figure 12..	43
Figure 14. Soil VWC threshold and well heat flux.....	44

Figure 15. Precipitation Intensity and rate of change in soil VWC (field 50 and 100cm).
Precipitation and soil moisture data were collected continuously from May 2013
to February 2014. 45

Figure 16. Precipitation intensity (in/hr) and runoff % of total flow in Jimmy Nolan
Brook. Stream discharge measurements were collected by the USGS Conte Labs
gauge at the confluence of Jimmy Nolan and Westbrook. 46

Figure 17. Precipitation events, soil VWC, streamflow, and groundwater potentiometric
surface elevations from wells MFS-1 and MFS-1. MIDDLE: Soil VWC
measurements from field, forest, and riparian locations. BOTTOM: JN Stream
level and precipitation measurements. 47

Figure 18. Westbrook stream stage and specific conductivity plotted against average
conductivity measurements from groundwater (MFS1, MFS2, and TAP) and the
MFS creek (SMC). 48

Figure 19. Dual isotope plot comparing the average climate zones of precipitation,
surface water, and groundwater. 49

Figure 20. Stable Isotopic composition of surface water, groundwater, soil pore water,
and precipitation from the Jimmy Nolan Brook catchment plotted against the
GMWL and SMWL 50

Figure 21. Stable isotope standard deviation of $\delta^{18}\text{O}$, $\delta^2\text{H}$, and deuterium excess for
precipitation, groundwater, surface water, and soil porewater at MFS from 2012-
2013. 51

Figure 22. Scaled graph of Stable Isotopic composition of surface water, groundwater, soil pore water, and precipitation from the Jimmy Nolan Brook catchment plotted against the GMWL and SMWL.....	53
Figure 23. Monthly averages of the stable-isotopic composition of precipitation from the Jimmy Nolan Brook Catchment.....	54
Figure 24. Stable Isotope composition of samples collected from streams and groundwater in the Jimmy Nolan Brook Catchment plotted against the GMWL and SMWL.....	55
Figure 25. Time series of precipitation and $\delta^{18}\text{O}$ samples of precipitation, stream, and groundwater in the Jimmy Nolan Brook Catchment	56
Figure 26. Time series of precipitation and $\delta^2\text{H}$ samples from precipitation, stream, and groundwater in the Jimmy Nolan Brook Catchment	56
Figure 27. Time series of precipitation and deuterium excess samples of precipitation, stream, and groundwater in the Jimmy Nolan Brook Catchment.....	57
Figure 28. Annotated temperature profile of the full DTS cable deployment at the MacLeish Field Station and upstream Jimmy Nolan Brook.....	59
Figure 29. DTS Cable distances (meters) in upstream Jimmy Nolan.....	60
Figure 30. Mean and standard deviation of DTS temperatures along cable distances 1000-1800m from Nov 13th to Nov 26th 2013.....	61
Figure 31. Mean calibrated DTS temperatures recorded at 0.25m intervals along JN brook from September 22 - November 26th.	64
Figure 32. Mean calibrated DTS temperatures recorded at 0.25m intervals along JN brook from September 25-30..	65

Figure 33. Mean calibrated DTS temperatures recorded at 0.25m intervals along JN brook from October 5-7.....	66
Figure 34. Mean calibrated DTS temperatures recorded at 0.25m intervals along JN brook from October 17-20.....	67
Figure 35. Mean calibrated DTS temperatures recorded at 0.25m intervals along JN brook from November 15-17.....	68
Figure 36. TOP: DTS temperature minimum (black) and maximum (black) and mean (green) in upstream JN over time.....	69
Figure 37. TOP: DTS seep locations from Figure 29 listed by cable distance, DTS temperature minimum (black), maximum (black), and mean (green) in upstream JN over time.....	70

CHAPTER 1

INTRODUCTION AND BACKGROUND

Stream temperature has long been used as an indicator of ecosystem health and suitability for aquatic species, particularly in sensitive areas crucial to the survival of declining important fish populations. In recent years, considerable attention has been paid to assessing the behavioral and life history response of fishes to differing thermal regimes in near-pristine headwater catchments. Assessments of native fish habitat the characterization of stream temperature conditions to support spawning and migratory thermal pathways has also become a major consideration in restoration designs. Of special importance is the detailed spatial and temporal distribution of thermal refugia created by localized inputs of groundwater entering a stream channel (Torgersen et al., 2012). Thermal refugia provide relatively cooler microhabitats during warm summer months and warm microhabitats during the cold or frozen winter months. Microhabitats play an important role in the growth and survival energetics of juvenile fishes, as they self-regulate their metabolisms based on external temperatures. Consequently, the spatial and temporal distributions of groundwater seeps within a stream reach play important roles in determining habitat fragmentation and connectivity for fish passage and migrations (Torgersen et al., 2012).

The principle components of the stream heat budget can be broken down into advective and non-advective contributors, where the major non-advective factors are net radiation, evaporation/condensation, sensible heat exchange, bed conduction, and fluid friction (Webb and Zhang 1997). Groundwater, which is recognized as the primary advective component, not including direct streamflow, acts as a systematic and seasonally

varying contributor to the stream heat budget. Seasonal contributions typically occur as heat losses during the summer and heat additions during the winter, spring, and fall; however, it is not uncommon for consistent heat losses to occur during the fall and early winter months. The total contribution to the river heat budget from groundwater has been shown to be as high as 45% of the daily total heat inputs, and 35% of heat loss along a stream reach (Webb and Zhang 1997). Over the course of a 495 day study period, direct advection of groundwater was found to account for 5% of the total stream heat storage, while bed conduction contributed up to 10% of the non-advective heat budget (Webb and Zhang 1997).

Common approaches to surveying stream temperature are typically limited in spatial extent, and often rely on trends in air temperature to predict how stream temperatures will respond to yearly and decadal variability in climate (Morrill et al., 2005, Johnson 2004). As a result, rising air temperature and decreasing stream flow trends are predicted to result in corresponding increases in stream temperatures (Arismendi et. al. 2013). This belief is problematic as recent studies have found air temperature to be poorly correlated with stream temperature trends in forested headwater catchments, in fact some studies have found almost no connection between the two (Arismendi et. al. 2013).

We can better identify the principle drivers of an individual streams heat budgets by considering how the magnitude of each component varies with respect to a unique stream environment (Johnson 2004). For example, streams that show poor temperature correlation with air temperature help support that non-climatic variables, such as baseflow indices and catchment geologic structure, may have an important confounding influence on the future of stream temperature (Arismendi et al., 2013). Small stream size, riparian

cover, and baseflow indices have all been found to result in decreased sensitivity to changes in air temperature and even show completely inverse relationships with long term air temperature trends (Arismendi 2013, Kelleher 2012).

1.1 Heat Transport

While often overlooked, the heat flux from groundwater inputs plays a fundamental role in mitigating large swings in stream temperature and has long been recognized as an important contributor to the advective heat budget of streams (Webb et al., 2008). Therefore, a clear understanding of heat transport in groundwater is a necessary piece to comprehending a detailed stream heat budget.

The fundamental theory of heat transport through aquifer systems is an adaption of Fourier's Law of Heat Flow (1822) and has been summarized in several important review publications and papers (notably Beck et al, 1989 and Anderson, 2005). The adapted equation for three-dimensional heat transport in a fully saturated aquifer system is expressed as:

$$\frac{\partial T}{\partial t} = \frac{K_e}{\rho c} \nabla^2 T - \frac{\rho_w c_w}{\rho c} \nabla \cdot (Tq)$$

$$K_e \rho c \nabla^2 T - \rho_w c_w \rho c \nabla \cdot (Tq) = \partial T \partial t$$

Where K_e is the effective thermal conductivity of the saturated substrate, T is temperature, ρ is density, c is specific heat of the saturated fluid-rock matrix, q is seepage velocity, and the subscript w indicates water (Domenico and Schwartz, 1998). The change in temperature with time is governed by heat flow by conduction (the first term), and heat flow by advection (convection; the second term).

Under low groundwater flow conditions, conductive heat transport dictates the temporal and spatial distribution of temperature throughout the subsurface, and the thermal properties of the subsurface and the temperature gradient between the atmosphere and the ground act as primary physical controls on heat transport. Furthermore, in aquifer environments with significant ground water flow, the conductive signature is modified by the advection of heat by ground water (Taniguchi, 1999; Taniguchi, 2002); this process is emphasized in recharge zones and shallow ground water flow systems (Beck et al, 1989; Anderson, 2005). Correspondingly, seasonal variations in temperature conduction between the land surface and atmosphere are translated by advection and preserved in deeper groundwater temperature signals; making heat flow an effective and widely used tracer for groundwater flow (Anderson, 2005). Characteristically, highly advective systems (with correspondingly high thermal Peclet numbers) with downward vertical flow (recharge areas) show a greater terminal depth of thermal influence from surface temperature.

While the importance of ground water flow on the subsurface heat distribution has been acknowledged for decades, quantification of how climate variability impacts subsurface temperature remains obscured by the complexity of near-surface hydrodynamics, air and ground temperature coupling, and the extent of heterogeneity in surficial materials.

1.2 Threshold Discharge

The evolution of catchment theory has evolved from the infiltration-excess theories of R.F.Horton to the Variable Source Area concept introduced by Hewlett and Hibbert in the late 60's in hopes of addressing the fundamental question: 'where does water go when it rains?'. Catchment theory has branched out to investigate controls on subsurface storm

response with respect to pressure wave propagation, macropore, and dynamic flows. However, the inherent heterogeneity and difficulty in measurement of the controlling properties of catchment water flux have made it so that a unified physically-based catchment flow theory has remained undiscovered (Kirchner 2009, Ali et al 2013, Bevan and Germann 2013). Heterogeneity throughout all aspects and scales in catchment hydrology is difficult to capture through traditional point-scale measurements: pore and fracture geometry, soil strata, vegetation structure, transpiration rates, throughfall variation, precipitation timing and magnitude, bedrock topography and composition, soil moisture, and subsurface flow paths all account for the system-wide heterogeneity (McDonnell et al 2007). This is reinforced through the fact that the Darcy-Richards equation for matrix flow is unable to retain its utility at larger scales and increasing flow complexity (McDonnell et al 2007).

Unexplained paradoxes in stream temperature, discharge, and chemistry drive current theory and investigation in the field of catchment hydrology. For example, the ‘old water paradox’ occurs during large precipitation events, where the water isotope chemistry of rapid stream discharge responses have been shown to reflect water from old storage reservoirs within the catchment, rather than the current precipitation (Kirchner 2003, McDonnell 1990). This ‘Old Water’ has been stored for a period of weeks to months yet is released rapidly during storm events. (Kirchner 2003). Conceptual models such as piston flow, kinematic waves, transmissivity feedback, and macropore flow have been used to explain this phenomenon, however, none has yet to adequately describe a physical account of the paradox (Kirchner 2003). As result, researchers are stepping back to reevaluate

traditional catchment flow through non-linear approaches (Ali et al 2013, McDonnell et al 2007).

Non-linear catchment theory is centered on the concept of ‘threshold discharge’, an emergent property of the hillslope-stream continuum which results in a hydrologic response at a critical point in time or space at which the magnitude and nature of fluid flow rapidly changes (Ali 2013). Hydrologic threshold responses have been observed in runoff processes (Detty and McGuire 2010), interflow (Van Meerveld and McDonnell 2006, Penna et al 2011), and groundwater recharge (Cuthbert et al. 2012, Heppner et al. 2007, Gleeson 2009, Nimmo 2010, Rodhe 2006) and over a range of geographically diverse catchments.

Integral to each hydrologic threshold is the soil water retention curve (Torres et al 1998) which dictates the timing, magnitude, and type of discharge of an event (Heppner et al 2007). The hydraulic properties of the subsurface porous media become a critical in determining antecedent threshold conditions within distinct stratigraphic units and have been used to conceptualize subsurface storm discharge at the hillslope and catchment scale (McGuire and McDonnell 2010, Cuthbert 2012, Meerveld and McDonnell 2006). In the unsaturated zone, subcritical, or below, threshold physics are governed by diffuse (matrix or Darcy) flow mechanics (Mirus and Nimmo 2013, Cuthbert et al. 2012), whereas supercritical threshold flow mechanics are characterized by rapid preferential flow paths (pipe flow, film-flow, macropore discharge, overland flow) where inertial forces can potentially impact flow (Torres 2002, Uchida et al 2005). However, achieving supercritical threshold conditions has been attributed to a wide array of storage, intensity, and stratigraphic conditions (Ali et al 2013).

Despite unique system-scale threshold variables which have been identified between different catchments, each catchment appears to have an identifiable rate-limiting factor for threshold activation. In a homogenous isotropic watershed model, this may be reflected solely by the soil water retention curve (Genuchten 1980).

As system complexity increases, threshold controls are attributed to subsurface storage (Ali et al. 2013, Meerveld and McDonnell 2006) and the connectivity of macropore networks (McDonnell et al 2007, Cuthbert et al 2012), respectively. This has prompted current research to focus on inter-basin flow comparisons in hopes of characterizing catchment flow based on global (landscape scale) governing properties (Ali et al. 2013).

1.3 Expected Outcomes/Hypothesis

This study investigates how non-linear catchment theory applies to fluid flux and connectivity between hillslope aquifers and stream temperature within a test catchment in western Massachusetts. Hydrologic thresholds are hypothesized to increase connectivity between storage reservoirs and streamflow. I hypothesize that this connectivity could impact the thermal buffering that localized groundwater-fed seeps provide to stream. Threshold discharge and stream temperatures were observed using hydrometric, isotopic, and fiber-optic distributed temperature sensing methods to address the primary goals of this study: (1) Identify the extent to which the theory of threshold discharge applies to the soil, groundwater, and stream flow in the Jimmy Nolan Brook catchment; (2) Evaluate the impact of threshold discharge on stream temperature distributions.

CHAPTER 2

SITE DESCRIPTION

This study is focused on the headwater streams of a test basin established in a till-mantled fractured bedrock catchment in Whately, MA. The geology of the site consists of underlying fractured crystalline bedrock with till mantled uplands, which is characteristic of a broader region of headwater systems in New England. It experiences a humid temperate climate with average annual rainfall exceeding 50 in, and average annual snowfall exceeding 77 in. The streams of interest are the Jimmy Nolan Brook (JN) and an unnamed ephemeral tributary (SMC) adjoining the Smith College, MacLeish Field Station (MFS) which are co-located with an on-going long-term fish movement study on the Westbrook River Basin conducted by the USGS Fish Ecology Division at the Silvio O. Conte Anadromous Fish Laboratory in Turner's Falls, MA. MFS sits above JN on a hilltop to the west of the brook, which drains to the south. SMC cuts through the field station and then travels downhill to the southeast to converge with JN before entering into the Westbrook River. The hillslopes separating the field station from JN have a steep eastern aspect (400m horizontal distance from well-field to JN with 70m vertical drop) and contain numerous small outcrops of bedrock and eroded topsoil. Monitoring wells and meteorological instruments are located adjacent to the field station on top of the hill.

The landcover of the Jimmy Nolan Brook catchment is composed of forest regrowth from agricultural developments abandoned in the early 1900s (90% of land area) and the remaining 10% of land is considered rural and is used for residential, agricultural, and pastoral purposes. The larger watershed provides important rearing habitat for juvenile salmonids, the Spring Salamander (*Gyrinophilus porphyriticus*), and the endangered

Dwarf Wedgemussel (*Alasmidonta heterodon*). The total watershed area of Jimmy Nolan brook is approximately 2.4 sq km, the stream has a mean discharge of 0.003 m³/s (Xu et al. 2010), and the longitudinal profile of the stream has an average slope of 2.6% and sinuosity of 1.17.

The bedrock of the Jimmy Nolan Brook watershed comprised of Paleozoic metamorphic and igneous crystalline rocks. The Conway Formation, which accounts for the majority of the basin, is composed of a garnetiferous quartz-mica schist interbedded with quartzite and marble. Marble beds within the formation are found to weather into a friable aggregate, and range in thickness from a few inches to 100ft. Quartzite beds remain thin, composed of fine-grained equigranular crystals. The Williamsburg formation is a younger intrusive igneous rock, underlying the Conway Formation to the West. It is composed of granodiorite and pegmatite dikes and sills. Abandoned open pit metal mines can be found within this formation where galena, silver, and gold ores have been located in 3-4' wide quartz veins (Willard 1956).

The surficial geology of the area is characterized by numerous rock outcrops covered with glacial sediments from the Pleistocene. Glacial deposits are present primarily as Illinoian (lower till) and Wisconsinian (upper till) ice advances. Lower till is generally present in deposits which can reach thickness of up to 80ft in isolated locations. Upper till is more commonly found at surface level with thickness of 0-20 ft. Bedrock outcrops are common as surficial material thickness is highly variable. Stream channels primarily contain modern alluvium and a mixture of poorly sorted sand and gravel layers. Thin layers of weathered clays and fine-grained deposits are also found between beds of glacial sediment.

2.1 Vegetation

The vegetation of the field site is characterized by abandoned pasture and stands of mixed hardwood and softwood forest. Near complete forest removal occurred in this area during colonial periods (~one hundred and fifty years ago). As a result, nearly all forest cover in Whately is considered to be second and third growth successional forest. Walking through the forest, the remnant stone walls that once bordered pastoral lands are visible and give insight to the landscape evolution. Presently, roughly 2/3rds of the total land area of the Town of Whately is forested (Whately OSRP).

The dominant vegetation at the MacLeish Field Station is characterized as mixed hardwood softwood forest. Mixed forest stands include northern red oak (*Quercus rubra*), red maple *acer rubrum*, black birch *betula lenta*, eastern white pine *pinus strobus*, eastern hemlock *tsuga canadensis*.. The riparian corridors often have sandy flats of alluvial sediments along their banks, which support white pine and northern red oak. The high water tables in the riparian area surrounding Jimmy Nolan Brook support an eastern hemlock dominated forest. Upland and hillslope sites with sandy soils and good drainage support hardwood species such as northern red oak, white ash, sugar maple, and white birch. Sugar Maple is widely tapped and exploited for sap during the spring.

The large deciduous stands present at the field site create a large swing in transpiration during leaf drop in the fall, while the exact rate and termination of leaf drop changes each year and at different elevations, the event typically occurs in early to mid October. During leaf drop forest stands transition from ~90% canopy cover at full foliage to ~%35 cover However, thick hemlock stands at the site create year-round canopy cover and source of transpiration (Whately Open Space and Recreation Plan Sec 4 EIS).

2.2 Soils

The upland soils of the field site (Figure 1) include the Chatfield-Hollis complex (109, map below), Charleton-Chatfield Hollis complex (125). Letters A-F indicate relative slope of the soil deposit 1-25% grade. All soils are well drained and found in areas with shallow bedrock or numerous bedrock exposures. Both soils are classified as yellowish brown fine sandy loam with a thickness of 75cm. Below which a light brownish gray sandy loam extends to a depth of 150cm before transitioning into surficial geologic parent material.

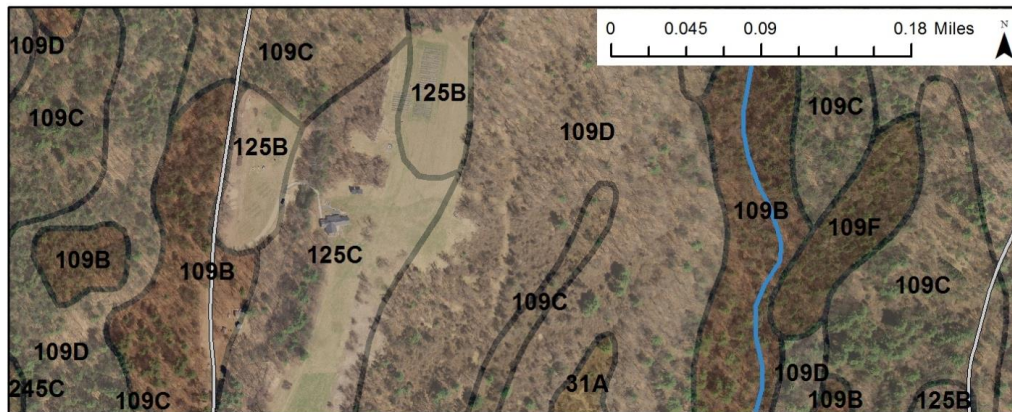


Figure 1. NRCS soil classification at the MacLeish Field Station, Whately MA.

2.3 Surficial geology

The surficial geology of the Westbrook watershed is characterized by rugged hills with numerous bedrock outcrops and mantled glacial sediments. During the Pleistocene multiple continental ice sheets exhumed most of the preexisting mantle and eroded the underlying bedrock (Heeley et al., 1980). As glacial lobes advanced and retreated they left remnants which can be categorized into two primary glacial deposits: glacial till and stratified drift. The surficial geology of the Westbrook was originally mapped by Kenneth Segerstrom in 1955, and was later simplified by Stone and DiGiacomo-Cohen in 2010.

Segerstrom discriminated the two primary glacial deposits into further categories based on the depositional environment.

The general regional ice flow of the continental glacier advanced in a S/SE direction and retreated from the South to the North. During glaciation a layer of till was deposited directly on top of the bedrock. Thicker deposits are thought to have been emplaced in the incised bedrock valleys as opposed to thinner till deposits on the higher elevation bedrock surfaces (Heeley et al., 1980).

During the retreat, stagnant ice blocks remained in the now uncovered valleys. Large volumes of glacial meltwater flowed through the valleys, travelling either over, through, or around the edges of the remnant ice blocks. In each valley a local temporary drainage was established based on the elevation of the existing bedrock, till, or standing ice. Meltwater streams then accumulated or eroded sediments based on these temporary base levels and cut rapidly through the previously deposited till. In some cases, till was completely eroded and the preglacial channel valleys became filled with glaciofluvial sediments. In other cases, glacial streams were able to cut terraces in till walled valley slopes. Bedrock spillways were also gradually eroded by the glacial meltwater streams, creating a procession of new spillways further upstream (Segerstrom 1955; Heeley et al., 1980).

In some instances the process of incremental melting and drainage of valley ice blocks has made some preglacial, glacial, and postglacial drainage channels system totally different from those existing today (Heeley et al., 1980). Glacial erosion and alteration of the basin drainage networks can be seen today in areas where there are poorly drained swamps and numerous waterfalls and rapids. However, past and present drainage patterns

in the Westbrook watershed are thought to be integrated better than many glaciated regions in the US due to the strong topographic relief of the valleys (Segerstrom 1955).

During the Wisconsinian Stage (the most recent Pleistocene glaciation), southward drainage was dammed by natural deposits and the Connecticut Valley filled with meltwater to become Glacial Lake Hitchcock. The elevation of Lake Hitchcock's banks were at approximately 300ft above modern sea level in Whately, the shoreline is tilted upward to slightly higher elevations in the north due to isostatic crustal rebound. Following the impoundment of Glacial Lake Hitchcock, standing water elevations rose in the highlands and tills and coarse glaciofluvial valley deposits were blanketed by large quantities of silty fine sand which graded upward into varved clay (Heeley et al., 1980). These glaciolacustrine backwater deposits created a relatively impervious aquitard over prior deposits. After thousands of years of fine sediment deposition the dam to Glacial Lake Hitchcock was breached and the dominant deposition processes switched from subaqueous to subaerial and subsequent anastomosing streams left relatively thin layers of sand on the top of glaciolacustrine sediments. As a result, stream channels primarily contain modern alluvium deposited over a mixture of poorly sorted glacial sands and gravels. Glaciolacustrine clays and fine sand and silt deposits are also found between beds of coarser glacial sediments. This layering has created the existence of partially confined sediment layers which are referred to as the 'upper' and 'lower' aquifers in the stream valleys (Heeley et al 1980). The 'upper' or shallow phreatic aquifer, is characteristically underlain by confined pre-glacial sediments which are capped by glaciolacustrine morphosequences. Where pre-glacial deposits are extensive, the 'lower aquifer' acts as a source of

groundwater supply for local municipalities such as the town of Williamsburg, MA (Storms and Motts 1987).

Coarse stratified drift is one of the major categories of glacial sediments mapped by Segerstrom and Stone. Glaciolacustrine and glaciofluvial deposits are concentrated in valleys and lowland areas and were laid down by glacial meltwater in streams and lakes. While Stone delineates only one lumped category, Segerstrom categorizes these sediments as (Qsg) Local thin deposits of gravel sand and silt, deposits on floors of ice-block basins, (Qld) Glacioalustrine deposits of gravel sand silt, trace clay, and (Qkt) kame terrace deposits.

Glacial drift that comprises most of the surficial deposits in the quadrangle is sourced from unsorted till that was transported and deposited directly by the ice and later sorted according to grain size by glacial meltwater. Deposition either occurred as ice-contact deposits where the place of deposition was bordered by ice blocks, or as outwash if downstream from the melting ice front (Segerstrom 1955).

Grain size of the stratified drift deposits with the Westbrook watershed are mapped as 'coarse' due to the relatively higher elevation above the shoreline level of Glacial Lake Hitchcock, fine stratified drift sediments are found at lower elevations. This sorting with elevation is a product of meltwater eroding fine sediments from the highlands and transporting to deposition locations closer to the elevation of Glacial Lake Hitchcock (Stone et al. 2004, Segerstrom 1955). Stone describes the typical grain sizes of Coarse Stratified Drift found in the watershed:

"Coarse Stratified Drift deposits include Gravel deposits composed of at least 50 percent gravel-size clasts; cobbles and boulders predominate; minor amounts of sand occur

within gravel beds, and sand comprises few separate layers. Gravel layers generally are poorly sorted, and bedding commonly is distorted and faulted due to post-depositional collapse related to melting of ice. Sand and gravel deposits occur as mixtures of gravel and sand within individual layers and as layers of sand alternating with layers of gravel. Sand and gravel layers generally range from 25 to 50 percent gravel particles and from 50 to 75 percent sand particles. Layers are well to poorly sorted; bedding may be distorted and faulted due to post depositional collapse. Sand deposits are composed mainly of very coarse to fine sand, commonly in well-sorted layers. Coarser layers may contain up to 25 percent gravel particles, generally granules and pebbles; finer layers may contain some very fine sand, silt, and clay (Stone and DiGiacomo-Cohen 2010)."

2.4 Bedrock geology

The bedrock of the Jimmy Nolan Brook watershed comprised of metamorphic and igneous crystalline rocks from the Paleozoic. The Conway Formation (SO), which accounts for the majority of the basin, is composed of a garnetiferous quartz-mica schist interbedded with quartzite and marble. Marble beds within the formation are found to weather into a friable aggregate, and range in thickness from a few inches to 100ft. Quartzite beds remain thin, composed of fine-grained equigranular crystals. The Williamsburg formation is a younger intrusive igneous rock, underlying the Conway Formation to the West. It is composed of granodiorite and pegmatite dikes and sills. Abandoned open pit metal mines can be found within this formation where galena, silver, and gold ore is located in a 3-4' wide quartz vein (Willard 1956). At many places for example the Conway formation is so thoroughly invaded by pegmatite, particularly along foliation planes that the resulting rock

might be called injection gneiss. at other places the granite and pegmatite show a well-developed foliation.

Schistosity cuts across bedding in troughs and crests of large folds and trends in a N/NE direction and dips slightly to the southeast (Willard 1956). Along poplar hill rd parallel bedding features strike N/NE and dips to the S/SE at ~45 deg. Much of the fracture cleavage in the Conway formation is oriented across the regional trend in schistosity. Slip cleavage is parallel to the exposed contact between the Williamsburg granodiorite intrusive and the Conway schist formation. Williamsburg granodiorite and associated pegmatites intruded the Conway formation, forcing its way into earlier foliation planes, bending them apart and deflecting the regional trend in schistosity. At the contact, the intrusive created local shear couples that resulted in the slip cleavage that surrounds and dips away from it. This is the slip cleavage in which the footwall appears to have moved up. Figure 2B Willard 1956. NW trending slip cleavage corrugations suggest that the deformation resulted from rocks in the East moving up and to the north relative to those in the West (Willard 1956).

2.6 Conceptual geologic model

An Electrical Resistivity Tomography survey was conducted to create a conceptual map of the geologic setting of the well site, hillslope, and stream catchment across an exposed transect on the hilltop. The transect starts at the west edge of the wellfield and travels across the ephemeral creek and the abandoned pasture to the east where it terminates at the precipice of the steep slopes of the river valley (Figure 2). The resistivity survey was conducted using the SuperSting™ with Swift™ automatic resistivity system made by Advanced Geosciences Inc. A 25 electrode array was installed using 10m spacing. Field testing occurred on 6/10/2013 using standard protocol including preliminary contact

resistivity testing prior to the administration of a dipole - dipole survey using the programming order for electrode induction consistent with the Superstring software.

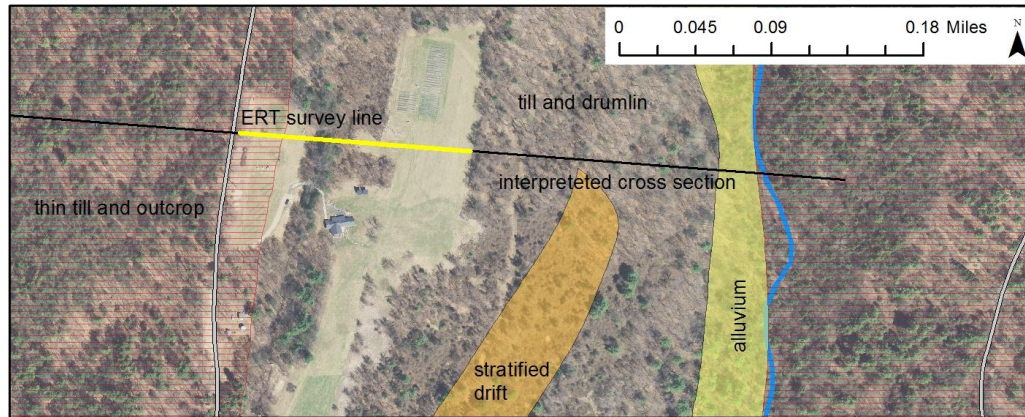


Figure 2. Map of ERT transect (yellow line) and the surficial geology extending to Jimmy Nolan Brook (black line). Surficial geology polygons from (Stone and DiGiacomo-Cohen in 2010).

The resulting voltage readings from each electrode were processed using commercial geophysical inversion software RES2DINV to create a representative matrix of earth-material resistivity values at various depths across the length of the transect. Using general reference values for directly measured and known resistivity values for earth materials and observed stratigraphic information from well borings and surficial geologic interpretations, the modeled resistivity values from the ERT survey were interpreted to create a conceptual model (Figure 3).

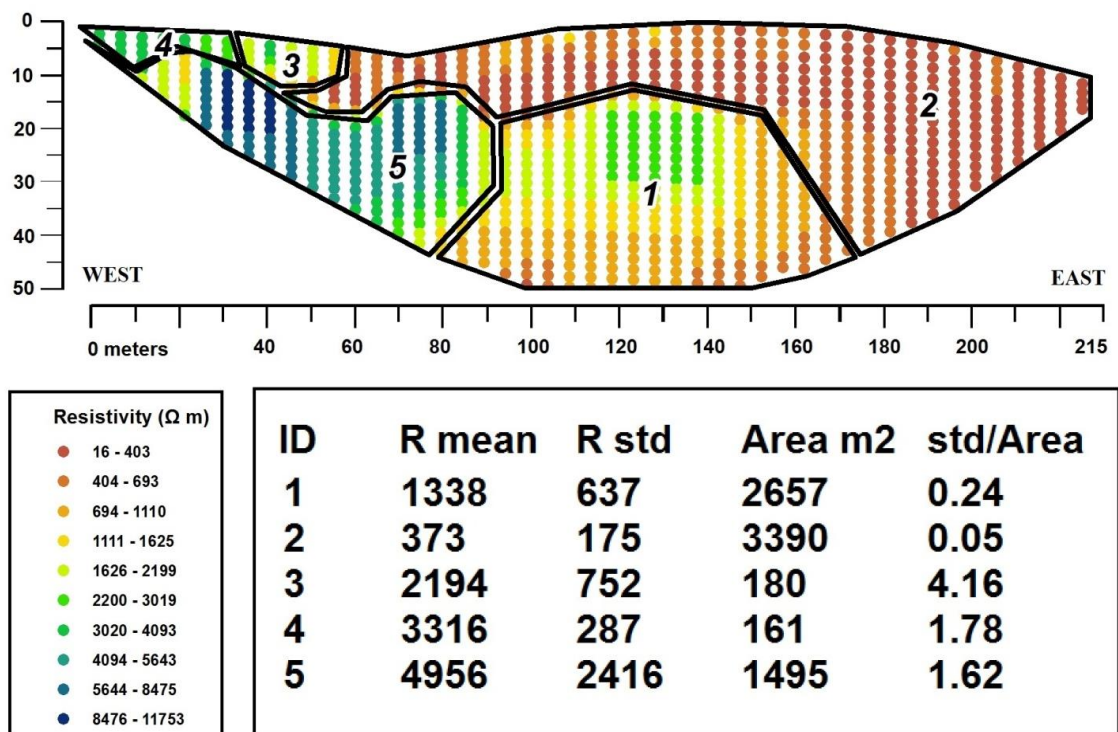


Figure 3. Cross section of ERT model and interpreted polygons with calculated mean resistivity and standard deviation. Vertical axis shown in depth in meters below ground surface.

Individual resistivity points on Figure 3 represent modeled values of resistivity from the inversion solution solution (deGroot-Hedlin and Constable 1990). Polygons were created by hand to map areas into categorical geologic units based on similar resistivity values and known contact points between bedrock and surficial materials based on well logs and field observations (Figure 4). Polygons were used to generate mean resistivity values for the enclosed area along with the standard deviation of values measured within the shape. The deeper values (below 30m depth) and boundary values are less reliable as they are based on fewer observations and weaker signal strength at depth.

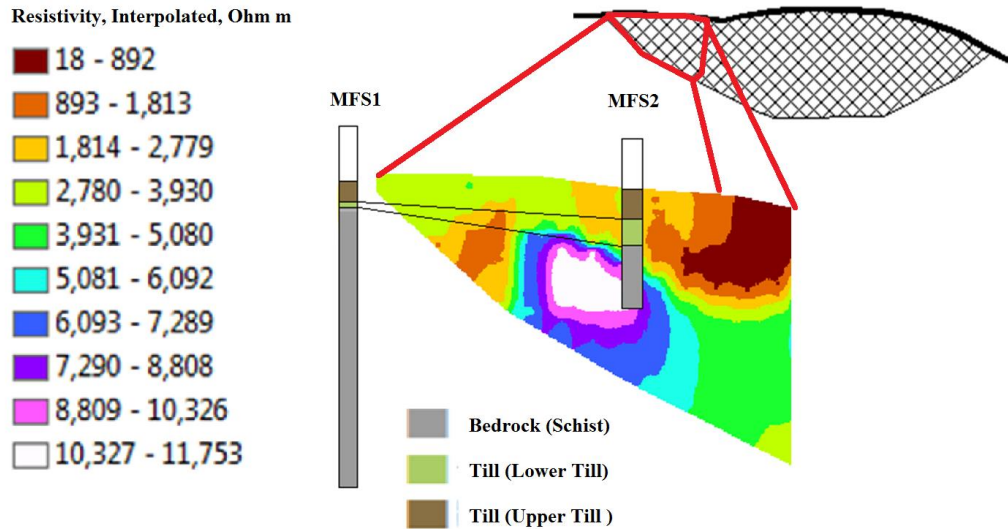


Figure 4. Interpolated resistivity values with well stratigraphy overlaid. The cross section from figure 3 is provided for reference. Wells MFS1 and MFS2 are located ~40 m apart. See scale on figure 3.

Polygon 4 in Figure 3 has a mean resistivity value of 3312 Ohm m which corresponds with the range of glacial sand and gravel deposits (Figure 4). Similarly, observations made in well borings of the sandy upper till unit correlate with polygon 4. This polygon appears to be well drained and above the water table throughout the summer, resulting in higher resistivity values compared to saturated sediments below the water table.

Polygon 5 in Figure 3 has a mean resistivity of ~ 5000 Ohm m which corresponds with typical R values found in crystalline bedrock with low saturation values. The top of this polygon also correlates well with the schist bedrock contact of the Conway formation recorded in the drilling logs from well MFS1 and well MFS 2. Similarly, an outcrop can be observed at the far West extent of the resistivity transect, which is presumed to extend into the ground towards the contact with nearby well MFS 1. An exceptionally high resistivity feature is seen in dark blue where modeled R values exceed 10,000 Ohm m, indicating a competent relatively less fractured bedrock section separating the two wells

(Figure 4). The high standard deviation is due to the lower resistivity section to the West which could represent a topographical trough in the bedrock surface which has been filled by lower till.

Polygon 2 in Figure 3 has the lowest resistivity values of each of the polygons with a mean value of 373 Ohm m. This area covers the largest extent and correlates with mapped surficial geologic units as drumlin composed of lower till. The low resistivity readings can be explained by the presence of clay in the sediment matrix.

Polygon 3 in Figure 3 has the highest standard deviation per unit area and represents a transitional zone where upper till in polygon 4 intersect drumlin deposits in polygon 2. Similarly, the water table cuts across the polygon area and can be seen by the decrease in resistivity at the bottom of the polygon.

Polygon 1 is likely a more complex area of till and bedrock, this polygon represents a large area and is at a greater depth in the model. The most uncertainty in interpretation remains here, however the standard deviation is relatively low, suggesting that it is more or less homogenous. It is likely that this zone is either drumlin or bedrock, or a mix of the two, however given that it is below the water table yet displays higher resistivity values, it is more likely weathered bedrock and its borders likely represent the interface of the drumlin deposit and schist bedrock of the Conway Formation.

The subsurface resistivity interpretation was extended to the lower hillslopes adjacent to Jimmy Nolan Brook by referencing the surficial geologic map (Segerstrom 1955, and Stone 2007) and project the subsurface locations of stratified drift, alluvium, drumlin, and till deposits. The remaining subsurface interpretations were based on field

observations and interpretive knowledge of modern stream geomorphology and descriptions of the depositional history of glacial sediments sequences in neighboring river valleys near the town of Williamsburg MA (Storms and Motts 1987).

Field observations support that the depth of the sediment layers underlying Jimmy Nolan Brook is variable and is best represented by a series of sediment filled troughs in between the numerous bedrock outcrops and eroded bedrock spillways. Greater depths of outwash and alluvial sediment layers are likely found at other locations along the stream reach where bedrock is steeply dipping towards the east at >45 degrees. Glaciolacustrine fine silt and clay sediments have also been excavated at low elevations along the stream reach, suggesting that preglacial sediment may also remain in a semi-confined position below the clay layers. This model is outlined in (Storms and Motts 1987). Additionally, coarse gravel deposit are located on abandoned stream terraces above the current stream channel. Active erosion by the present stream channel has carved multiple paths through the till, bedrock, and finer deposits leaving a network of interconnected sediment channels between bedrock outcrops. An abandoned rockwall which bordered 19th century pastoral and agricultural fields also gives insight into the development of topsoil which is now host to young succession of eastern hemlock.

The depositional history of sediments in stream valleys outlined by (Storms and Motts 1987) is based on well borings from public water supply aquifers in Williamsburg MA (Appendix D) and provides the basis for the cross section underlying Jimmy Nolan Brook. The characteristic depositional pattern is characteristic of the western highlands surrounding the connecticut river valley. Thin and thick till deposits mantle bedrock hillslopes, and cover depressions where pre-glacial stream channel sediments have

infilled. Stratified drift deposit are the most superficially exposed deposits in the stream valleys where glaciofluvial and lacustrine deposits are interbedded corresponding to the alternating melt and ice-dam series.

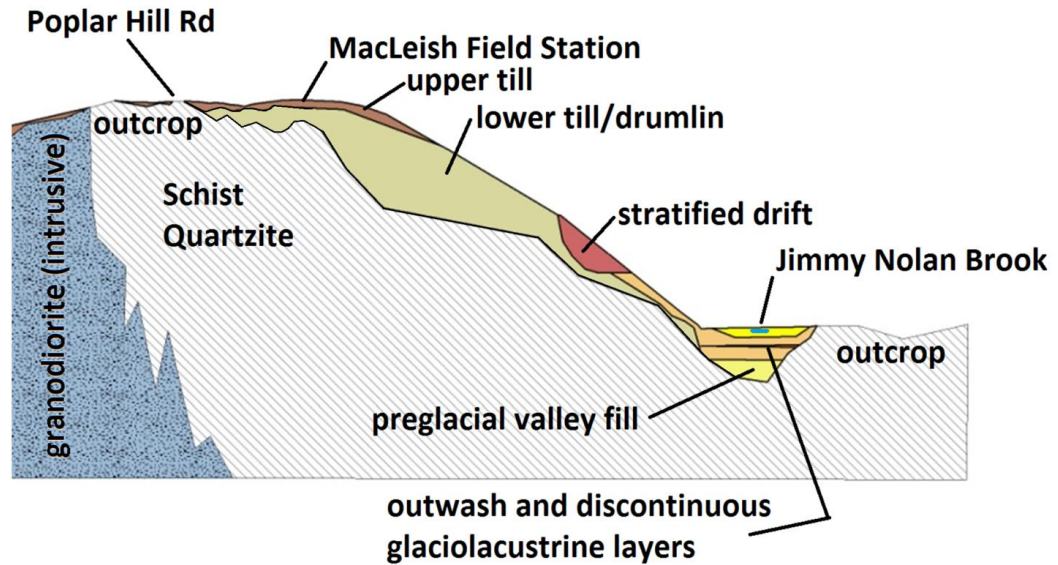


Figure 5. Conceptual Geologic Model of well site near Poplar hill road extending east towards Jimmy Nolan Brook. Vertical exaggeration x 3.

2.7 Hydrogeologic characteristics of Glacial units

Groundwater flow into the Jimmy Nolan Brook stream valley can be conceptualized by categorizing 3 different groundwater aquifers: the unconfined zone, confined zone, deep water zone (Appendix D). The connectivity of each aquifer zone is controlled by relative confining units such as till and glaciolacustrine sediments acting as aquitards. Stratified drift and preglacial valley sediments provide the greatest water storage, and fractured bedrock provides the most rapid groundwater flow routing (Garabedian & Stone 2004). The laying of these deposits results in the creation of discontinuous confined layers, perched water tables, and variable recharge fluxes to each aquifer.

The major deposits that characterize the unconfined zone include kame terraces, glaciolacustrine deposits and sandy upper till. In unconfined storage these aquifers hydraulic head corresponds with the water table. Perched aquifer water table elevations can also be present in these deposits where lower conductivity layers are present below. Similarly, perched aquifer tables can be found under transient duration where the addition of rainwater produces an upward extension of water table at a faster rate than lower, less-permeable sediments can wet-up (Buttle 1989).

Confining layers such as lower till, which can be considered to have a very-low permeability (Storms and Motts 1987), can create confined zone where extensive preglacial deposits are underneath, however it is not a continuous cap over all preglacial deposits. Lower till also blankets much of the bedrock and acts to limit the recharge flux to areas where bedrock outcrops and thin till cover are present (Gleeson et al. 2009). Confined layers are often connected to specific deposits such as Kame Terraces, where they can be recharged.

The Deep water zone includes the circulation of groundwater in fractured bedrock storage (Appendix E). Fractured bedrock permeability is typically greater at shallower depths due to larger aperture size and greater frequency of fractures (Gleeson et al. 2009). Where fractured bedrock outcrops are present, the deeper bedrock aquifer has the potential to be recharged, however in areas where fracture density is low, shallow bedrock acts as a barrier to flow.

CHAPTER 3

METHODS

This study uses a spatially distributed network of field instruments to characterize variability in the water flux and temperature in the Jimmy Nolan Brook Stream catchment. Upland groundwater reservoirs, hillslope, stream valley, and stream channel in sample locations were instrumented with continuous data loggers to record hydrometric and temperature data at high temporal frequency. Hydrometric field measurements were recorded for streamflow, soil moisture, groundwater head, and precipitation volume. Temperature data were collected in the stream channel, groundwater reservoirs, shallow soil profiles, and along the ground surface. Data were calibrated with overlapping measurements, where available, to remove errors during collection and processed to create a consistent timestamp for comparison purposes. The work described in the following sections details the instrumentation deployment, monitoring, data collection, and numerical modeling of ground water and heat flow.

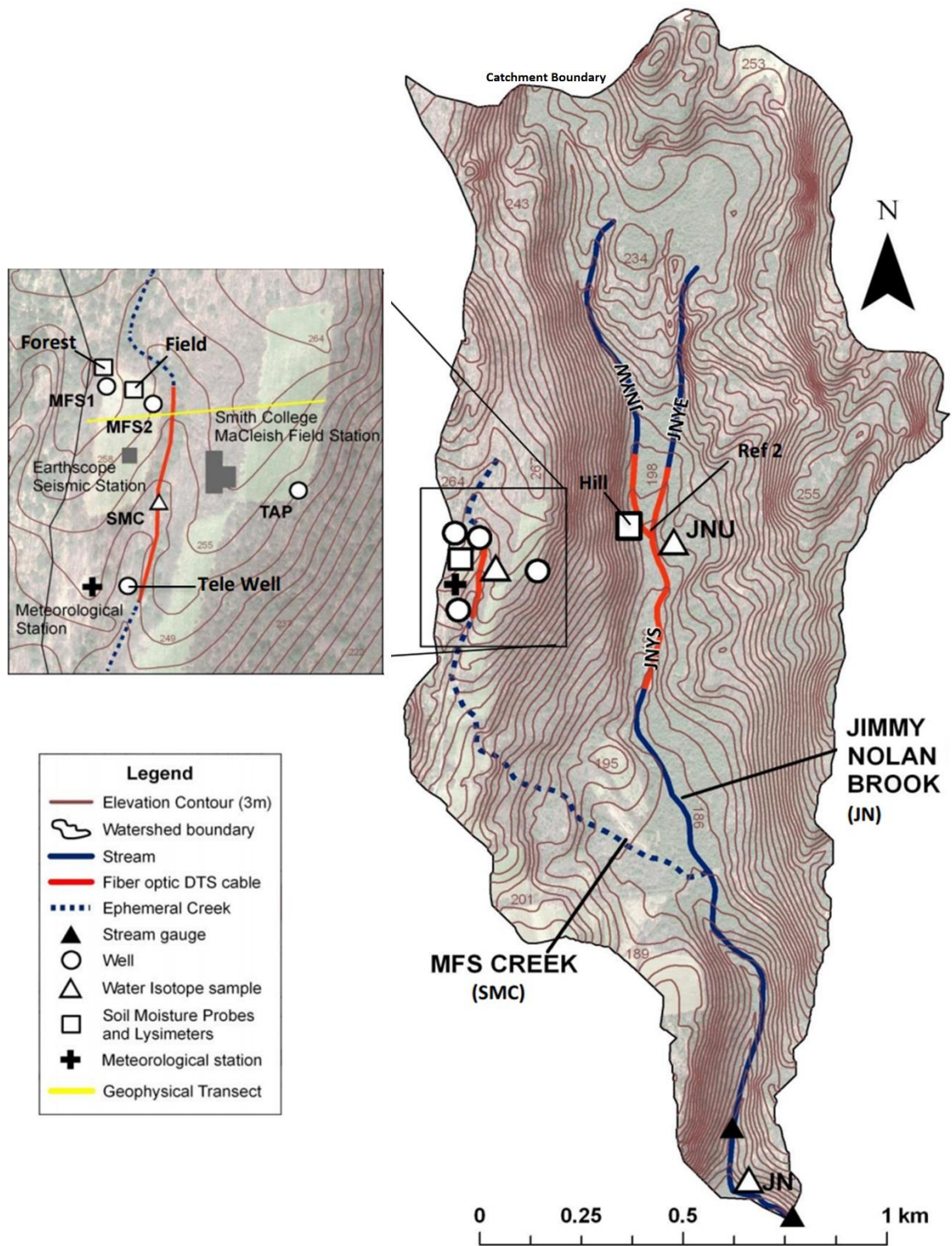


Figure 6. The Smith College MacLeish Field Station, Jimmy Nolan Brook catchment and location map of isotope samples, stream segments, fiber-optic DTS cable locations in streams, geophysical transect, and soil moisture probes. The field station is located at 42.449175 deg longitude and -72.679467 deg latitude in Whately Massachusetts.

3.1 Weather

Precipitation data was collected at ten-minute intervals from the MacLeish Field Station's weather station which is maintained by Smith College. Relative humidity, temperature, barometric pressure, wind speed, wind direction, and solar radiation are measured above the tree canopy from the top of 25.3 meter (83 feet) tall tower. Precipitation data is collected from a tipping bucket located at ground level. Data gaps from the MFS weather station were compensated for with data from the Weather Underground Station KMACONWA2 which is located less than one mile from the site. Minimum air temperatures typically occur in January and maximum air temperature typically occurs in July. Average temperatures below freezing are common from early November to late March most years. Hurricane's in late summer/early fall can result in increased precipitation, flooding, and high winds. In August 2011 Hurricane Irene was responsible for the loss of many bridges in western Massachusetts and resulted in significant spikes in stream runoff and flooding. To a lesser extent, Hurricane Sandy also resulted in increased precipitation and stream runoff during October 2012.

3.2 Soil Moisture TDR field measurements

Soil moisture content in the shallow subsurface was measured using time domain reflectometry (TDR) which is a widely used method used to measure the volumetric water content of a soil volume. TDR technology has readily been applied to commercial instruments such as the Decagon 5TM Em50-series data logger, which was used in this study. The data logger directly measures the apparent soil electrical conductivity of a bulk soil volume (715 ml effective measurement volume), which is then converted to volumetric water content using a capacitance/frequency domain and the Topp Equation. Temperature

data is collected with an additional attached thermistor prong with a resolution of 0.1°C and an accuracy: $\pm 1^\circ\text{C}$.

Apparent soil electrical conductivity is measured in 2 of the 3 adjacent prongs of the sensor in contact with the soil. Resistivity (inverse of conductivity) is measured based on the voltage drop recorded across the prongs similar to an ohmmeter. Apparent dielectric permittivity (ϵ_b) is calculated using the measured soil apparent electrical conductivity, the angular frequency of the circuit oscillator (ω), and the temperature (T) (Yu and Yu 2006). The apparent dielectric permittivity (ϵ_b) is then used to estimate the volumetric water content (θ) using the Topp equation, which provides an empirical reference for a wide range of soils. This provides a final Volumetric Water Content (VWC) accuracy of $\pm 0.03 \text{ m}^3/\text{m}^3$ ($\pm 3\%$ VWC), and resolution of $0.0008 \text{ m}^3/\text{m}^3$ (0.08% VWC).

Soil moisture probes were installed in 3 different locations: upland field, upland forest, hillslope forest, and hillslope riparian: electrodes were placed in pairs at depths of 50 and 100 cm beneath the soil surface. These depths correspond to the B and B/C horizons in the soil. The first pair, labeled “Field” were placed 3m' away from Well MFS1 in a fallow field, which also contains well MFS2 (Figure 6). The second pair of TDR electrodes was placed in a location labelled “Forest” which consisted of a stand of red maple and eastern hemlock located 7m west of well MFS1, near the highest elevation point on the transect from the well field to Jimmy Nolan Brook valley (Figure 6). The third pair of probes 'riparian' or 'Hill' was installed 2m to the west of the stream bank in a clay and organic rich riparian soil at an elevation 30cm below the adjacent stream stage (Figure 6). Only 1 of 2 TDR probes functioned after one of the cables was chewed by an animal.

Measurement frequency was set at 10 min intervals and recorded using a Decagon 3G transmitter so that the time-series could be accessed and record by offsite data servers.

3.3 Saturated conductivity lab measurement

Laboratory measurements of soil saturated hydraulic conductivity for field soil samples were conducted to better understand the relationship of field measurements of soil saturation to the variability in the hydraulic conductivity of the soil profile. Soil cores were collected from locations representing the upper till and lower till. The soil core taken representing the upper till was coordinated with the excavation of the soil pit for the installation of the TDR soil moisture probes located at the 'upland field' at a depth of 75cm below the ground surface. The soil sample is described as dark yellowish brown USCS soil class 'SP' or fine to coarse grained clean sand. The Soil core taken from the lower till (16-18' depth) was sampled from well MFS2 and can be described as medium dark gray USCS soil class 'ML' or silts of low plasticity inorganic silt and fine sand. A soil sample can be conceptualized as a bundle of capillary tubes connected through a variety of pore and pore-throat sizes with which a unique relationship exists between the water potential associated with a given pore. As a result, it is important to minimize sample disturbance during collection, which could alter the density of the soil, by using a specialized soil collection core ring apparatus, which also serves as the housing during the evaporation process. As the saturation state of a soil changes, the rate of water flux through the medium changes disproportionately depending on the specific relationship between saturation state (Volumetric Water Content, VWC, θ) and hydraulic conductivity for that soil type $K(\theta)$. In order to measure this relationship a HYPROP dual tensiometer soil water retention instrument was used to records the soil water retention curve (SWRC) by measuring

simultaneous weight and water potential of an undisturbed soil core (250 ml) during a evaporation dry-down curve. Soil cores were collected from the field site and underwent a laboratory standardized saturation and dry-down process using precision the HYPROP equipment for preparation and data recording. In this process two precision mini-tensiometers shafts 12.5 mm and 37 mm measure the differential water potential within the sample while recording weight measurement from precision scale (0.01g precision). Tensiometers are located in the middle of the sample where it is assumed that the most representative saturation conditions are present. This process assumes quasi steady state conditions, where the flux and hydraulic gradient are constant over the time interval, and that there is a linear decrease of water content and linear decreasing soil suction (Macek et al 2013). This assumption is met by conducting the evaporation recording process in a climate-controlled laboratory environment. Curve fitting to the soil-water retention model by van Genuchten 1980 was then to used to develop the relationship between $K(\theta)$ and VWC.

The SWRC is defined as relationship between the water content and the soil suction and it can be divided into the capillary saturation zone, desaturation zone, zone of residual saturation (Macek et al 2013). The capillary saturation zone where soil is fully saturated and water is able to leave freely through gravity drainage. The desaturation zone is where the matrix suction of the soil pores exceeds the air entry value, this is the part of the curve where saturation decreases rapidly. Maximum pore size at the soil surface has control over the value of this point. As a result, finer grained sediments have the highest air entry values. Hysteresis between wetting and drying curve is typical for the desaturation zone. Lastly the zone of residual saturation: in this zone water content can be changed only by vapor

transport. Porosity structure in the soil sample plays a large role in shaping the SWRC (Macek et al 2013).

3.4 Groundwater

Monitoring wells 'MFS-1' and 'MFS-2' were constructed on the MFS property owned by Smith College in June 2012. The wells were drilled using an 8" hollow-stem auger and an air-hammer to advance through the surficial materials and bedrock, respectively. MFS-1 was drilled to a depth of 140 ft bgs and completed as an open borehole in the bedrock with steel-casing extending from ground surface to 2 ft below the bedrock contact (12.5 ft bgs). MFS-2 was drilled to a depth of 50 ft bgs and completed with a 2 in PVC well screened across the till and bedrock contact (27 ft bgs REF attached borehole logs). An existing well which supplied drinking water to the field station (TAP) is also located east of the field station.

MFS-1 (bedrock well) is located at 856 fasl on the hilltop near the highest elevation along the E-W transect from the MFS to Jimmy Nolan Brook. The top 9 ft of the overburden surrounding the well consisted of 'sandy upper till' with a 2.5 ft thick layer of gravel from 9-11.5 ft bgs and a thin, 1 ft layer of 'clayey lower-till' material existed above the bedrock contact (843.5 fasl). The remaining length of the well is open to fractured micaceous schist (Conway Formation) with intermittent quartzite beds. Fracture angles tend to increase with depth in the well. Core samples of the bedrock and surficial materials were recorded by hand upon excavation from the drill bore.

MFS-2 (surficial till well) was drilled at an elevation of 845 fasl and 110 ft to the East of MFS-1 along the transect at an elevation of 845 fasl. The well screen is open to the

bottom 5 ft of overburden material, below this depth the bedrock is considered competent and relatively impermeable. Overburden material extend to 27 ft below ground surface (818 fasl). The top 14 ft of material is consistent with 'sandy upper till' with zones of fine sand silt and clay at 10-12 ft below ground surface. From 14-27 ft below ground surface, the materials are consistent with 'lower till' and contain primarily fine sand silt and clay with large gravel clasts > 4" diameter. Sulphide minerals were present at the bedrock contact, suggesting that this may be an active zone of fluid transport.

Monitoring wells MFS-1 and MFS-2 were instrumented with autonomic data loggers (Solinst levelogger gold, Temp. Sensor Accuracy: $\pm 0.05^{\circ}\text{C}$, Temp. Sensor Resolution: 0.003°C , pressure resolution and an accuracy of ± 0.5 cm) to record temperature and pressure. Well tests included pumping tests and geophysical borehole logging. Pumping tests were conducted on well MFS1 using a step increase pump rate, however after 6 hours of pumping less than 5cm of drawdown was observed, indicating that there is a minimal hydraulic connection between the wells. Borehole geophysical logging was conducted by Geophysical Applications, Inc. Profiling included the use of an ambient and heat pulse flowmeter, temperature/resistivity profile, and acoustics. This process was able to resolve the distribution of fractures intersecting the well bore and determine relative flow rates corresponding with each fracture intersection point. The extent of the connectivity of each well to the corresponding aquifers was examined by Hudson, 2016 who found that the active flow in well MFS-1 occurred primarily at discrete fracture interval 28 ft bgs in the borehole. MFS-2 was found to be representative of the lower-till aquifer, despite being screened across the till/bedrock contact, the well screen does not interface with any hydraulically active fractures within the bedrock.

3.5 Streamflow

Streamflow measurements were recorded at a long term gage operated by the USGS on the downstream reach of Jimmy Nolan Brook , 300 ft upstream of the confluence with the Westbrook River. The stream gage has been monitored at 60 minute frequency since 2004, however Tropical Storm Irene caused damage to instruments and the gage was replaced after 2011. Water temperature data were collected using data loggers recording every 2 h. Stream flows were estimated by the USGS using a flow extension model (Nielsen, 1999) based on data from the nearby USGS stream gauge at the Mill River, Northampton, MA. Correlation between flow extension estimates and flow estimates based on a stage–discharge relationship developed at the study site (using a continuous stage record and several direct measurements of discharge) were high ($r = 0.94$, $n = 506$, $P < 0.001$), however the flow extension method was preferred to the stage-discharge relationship due to the observation that the flow extension method provided a more consistent record of stream flow over long time periods. Baseflow separation was conducted using a one-parameter digital filter method using the following equation (Lyne and Hollick, 1979; Nathan and McMahon, 1990; Arnold and Allen, 1999):

$$q_k = aq_{k-1} + \frac{1+a}{2}(y_k - y_{k-1})$$

Where, q_k is direct runoff at time step k , q_{k-1} is direct runoff at time step $k-1$, y_k is total streamflow at time step k , y_{k-1} is total streamflow at time step $k-1$, and a is a filter parameter.

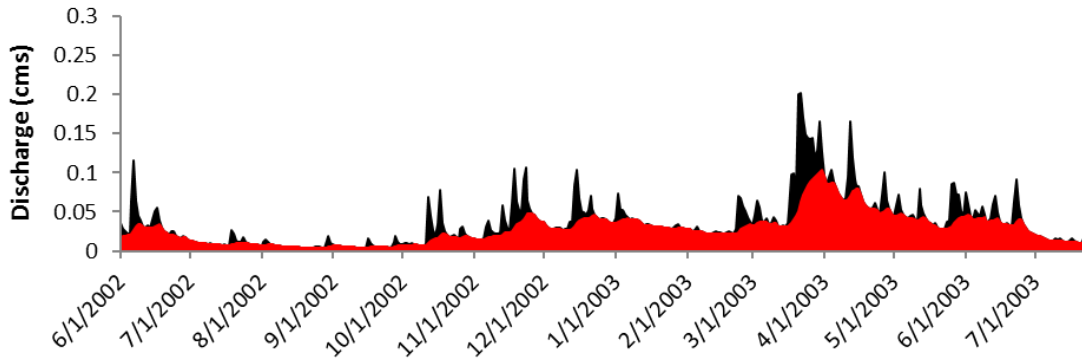


Figure 7. Baseflow separation for Jimmy Nolan Brook. (Red area = baseflow contribution, black = total discharge).

3.6 Stable water isotope tracers

Stable isotope samples were collected from stream, groundwater, precipitation, and soil sources at weekly to bi-weekly intervals. These observations were then used to help determine sources of different waters in the catchment. Hydrogen and oxygen isotopes are ideal natural conservative molecular tracers for surface and groundwater as their weight, composition, and therefore behavior is similar to natural waters (Clark and Fritz, 1997). Water isotopes act as natural tracers as they are introduced to the hydrologic system through precipitation and mix with older and more recent source waters along a flowpath. Hydrologic environments can be distinguished based on their Isotopic composition which is distinguishable on the basis of fractionation which creates a unique signature that can be seen in the seasonal distribution of precipitation and/or other source waters (Clark and Fritz, 1997). The process of fractionation of isotopes occurs primarily through preferential evaporation of lighter isotopes, resulting in the enrichment of heavier isotopes in relative proportion to the timing and duration of evaporative loss. Common stable isotopes of water are deuterium ^2H and oxygen-18 ^{18}O , with the most common molecular forms being $^2\text{H}^1\text{H}^{16}\text{O}$ and H_2^{18}O . Deuterium excess, a measure of preferentially fractionated $^1\text{H}_2^{16}\text{O}$ relative to the Global Meteoric Water Line (GMWL), can be used to further delineate the path of isotopes through a groundwater system. The GMWL represents an average humidity just slightly greater than 85% which produces precipitation values displaced from the seawater by + 10 ‰ deuterium, resulting in the

general equation for global meteoric precipitation, $\delta^{18}\text{O} \text{‰ VSMOW} = 8.17(\delta^2\text{H} \text{‰ VSMOW}) + 11.27$. Deuterium excess is controlled by humidity of the vapor source region and secondary evaporation effects. For example, continental evaporation sources preferentially contribute lighter $^2\text{H}^1\text{H}^{16}\text{O}$ molecules to the atmospheric vapor composition (Clark and Fritz, 1997). In the Northeast US, Deuterium excess is greatest during summer months due to the influence of tropical air streams from the Gulf of Mexico and Atlantic Ocean. Winter evaporation on the east coast falls close to the GMWL (Clark and Fritz, 1997).

Precipitation isotope samples were collected using a homemade precipitation collector with the addition of mineral oil to limit evaporative losses. Weighted monthly values were computed by adjusting sample volumes by the total volume recorded at the MacLeish weather station. Snow volumes were adjusted using the water equivalent and reported at the time of sampling, not the time of melting. Soil pore-water samples were collected using suction lysimeters at 30 cm and 60 cm depths below the soil surface at locations coinciding with the Soil moisture probes. Samples were collected opportunistically after precipitation events, producing a discontinuous record of measurement. Plant water was sampled by cutting invasive vines and allowing water to drip collect into a sample vial. Stream, well, and lysimeter samples were collected via grab samples.

Samples were analyzed using a Picarro L2130-*i* Analyzer using the later 3 of 6 sample runs to calculate the final sample values. Three separate standard samples were also used to maintain relative uncertainties of less than 0.001% for $\delta^{18}\text{O}$ and 0.02% for $\delta^2\text{H}$.

3.7 Distributed Temperature Sensing

High spatial and temporal resolution stream temperature data were collected using a fiber-optic distributed temperature system cable (DTS) deployed in the ephemeral creek (SMC) running through the MacLeish Field Station and segment of the Jimmy Nolan Brook stream channel 1.7 km upstream of the confluence with Westbrook River. The cable Temperature measurements were recorded at 10 min intervals along 2000 meters of cable that was submerged in the stream channel and along the ground surface between the power source and the collection target (stream channel). A Sensortran DTS system was used to measure temperature with a precision of 0.01 deg C with a spatial resolution of 0.25m averaged every 10 minutes. The DTS system works by tracking light emissions fired by the laser as they travel down the length of the cable, during the process light waves are backscattered to the recording instrument where the travel time and ratio of temperature-dependent wavelength to the temperature-independent wavelength provide a measure of temperature along the cable. (*Selker et al.*, 2006). DTS is a well-established temperature sensing technology and is further detailed in Tyler et al. (2009).. The 2000 m long cable installation required two cables of 1000m each to be joined together using an fusion splicing tool, which was housed in a protective waterproof heat-shrink casing to minimize signal loss due to environmental stress such as pressure. The MacLeish Field Station Meteorological Bunker, which is maintained and operated by the Smith College CEEDS, housed the Sensortran system and provided a constant power source and climate-controlled environment.

Stream temperature data in SMC were sampled along a 230 m segment extending from the MacLeish Meteorological station which supplied power and housed the laser and

data recording hardware. The section of DTS cable deployed in upstream Jimmy Nolan brook stretched across a 500m section of the main channel, a 200m section along the east fork (JNYE), and a 200m section along the west fork (JNYW).

DTS temperature calibration was based on an upstream and downstream temperature reference coils and georeferencing the cable with field measurements. Calibration coils of cable >20m in length coincided with a temperature logger in the telescope well adjacent to the Meteorological station and a temperature logger in a pool in upstream Jimmy Nolan, providing references at each end of the deployed cable. Temperature reference points were collected in the open stream channel in 2 locations using autonomous temperature loggers (Hobo Pro v2 Water Temperature Data Logger – U22-001, 0.2 C accuracy, 0.01 C resolution), and an additional ice bath for a lower range reference point. An upstream reference bath in a telescope cooling cistern near the meteorological station functioned as a shallow groundwater well to provide reference points at both ends of the cable (6ft below ground surface, TOC, 824 fasl), which provided a cold temperature reference. The temperature difference between the DTS cable and hobo logger measurement were calculated at corresponding time intervals, the mean measure of this value was then used to correct a direct offset in temperature at this point. This process was repeated for both the upstream JN reference hobo (end of cable) and the MFS Met station well (beginning of the cable). The difference between these two points was then used to determine a correction of +3.8 deg to be applied to the entire length of cable (Figure 8 and 9). Sontaran software provides user-friendly deployment of DTS cable for temperatures sensing and additionally corrects trends for signal recovery loss along the cable length. Field locations were calibrated using measurements from a hand-held GPS

device which were then incorporated into a geodatabase and compared to orthophotography to match the corresponding geomorphology of the stream channel. Observed cable temperatures were then compared to field notes to determine the transition areas between land and water, and sections of the cable extending above the stream level.

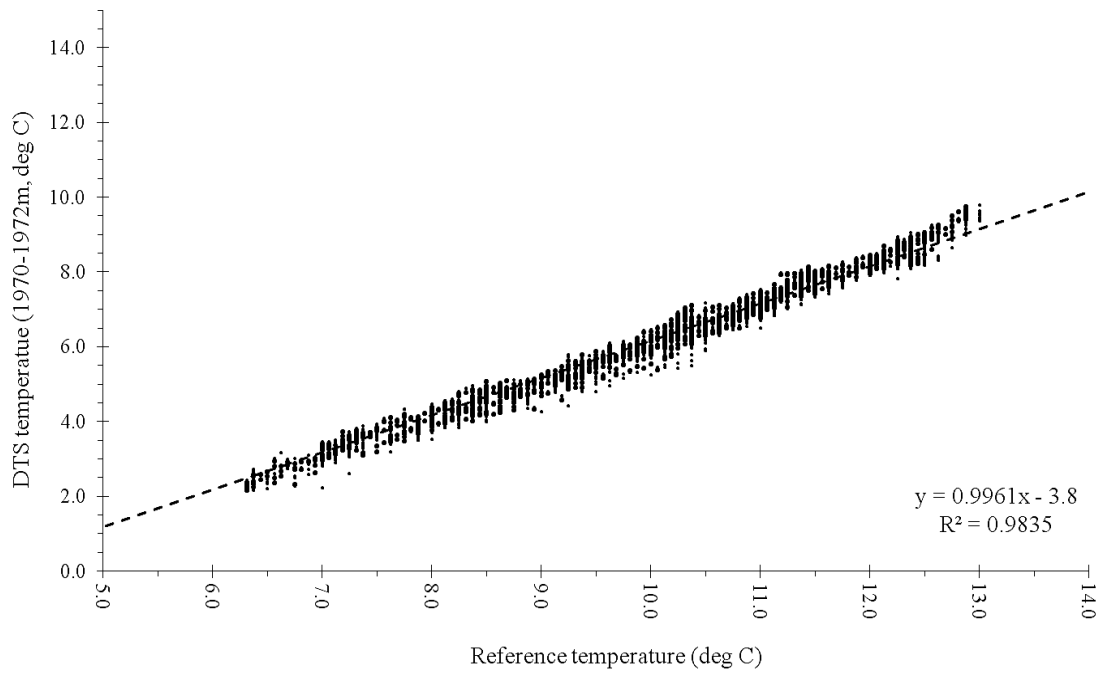


Figure 8. DTS downstream calibration coil with straight-line fit. Temperature offset of 3.8 deg C between DTS temperature and reference.

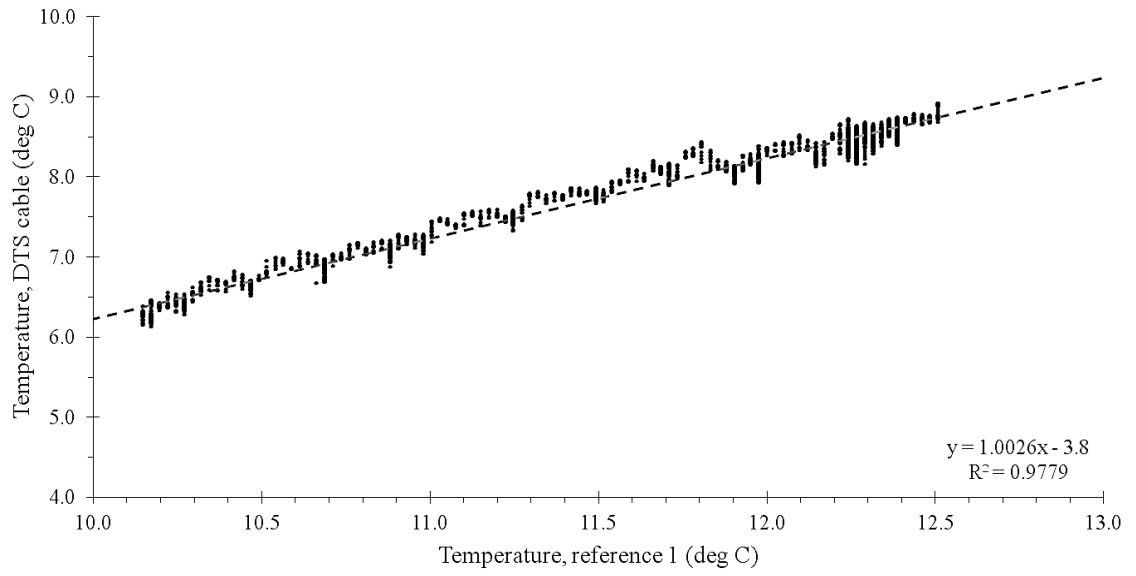


Figure 9. DTS Upstream calibration coil in telescope well with straight-line fit. Temperature offset of 3.8 deg C between DTS temperature and reference.

CHAPTER 4

RESULTS AND DISCUSSION

4.1 Soil Moisture Thresholds

Saturated hydraulic conductivity lab analysis of the B/C soil horizon located adjacent to the ‘field’ soil moisture probes depict hydraulic conductivity increasing as volumetric water content (VWC) increases (figure 10). When the VWC begins to exceed 19% in a wetting-up phase, the hydraulic conductivity increases at a rate that is approximately ten times faster than below ~19%. On a pore scale this can be explained by flow within the soil matrix exploiting larger pore spaces or preferential flow paths at higher water content. Threshold behavior impacts the physical fluid movement through a soil medium, in effect, water added to the soil while $VWC < 0.19\%$ will result in increased VWC, while water added to the soil when $VWC > 0.19\%$ will result in a relative increase in transmittal of water through the soil horizon (field capacity). Within the range of typical field saturation values the measured hydraulic K changes by 2-3 orders of magnitude, while the thermal conductivity measurements recorded by the MA State Geologist at the site remain within 1 order (fully-saturated soil = 0.63 W/m/K, dry soil = 0.166 W/m/K). As a result, changes in soil saturation will result in larger increases in advective relative to conductive heat flux.

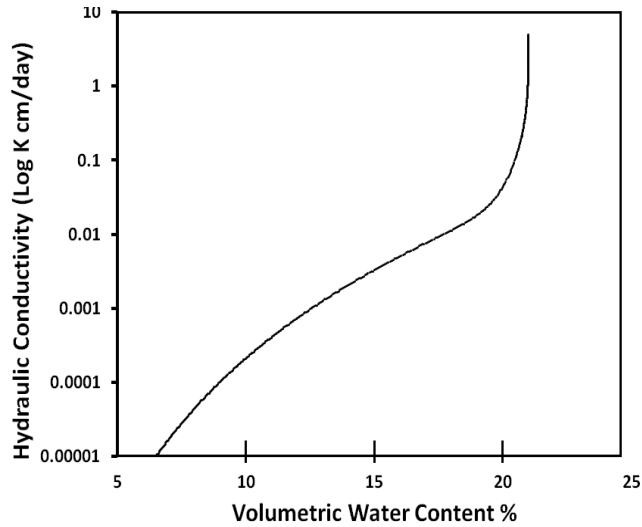


Figure 10. Saturated hydraulic conductivity curve results from Hyprop testing of the B/C soil horizon sample collected from ~150 cm depth. VWC % was recorded from the dry-down curve.

In-situ field measurements of water content over time also show non-linear trends with inflection points occurring at an average VWC of 20%. Semi-log plots of the mean change in volumetric water content over a 60 min interval for scaled values of VWC recorded in the soil moisture probes installed in the 'Field' (Figure 11) and 'Forest' (Figure 12) at 100 and 50cm below ground surface depict higher rates of change once saturation values surpass the inflection points A,B,C and D (VWC values listed in Figure 13). Data were collected from May 2013 to Feb 2014 at the MacLeish Field Station in Whately MA. VWC values were interpreted as soil saturation by scaling from 0 to 100% based on the maximum values recorded in the field over this time period. Inflection points in VWC correspond with point A=0.28, B=0.39 point c=0.35, d=0.11, C=0.80, and D=0.38. The scaled values correspond with measured values in Figure 13., ranging from 17 to 24 %, with an average measured value of 20%.

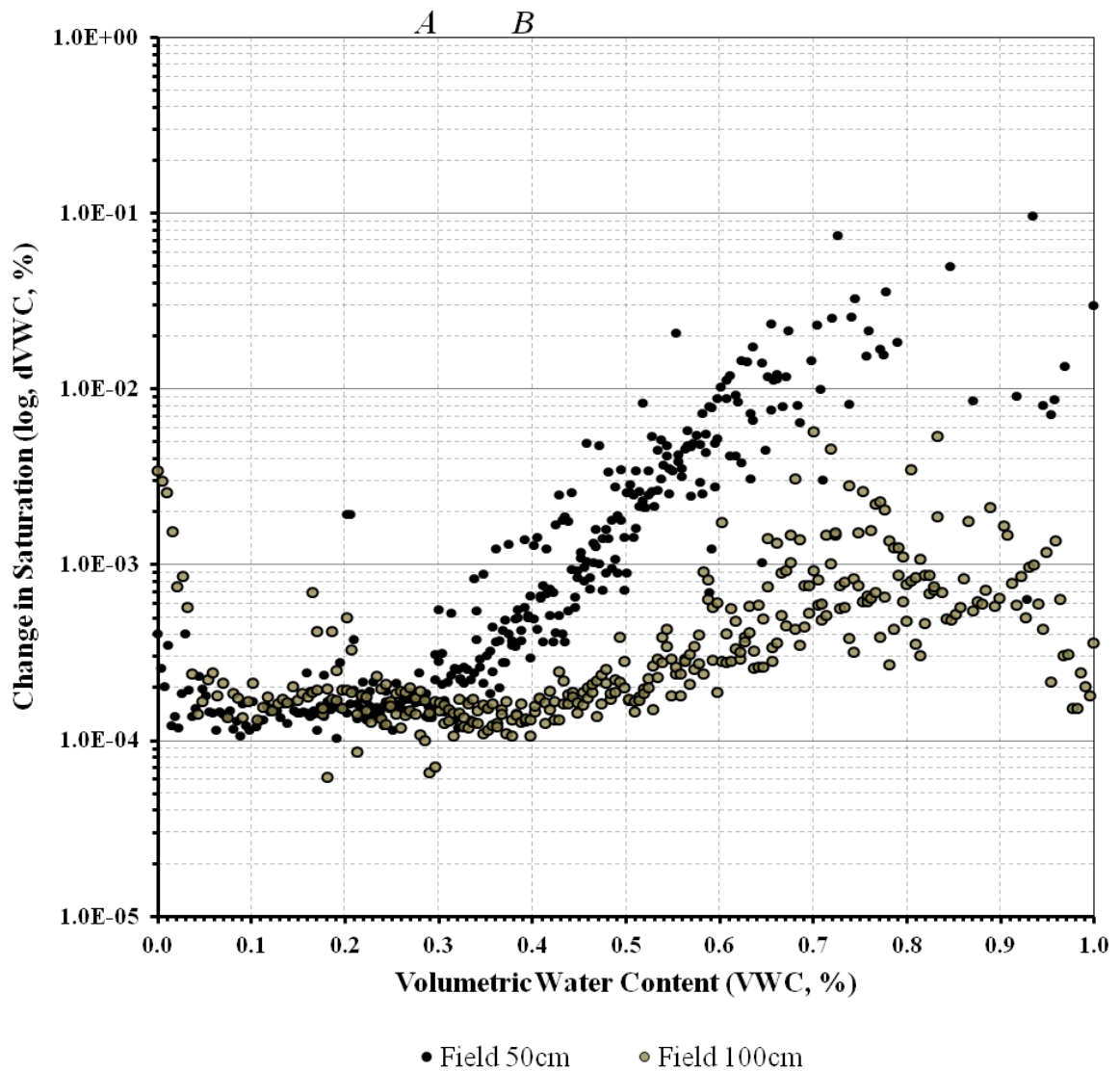


Figure 11. Semi-log plot of the mean change in VWC over a 60 min interval for scaled values of VWC recorded in the soil moisture probes installed in the 'Field' at 100 and 50cm below ground surface from May 2013 to Feb 2014. Inflection points in VWC correspond with point A=0.28, B=0.39. Sample counts Field 50cm n=354; Field 100cm n=337.

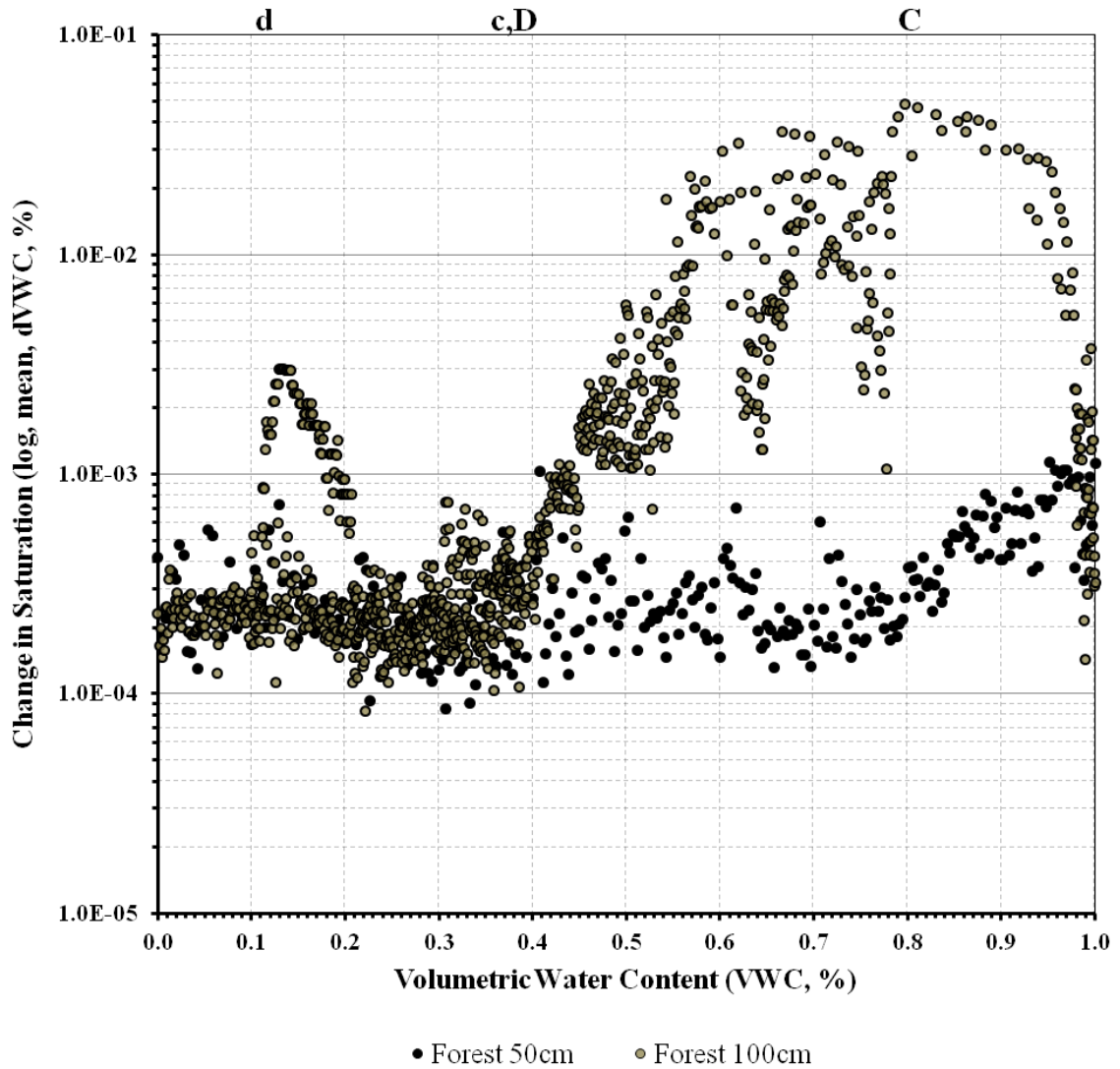


Figure 12. Semi-log plot of the mean change in VWC over a 60 min interval for scaled values of VWC recorded in the soil moisture probes installed in the 'Forest' at 100 and 50cm below ground surface from May 2013 to Feb 2014. Inflection points in VWC correspond with point c=0.35, d=0.11, C=0.80, and D=0.38. Sample counts Forest 50cm n=292; Forest 100cm n=1029.

Point	Scaled VWC %	Measured VWC (mean, %)	Probe
<i>A</i>	28%	0.20	Field 50cm
<i>B</i>	39%	0.17	Field 100cm
<i>c</i>	35%	0.13	Forest 50cm
<i>d</i>	11%	0.14	Forest 100cm
<i>C</i>	80%	0.18	Forest 50cm
<i>D</i>	38%	0.24	Forest 100cm

Figure 13. Table of VWC inflection points for scaled and measured (uncalibrated) values from TDR soil moisture probes and annotation points corresponding to Figure 11. and Figure 12. The average measured VWC of inflection points in each measurement point was ~ 20%.

A graphical inflection point was identified in soil moisture saturated conductivity curves (Figure 10) and tested using a binomial model to simulate above or below threshold values which will be derived from observed field data. Soil moisture data was converted to binomial scale data using a threshold of 20% VWC as a positive indicator of threshold conditions, based on the measured inflection point from variably saturated K curve. Binomial logistic regression was computed using change in MFS-1 well temperature as the dependent variable, and binomial soil saturation from the Feld 100cm sensor as the independent variable. Overall Model fit produced a Chi Square = 2012.3383, df = 1, p = <.00001. Thereby confirming that these data can be modelled as 2 distinct domains (sub- and super-critical).

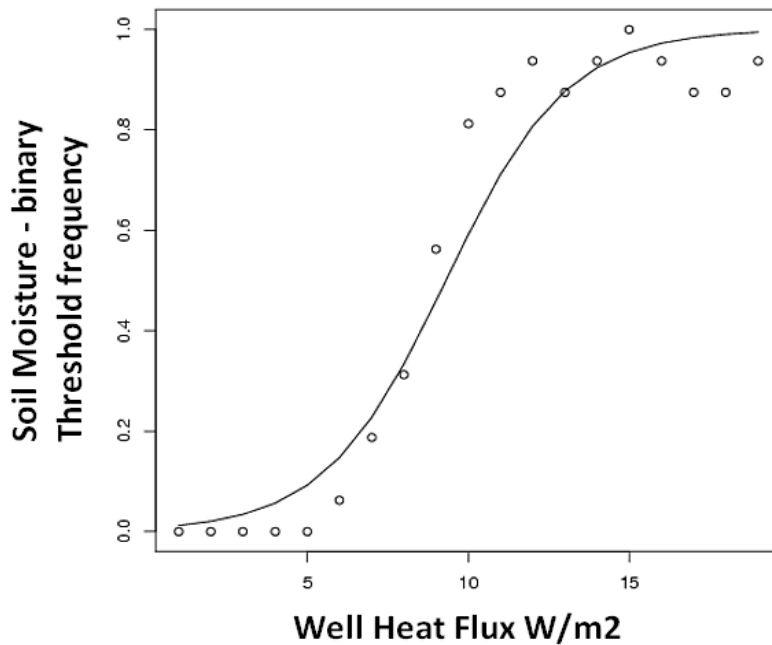


Figure 14. Soil VWC threshold and well heat flux. Soil moisture data was converted to binomial scale data using a threshold of 20% VWC as a positive indicator of threshold conditions, based on the measured inflection point from variably saturated K curve. Binomial Logistic regression was computed using change in well temperature as the dependent variable, and binomial soil saturation as the independent variable. Overall Model fit produced a Chi Square = 2012.3383, df = 1, $p = <.00001$.

Precipitation intensity doesn't show a direct relationship with the rate of change in soil saturation (Figure 15). The rate of change in VWC in the soil, as demonstrated by Hyprop lab results, is dependent upon the antecedent saturation in the soil. Prior to threshold or non-linear changes to occur in the soil, a sufficient volume of precipitation is first required to wet-up the soil to the 19% VWC.

Although soil moisture does not show a direct response to precipitation intensity, stream runoff in Jimmy Nolan Brook demonstrates a distinct non-linear response to the intensity of a precipitation event (figure 15). The blue and red annotation lines in Figure 16 depict the trends in stream runoff above and below the inflection point of 0.2 in/hr. A

distinct shift in the rate of increase of stream runoff occurs during more intense precipitation events, however it is unlikely that this is occurring entirely as overland flow.

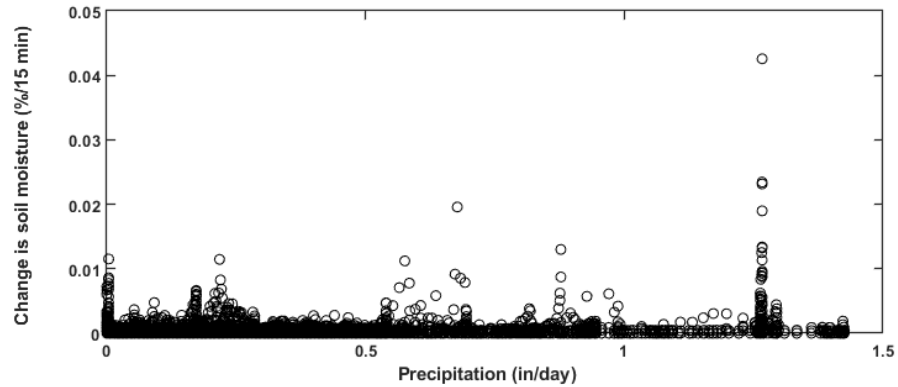


Figure 15. Precipitation Intensity and rate of change in soil VWC (field 50 and 100cm). Precipitation and soil moisture data were collected continuously from May 2013 to February 2014.

Timeseries data of streamflow and soil moisture responses show how threshold or non-linear behaviors look in real time with respect to precipitation intensity and antecedent conditions. In figure 17, a time series of water levels in the glacial till, fractured bedrock, upland forest and field soil moisture, riparian soil moisture, and stream stage are compared to precipitation events occurring in fall 2013. Precipitation events are annotated with dashed lines and letters *a-f*. For example, the precipitation intensity of event *a* is proportional to event *f*, however event *a* shows little or no response in groundwater or soil moisture, while event *f* corresponds with increases in till and bedrock water levels, and all 5 soils horizons. Streamflow appears to be sensitive to each precipitation event and varies non-linearly according to precipitation intensity (Figure 16). Soil moisture measurements in the forest appear to be the least sensitive to precipitation events, and also maintain the lowest VWC of the soil horizons measured. Diurnal fluctuations in VWC cease in the forest 50cm and 100 cm depths after October 7th, which corresponds with leaf drop in the

deciduous maples. In the month following leaf drop, the groundwater table elevation in the fractured bedrock and the forested soil saturation gradually rise due to the decrease in loss through evapotranspiration. The progressive wetting-up of precipitation events *d*, *e*, and *f* show initial increases in the till groundwater levels, streamflow, and shallow field VWC in response to event *d*. Event *e* subsequently triggered responses in the 100cm depth field VWC, an initial response in the riparian soil VWC, and fractured bedrock water table. The connection between the fractured bedrock, riparian zone, and 100cm depth soil horizon in the field is reinforced by the presence of fractured bedrock outcrops both along poplar hill road and in the stream channel. Event *f* triggers a rapid increase in the riparian VWC, and larger saturation increases in the groundwater and soil horizons compared to events *d* and *e*.

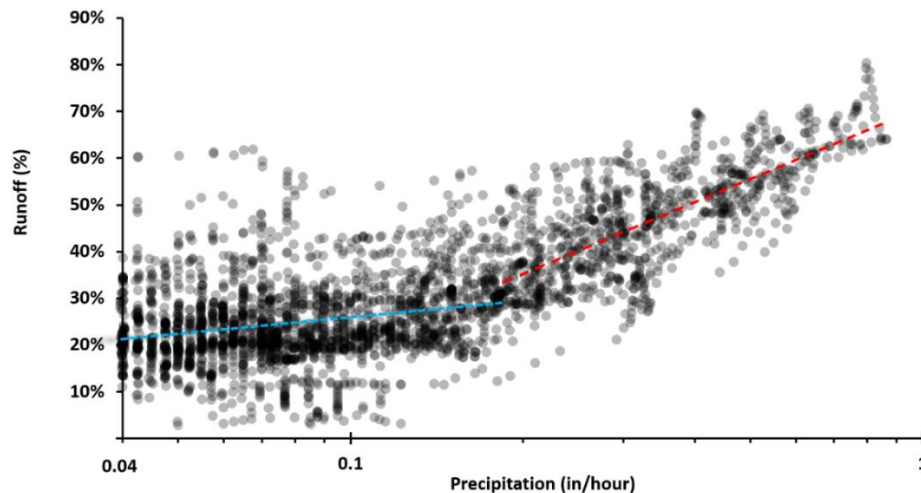


Figure 16. Precipitation intensity (in/hr) and runoff % of total flow in Jimmy Nolan Brook. Stream discharge measurements were collected by the USGS Conte Labs gauge at the confluence of Jimmy Nolan and Westbrook.

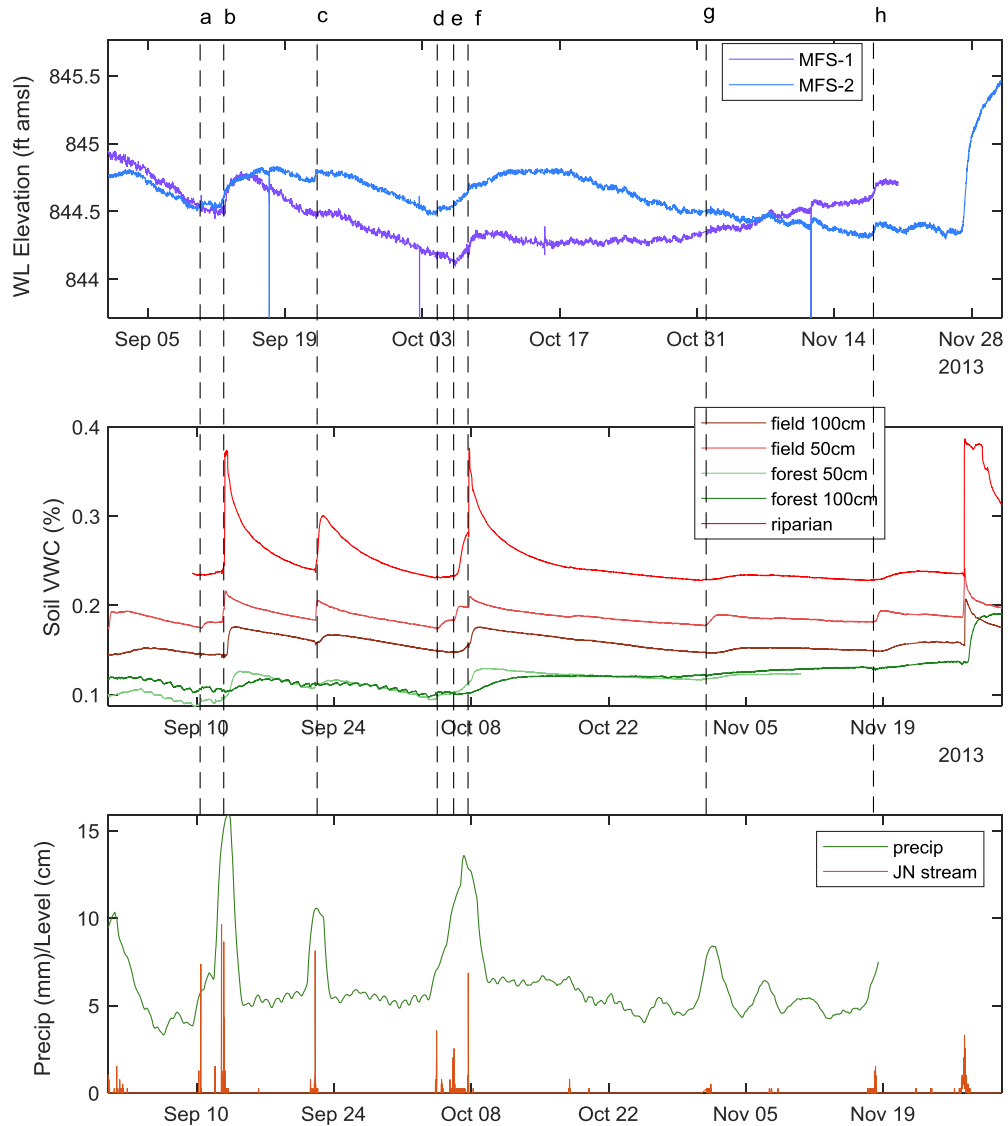


Figure 17. Precipitation events, soil VWC, streamflow, and groundwater potentiometric surface elevations from wells MFS-1 and MFS-1. MIDDLE: Soil VWC measurements from field, forest, and riparian locations. BOTTOM: JN Stream level and precipitation measurements. Dashed lines annotate precipitation events a-h.

Conductivity and streamflow measurements recorded in the larger Westbrook catchment can help identify which the storage reservoirs contribute to the flow regimes of Jimmy Nolan Brook (Figure 18). While investigating threshold behavior within the Jimmy Nolan Brook catchment, fluid flux in glacial till, fractured bedrock, upland soils, and riparian soils show non-linear responses which represent the interaction of precipitation

intensity, antecedent moisture, and geomorphology. The specific conductivity (SpC) of baseflow is generally higher, suggesting that soils and tills have a higher contribution to streamflow during this time: ‘TAP’, ‘MFS 2’, and ‘SMC’ sample locations are located in glacial till. SpC values decrease during peak streamflow events, which is consistent with the SpC values measured in the fractured bedrock storage (‘MFS 1’) and direct precipitation (‘Rain’). This helps simplify the conceptual model of transient advective threshold-controlled recharge and shallow soil water fluxes in the upland soils, hillslope, and riparian areas by showing the progressive contribution of different storage reservoirs to stream discharge.

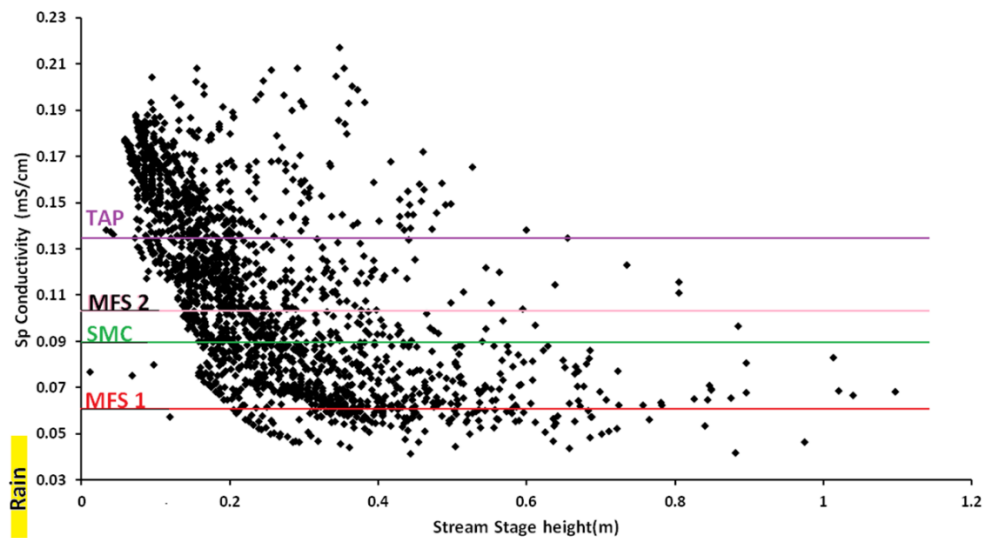


Figure 18. Westbrook stream stage and specific conductivity plotted against average conductivity measurements from groundwater (MFS1, MFS2, and TAP) and the MFS creek (SMC).

Low flows in the watershed correspond with SpC values similar to till and thick post-glacial surficial materials. Whereas high flow values in the catchment elicit SpC values coinciding with those measure in the fractured bedrock and recent precipitation. Due to the low storativity and high hydraulic conductivity of bedrock fractures, it is

coincident that discharge responses to fluid flow in fractured bedrock would be greater than to surficial materials, given a proportional increase in head provided driven by a rainfall/streamflow response event. In summary, these data suggest that stream runoff is directly supplied by the immediate rainfall and fractured bedrock discharge.

4.2 Stable Isotope tracers

Stable Isotopic analysis of field samples capture the annual variability of the Jimmy Nolan Brook catchment from October 2012 to November 2013. The average isotopic compositions are consistent with Climate Zone 3 from the statewide data compiled by Cole, in progress (Figure 19), and samples generally trend along the SMWL (Figure 20).

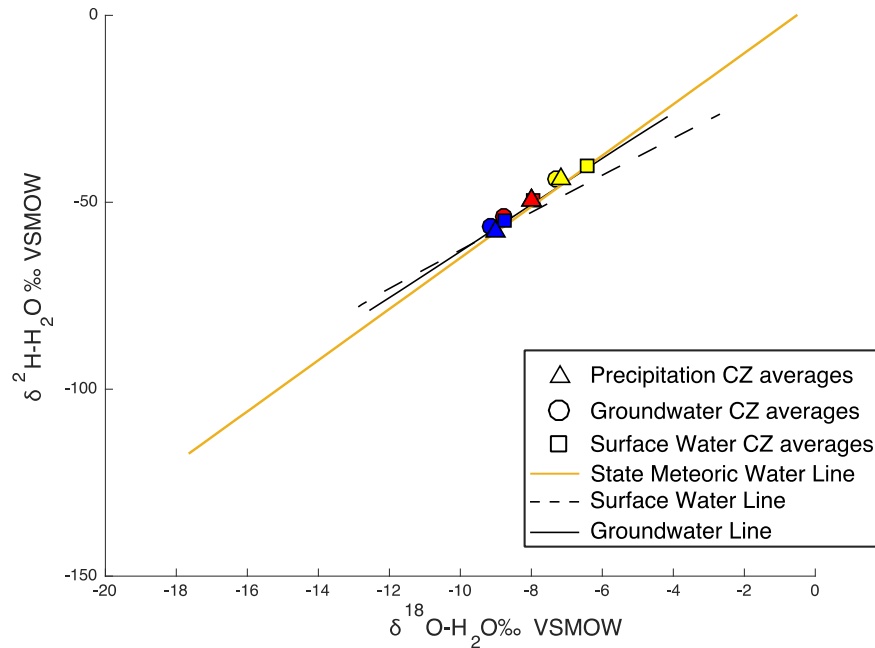


Figure 19. Dual isotope plot comparing the average climate zones of precipitation, surface water, and groundwater. Climate Zone I (CZ I, blue) represents isotope samples collected from west of the Connecticut River in MA, CZ 2 (red) represents samples collected in central MA, and CZ 3 (yellow) represents samples collected from eastern and coastal areas in MA. The State Meteoric Water Line (SMWL, n=399), Surface Water Line (n=1917), and Groundwater Line (n=1405) represent trend lines for all 3 climate zones (Cole, A. in progress).

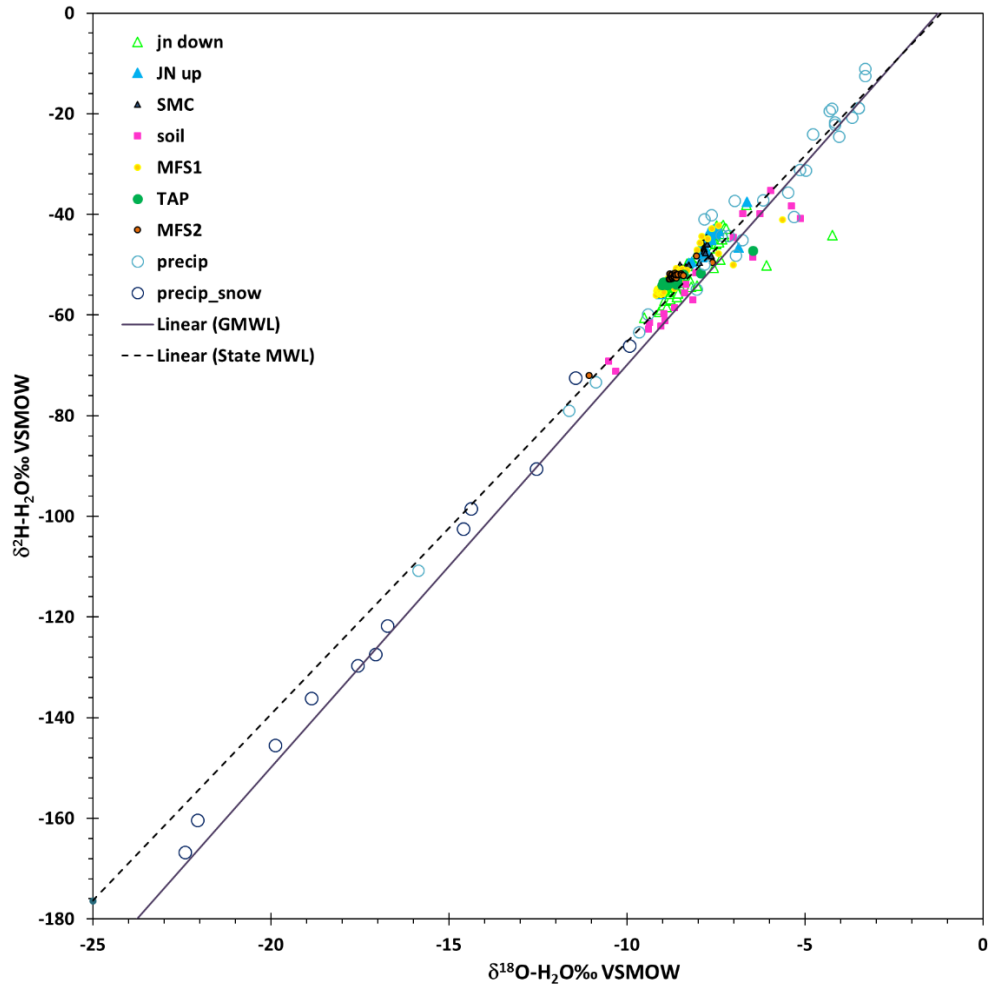


Figure 20. Stable Isotopic composition of surface water, groundwater, soil pore water, and precipitation from the Jimmy Nolan Brook catchment plotted against the GMWL and SMWL (SMWL from Cole, in progress).

The variability in the isotopic enrichment of samples from MFS illustrate travel times for recharge and discharge paths within the catchment. The standard deviations of $\delta^2\text{H}$ and $\delta^{18}\text{O}$ decrease as mean residence time (MRT) increases. Hudson 2016 used geochemical data to estimate the MRT of MFS-1 to be 0.7 years and MFS-2 to be greater than five years. This difference in residence times was attributed to the low hydraulic conductivity of the till aquifer surrounding the MFS-2 and TAP wells, which increased the time for mixing to occur within the system. This can be seen in Figure 21 where the standard deviation of stable isotope values decreases in groundwater samples, with the

deep till (TAP) aquifer showing the least amount of variation and therefore, it can be inferred, the longest MRT. Upstream JN Brook has the second lowest variability and is lower than the other groundwater samples. This may be due to the location of MF1 and MFS2 in upland areas with exposure to outcropping fractured bedrock and thin soil/till cover, while JN upstream sample location is at a discharge point in the catchment, representing the longest flowpaths in the system. SMC creek appears very similar to MFS1 and MFS2 and is likely fed by the same groundwater sources.

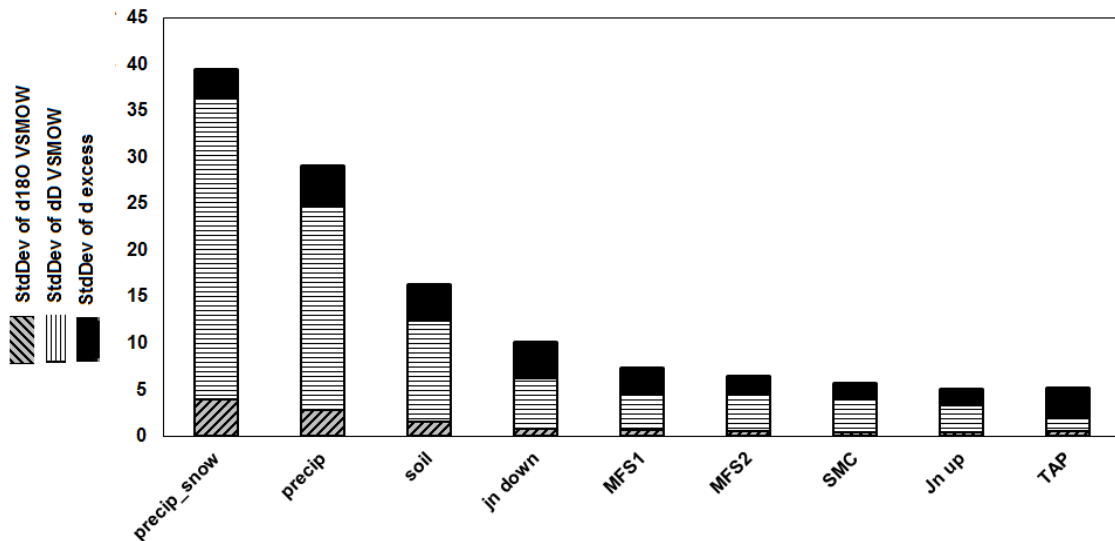


Figure 21. Stable isotope standard deviation of $\delta^{18}\text{O}$, $\delta^2\text{H}$, and deuterium excess for precipitation, groundwater, surface water, and soil porewater at MFS from 2012-2013.

Soil moisture ('soil') and the downstream Jimmy Nolan brook stream samples ('jn down') show higher variability than 'SMC' and 'Jn up' suggesting that the downstream reaches of JN receive direct input from relatively unmixed precipitation and soil water inputs. The low deviation of values recorded in 'Jn up' supports the idea that the headwater area of the catchment receives isotopically well-mixed water from groundwater storage in the glacial till reservoirs. SpC measurements in Figure 18 also

support this as the average conductivity from the thickest till unit corresponds the closest to the baseflow SpC of the stream. Higher standard deviation of deuterium excess in the ‘TAP’ samples indicates that the lower till units are recharged from a greater range of seasonal precipitation. Similarly, well-mixed isotopic signatures can be found in SMC, which is perched in the till. Well-mixed and low-evaporative signature isotope data are observed in both SMC and JN up, which is also characteristic of groundwater recharged in late fall and early spring (Figure 20). Although upstream JN has more enriched isotopic signature compared to groundwater and SMC, all 3 can be plotted along the same rough trendline. Soil and downstream JN show an increased isotopic variation (Figure 21) suggesting that they receive more direct inputs from precipitation events and are somewhat unbuffered from longer residence time mixing processes.

Fractured bedrock isotopes have the highest variance of the 3 wells sampled (Figure 21), this is likely due to threshold-recharge perturbations where precipitation events access fracture networks in shallow outcrops and thin soil or till cover. Isotopic signatures in the deep till represent the mean groundwater isotopic values, however the standard deviation of TAP and MFS-2 is comparable. The fractured bedrock/MFS-1 values within the black circle on Figure 22 show more depleted grouping of samples (Figure 22) corresponding with recharge from snow and a spread of samples higher deuterium excess isotopic enrichment corresponding with humid spring rain events (Figure 23). This supports the conclusion that groundwater in both fractured bedrock and till appear to recharge during the late winter and early spring months.

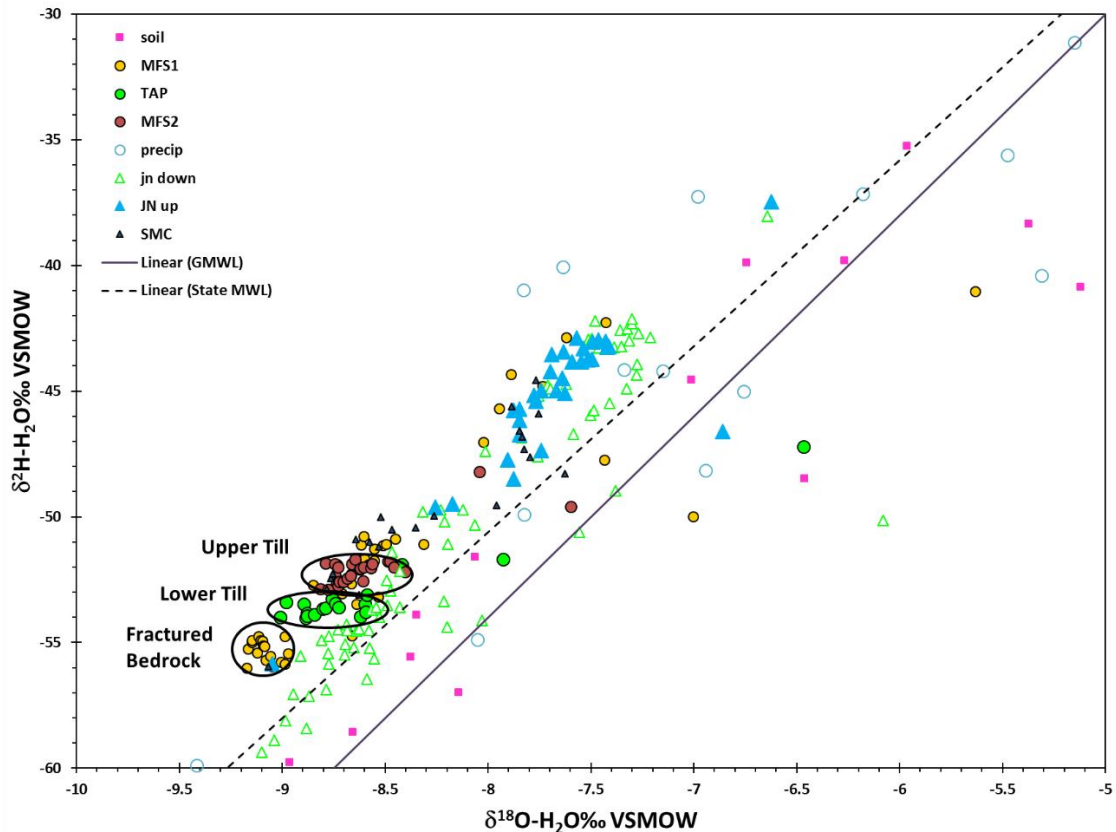


Figure 22. Scaled graph of Stable Isotopic composition of surface water, groundwater, soil pore water, and precipitation from the Jimmy Nolan Brook catchment plotted against the GMWL and SMWL (SMWL from Cole, in progress). Sample clusters from fractured bedrock (MFS1), lower till (>10m bgs, TAP), and upper till (0-10m bgs, MFS2) are outlined in black.

The isotopic composition of precipitation in Jimmy Nolan Brook catchment varies by over 170 ‰ δ^2H and 20 ‰ $\delta^{18}O$ (Figure 20). The average non-weighted monthly δ^2H -H₂O and $\delta^{18}O$ -H₂O values for precipitation samples collected at the MFS are shown in Figure 23. Precipitation falling as rain in late summer to early fall shows the most isotopically-enriched values and lowest variability. Precipitation falling as snow and rain in late winter and spring appears the most isotopically-depleted and has the highest variability. Precipitation at the site falls slightly above the GMWL and is consistent with the SMWL (Figure 23), with the greatest offset occurring during the winter months where

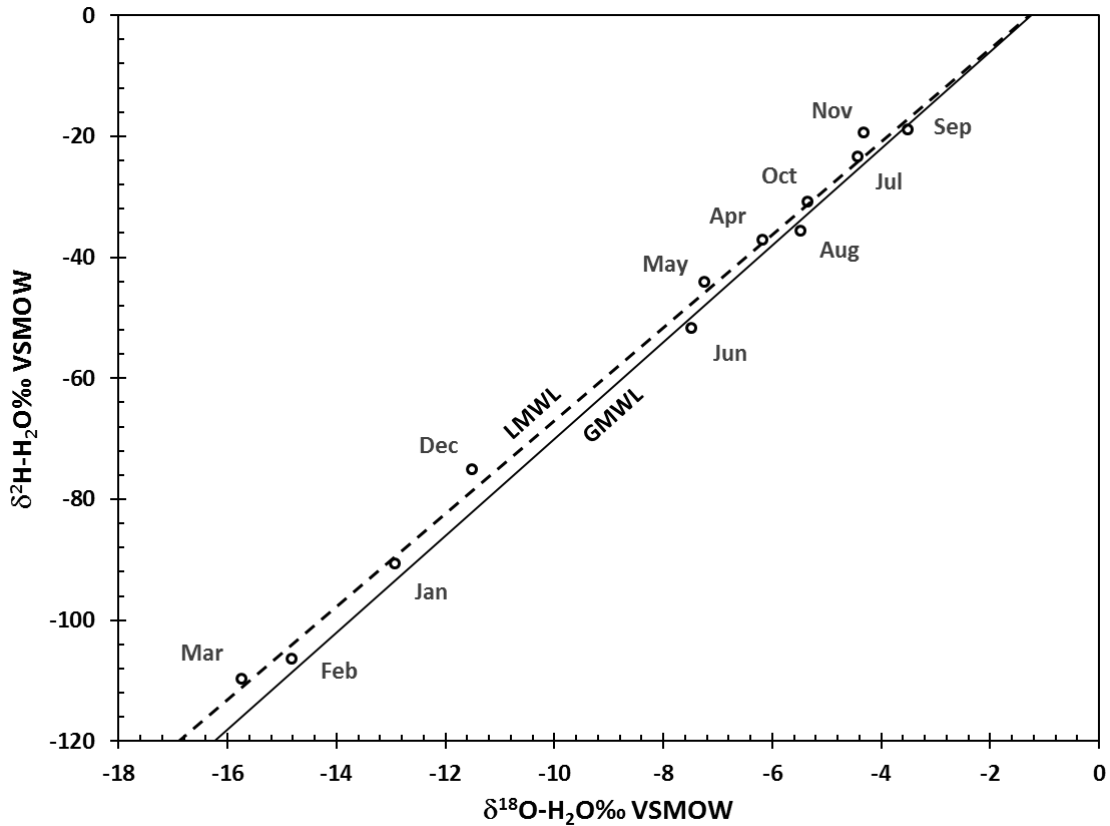


Figure 23. Monthly averages of the stable-isotopic composition of precipitation from the Jimmy Nolan Brook Catchment. Non-weighted values were used to compute the simple means for monthly bins of $\delta^{18}\text{O}$, $\delta^2\text{H}$.

precipitation is sourced from a more arid landmass. Summer months of June, July, and August show the highest evaporative offset due to the increased thermal input during that time. The annual distribution of isotopic signatures helps explain how spring streamflow during episodic snowmelt could contribute to greater isotopic variability in downstream vs. upstream JN. The isotopic signatures of precipitation, soil, streams, and groundwater are most stable in the early fall months and therefore don't provide contrast to distinguish specific threshold recharge and discharge events during the study period.

Seasonal trends in the isotopic composition of precipitation, stream, and groundwater samples for $\delta^{18}\text{O-H}_2\text{O}$, $\delta^2\text{H-H}_2\text{O}$, and deuterium excess are shown in Figures

25, 26, and 27 (respectively). Groundwater samples show the least response to seasonal precipitation input, whereas stream water shows a muted or buffered response to precipitation throughout the year. Deuterium excess values in stream samples show the most enrichment during the summer months when surface waters experience the most evaporation. It is likely that during the summer time water from standing bodies contributes to both groundwater recharge and stream discharge.

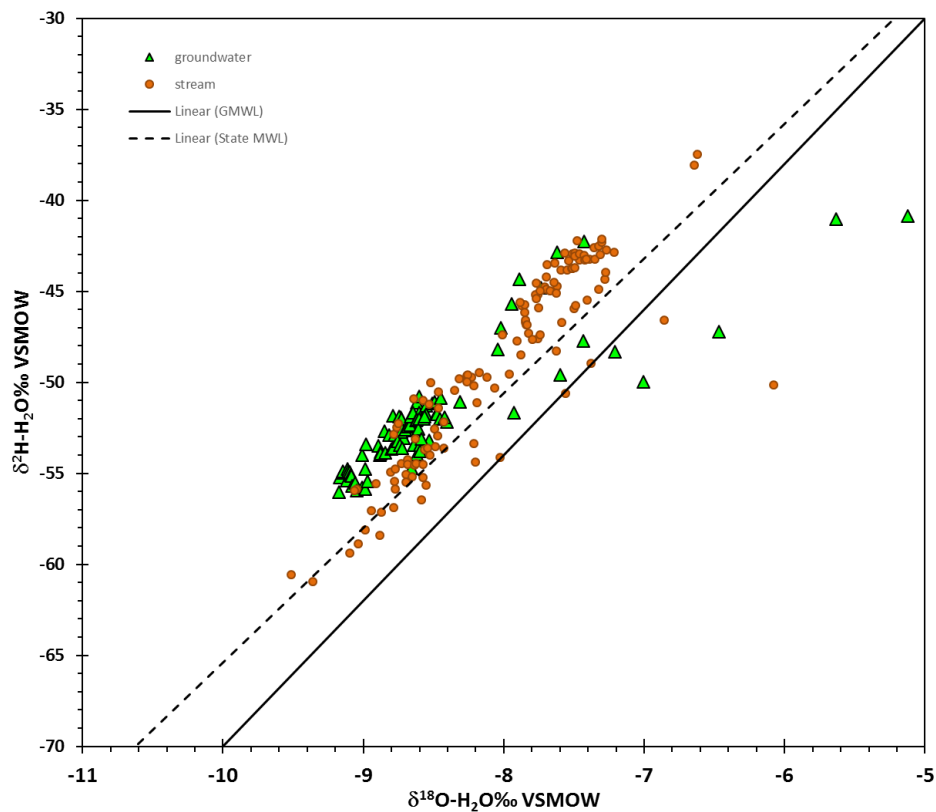


Figure 24. Stable Isotope composition of samples collected from streams and groundwater in the Jimmy Nolan Brook Catchment plotted against the GMWL and SMWL (SMWL from Cole, in progress).

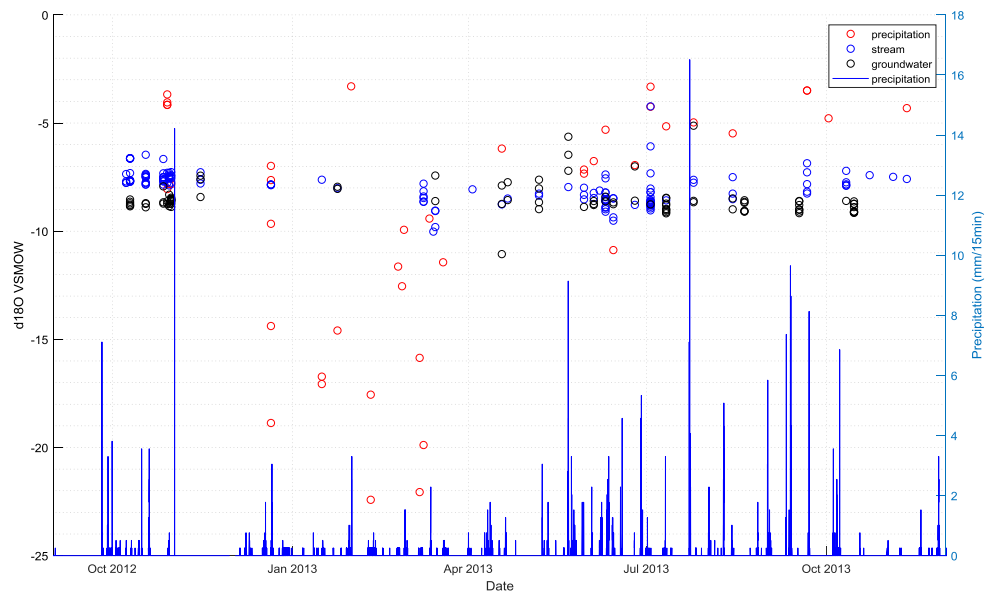


Figure 25. Time series of precipitation and $\delta^{18}\text{O}$ samples of precipitation, stream, and groundwater in the Jimmy Nolan Brook Catchment. Precipitation sample collected during snowfall are plotted as the snow-water equivalent.

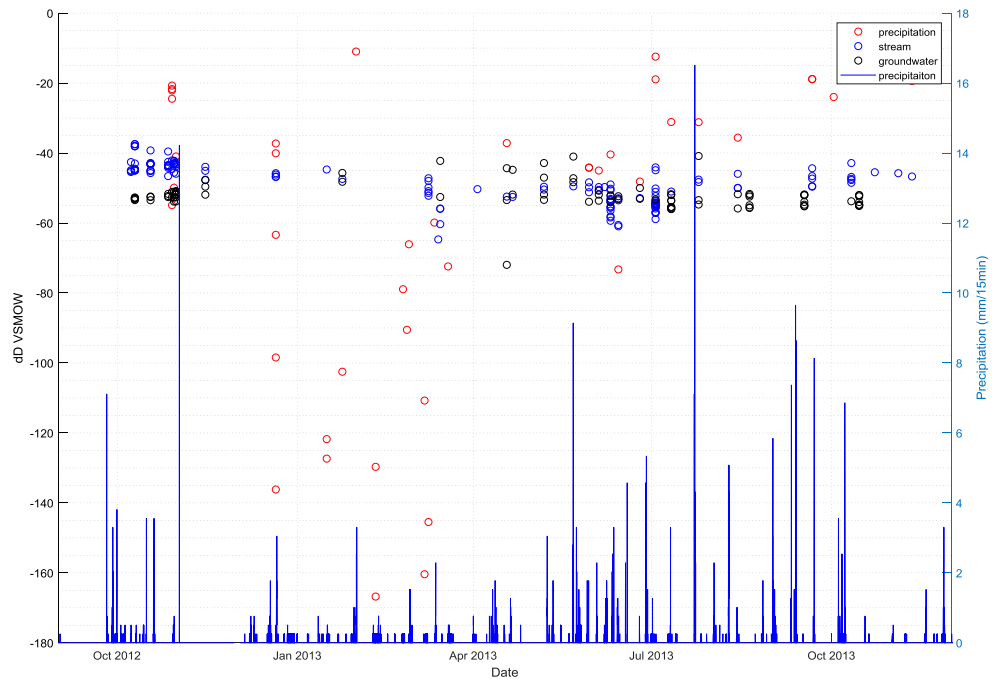


Figure 26. Time series of precipitation and $\delta^2\text{H}$ samples from precipitation, stream, and groundwater in the Jimmy Nolan Brook Catchment. Precipitation sample collected during snowfall are plotted as the snow-water equivalent.

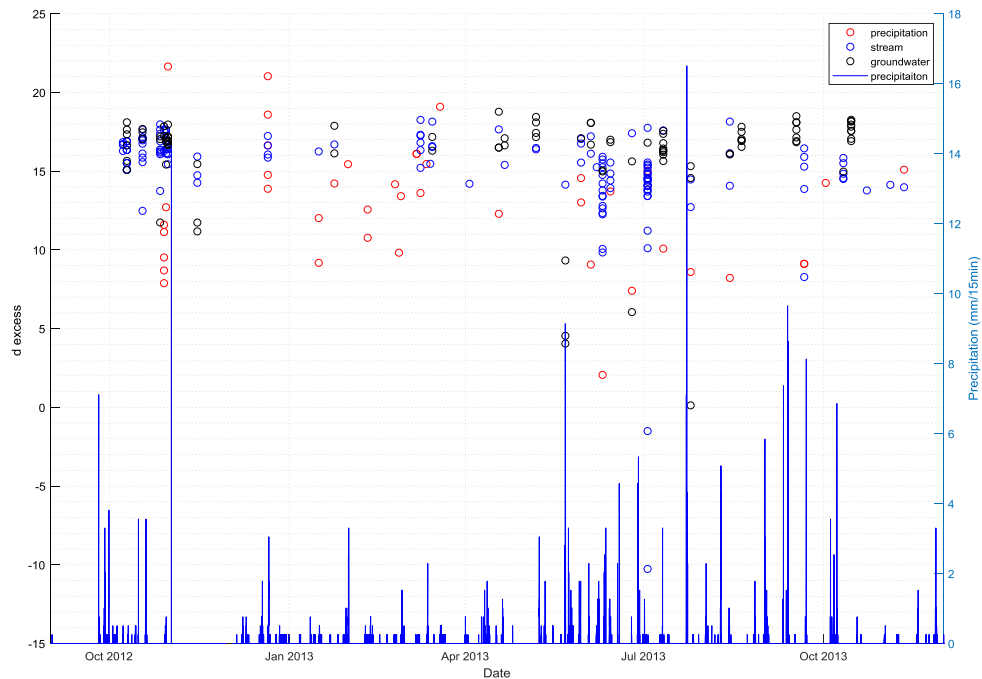


Figure 27. Time series of precipitation and deuterium excess samples of precipitation, stream, and groundwater in the Jimmy Nolan Brook Catchment. Precipitation sample collected during snowfall are plotted as the snow-water equivalent.

The standard deviation, regional isotopic trends, and sample distribution support the conceptual model of late winter and early spring recharge to fractured bedrock, increased MRT and mixing of waters recharged to deeper till aquifers, and the headwater discharge of water with the longest MRT to upstream JN and support baseflow during the summer months. Precipitation events more immediately impact the downstream catchment, where the culmination of a greater variety of flowpaths and transport mechanisms transmit water to the stream from soil, till, bedrock, and runoff.

4.3 DTS temperature distribution in JN

The distribution of temperature in upstream Jimmy Nolan was characterized using continuous distributed temperature measurement at 0.25m intervals. The spatial and temporal variation in stream temperature help to distinguish the location and behavior of discrete groundwater inputs or seeps. Figure 28 provides a general temperature profile of the full DTS cable deployment and Figure 29 shows the reference distances on a map. The DTS cable starts in an upland area at the MacLeish Field Station Observatory, continues through the SMC creek, and continues downhill to the headwater section of Jimmy Nolan Brook. The upstream section of JN is referenced in 3 sections: the west fork, east fork, and southern fork or confluence. The upland areas record ground surface temperatures exposed to air and varying amounts of shade. The cable deployment in the upland SMC creek adjacent to the field station was exposed to air frequently as water levels didn't stay high enough to cover the cable. Both the upland areas and SMC creek were not evaluated for the purpose of this study.

Seep locations were initially identified based on the mean and variance at distances along the cable in upstream JN (Figure 30). Cable distances from 1000-1800m are shown during the period of November 13th to 26th where mean air and stream temperature is colder than groundwater. Seep locations appear as relatively warmer points with lower variance as the groundwater input provides a buffer from air temperature oscillations and dampens the diurnal fluctuations. Corresponding cable distances are georeferenced in figure 29 for reference. The mean and standard deviation of temperatures along the cable are mapped by in Figures 31 through 35, locations are colored by temperature (see legend) and scaled by standard deviation (larger dot equals a proportionally larger standard deviation).

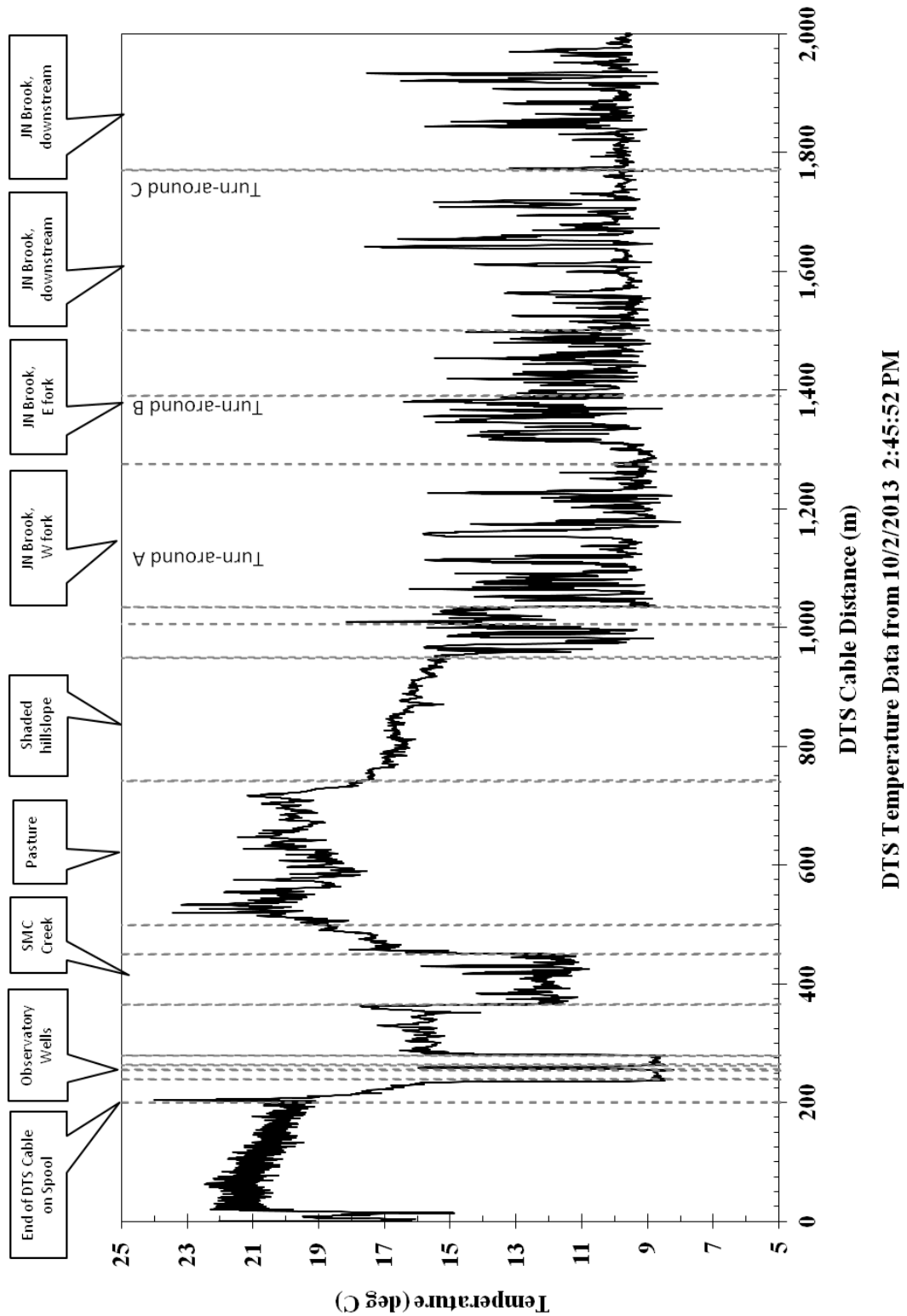


Figure 28. Annotated temperature profile of the full DTS cable deployment at the MacLeish Field Station and upstream Jimmy Nolan Brook. The beginning of the cable (0m) starts at the MFS observatory and the cable ends in stream valley below the field station.

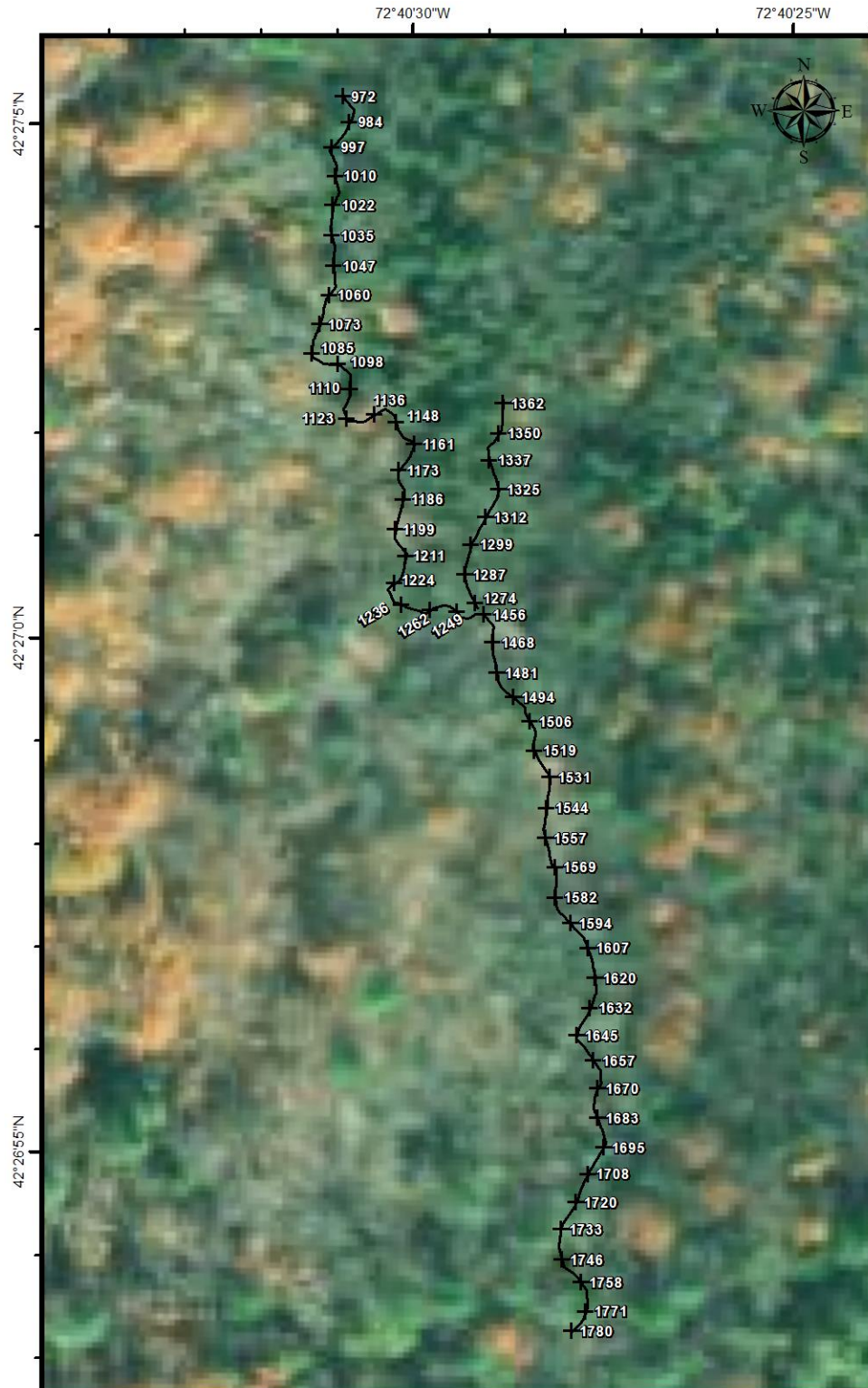


Figure 29. DTS Cable distances (meters) in upstream Jimmy Nolan. Overlapping sections of cable are now shown

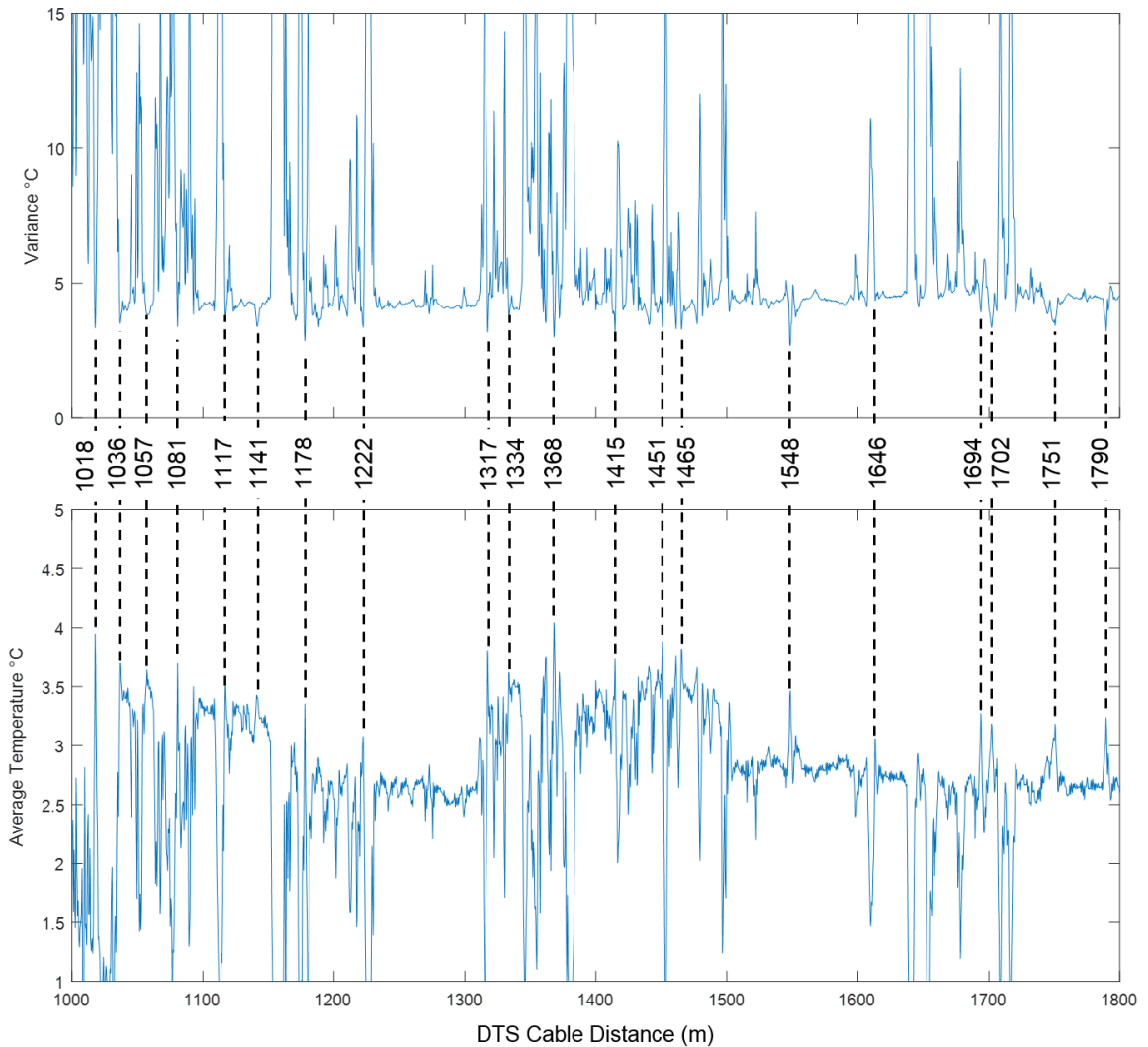


Figure 30. Mean and standard deviation of DTS temperatures along cable distances 1000-1800m from Nov 13th to Nov 26th 2013. Dashed lines are labelled with cable distances and indicate areas with relatively higher average temperatures and low standard deviation

The average DTS cable temperatures for the study period (Figure 31, September 22nd to November 26th) show areas immediately downstream of certain seep locations identified in Figure 30 maintaining warmer temperatures which are closer to groundwater than average values for the stream; specifically at cable distances 1036m, 1048m, 1081m,

and 1117m in the west fork; 1368m, 1334m , and 1317m in the east fork; 1451m and 1465m in the southern fork.

In Figure 32 (September 25th to 30th) the seeps identified in Figure 30 track average stream temperature fluctuations and oscillate above and below groundwater temperature in MFS-2 (11.8 deg C). The upstream section of the west fork shows higher temperature variation with averages closer to MFS-2 and riparian soil moisture temperatures. The southern section shows relatively uniform average temperatures without evidence of warmer seep locations, suggesting that seeps in that area are not active, or the temperature difference is masked due to the similarity of the means of stream and groundwater temperature.

Periodic precipitation and overcast skies from October 5th to 7th (Figure 33) correspond with a decrease in the range of stream temperatures. Seep locations consistently stay at the same values as upslope groundwater in MFS-2. Blue points on the map are consistent with upslope groundwater temperature (11.8 deg C), and orange points are consistent with riparian groundwater temperatures (14.1 deg C). The dark blue points north of the junction of the E and W branch are consistent with bedrock outcrops with shallow (1-3 ft) overburden, and could be areas where water is directly entering the system through bedrock fractures. Leaf drop in western Massachusetts typically occurs around these dates. Upslope and riparian groundwater is within the range of stream temperature in Figure 34 and seeps locations are hard to distinguish during the transition to colder late-fall weather (October 17th-20th). Figure 35 shows mean DTS stream temperature from November 15th to 17th. Mean stream temperatures are colder than groundwater and seeps appear as warmer locations. The furthest upstream sections show higher average temperatures and lower

standard deviations. Higher standard deviation areas show colder average temperatures, perhaps pools with less circulation. Sections of cable exposed to air above the stream show colder temperatures and higher deviations.

DTS stream temperatures, precipitation, soil moisture, stream stage, and groundwater temperatures are plotted vs time in Figures 36 and 37. Figure 37 shows the time series of seep locations identified in Figure 29. Precipitation events occur periodically from October 5th to 7th, soil moisture gradually increases until the last and most intense precipitation occurs on the 7th where a non-linear threshold response occurs in the upland and riparian soil saturation levels. Once this occurs, the intermittent seep located at 1018m begins higher amplitude diurnal temperature fluctuations, suggesting that it becomes disconnected from groundwater after this event.

The east fork of JN and upstream portion of the west fork show average temperature more consistent with groundwater. Overburden in these areas is thicker and potentially provides a more diffuse distribution of the groundwater flow from underlying fracture bedrock. These parts of the stream are mapped with less underlying surficial alluvium compared to downstream sections (Stone and Cohen, 2010). Alluvial sands and gravels effectively disperse point-source seeps of groundwater as can be seen from 1450m to 1600m where alluvial sands form the streambed. Bedrock outcrops scattered throughout the confluence and the west fork create transitional zones between the overburden and underlying bedrock where active fracture flowpaths contribute more discrete groundwater inputs. The ideal seasonal temperatures for observing discrete seep locations occur when average stream temperature is below groundwater temperature and flow is low enough so that mixing in the stream channel does not mask the location of

discrete seeps. Similarly, large threshold events can fully saturate the vadose zone and potentially mix discrete flowpaths from fractures or macropores before those paths intersect the stream.

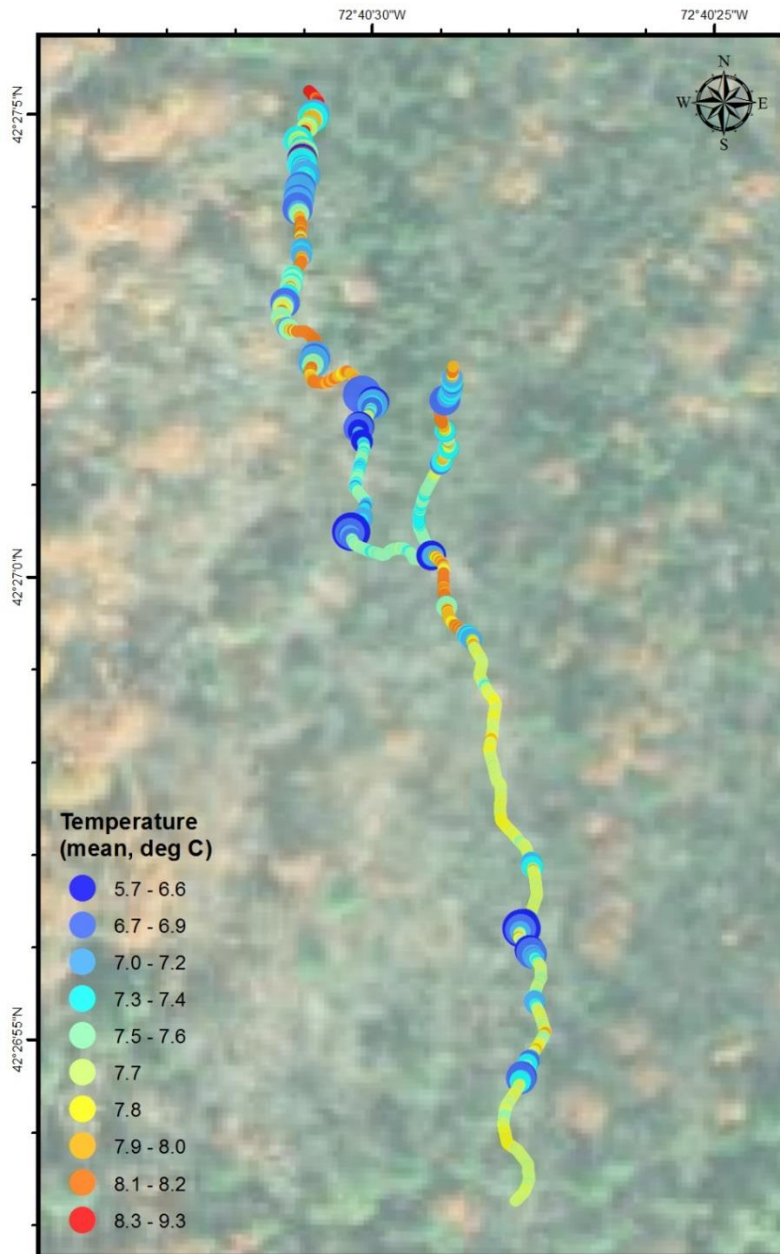


Figure 31. Mean calibrated DTS temperatures recorded at 0.25m intervals along JN brook from September 22 - November 26th. Measurement locations are colored by temperature (see legend) and scaled by standard deviation (larger dot equals a proportionally larger standard deviation).

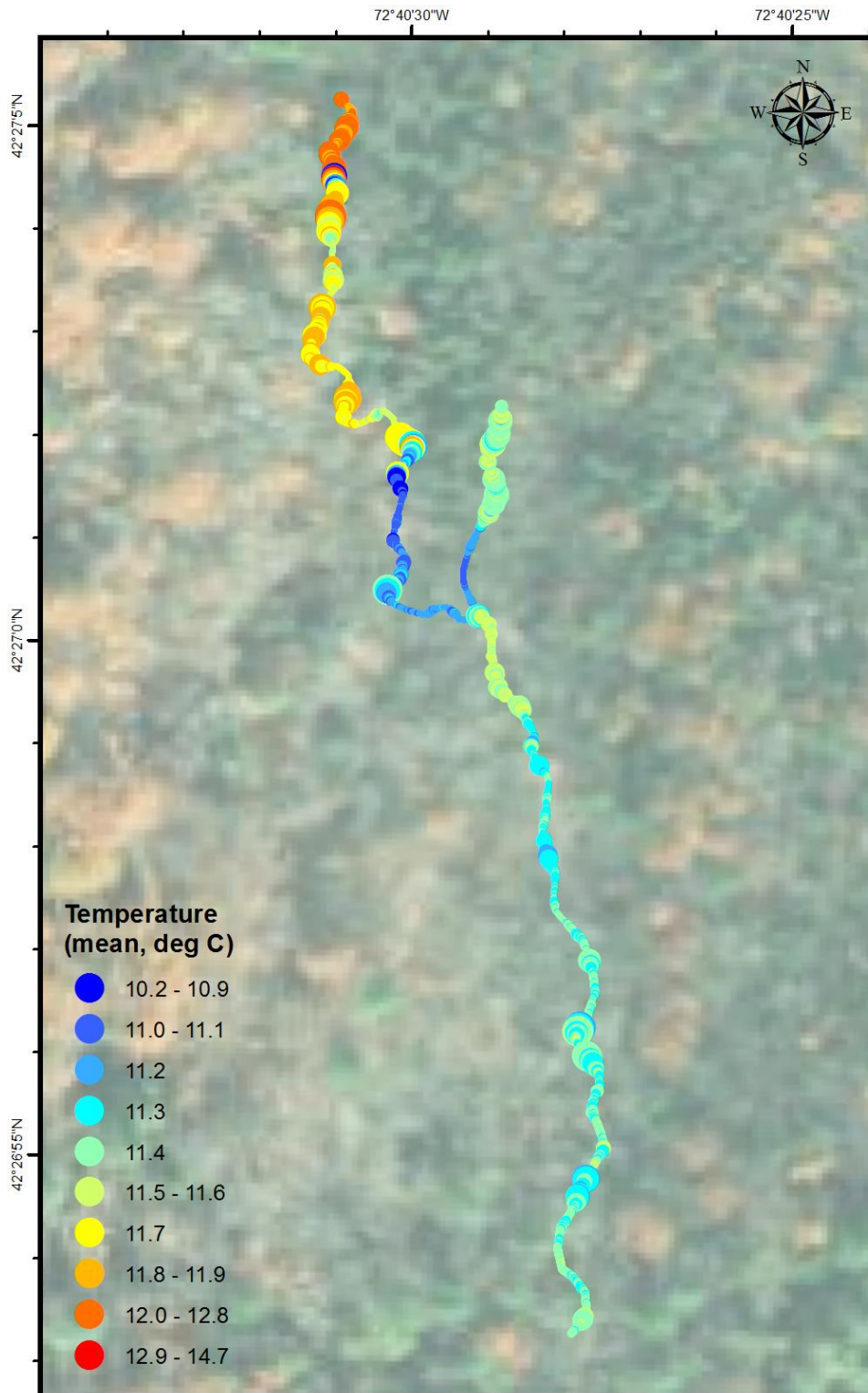


Figure 32. Mean calibrated DTS temperatures recorded at 0.25m intervals along JN brook from September 25-30. Measurement locations are colored by temperature (see legend) and scaled by standard deviation (larger dot equals a proportionally larger standard deviation).

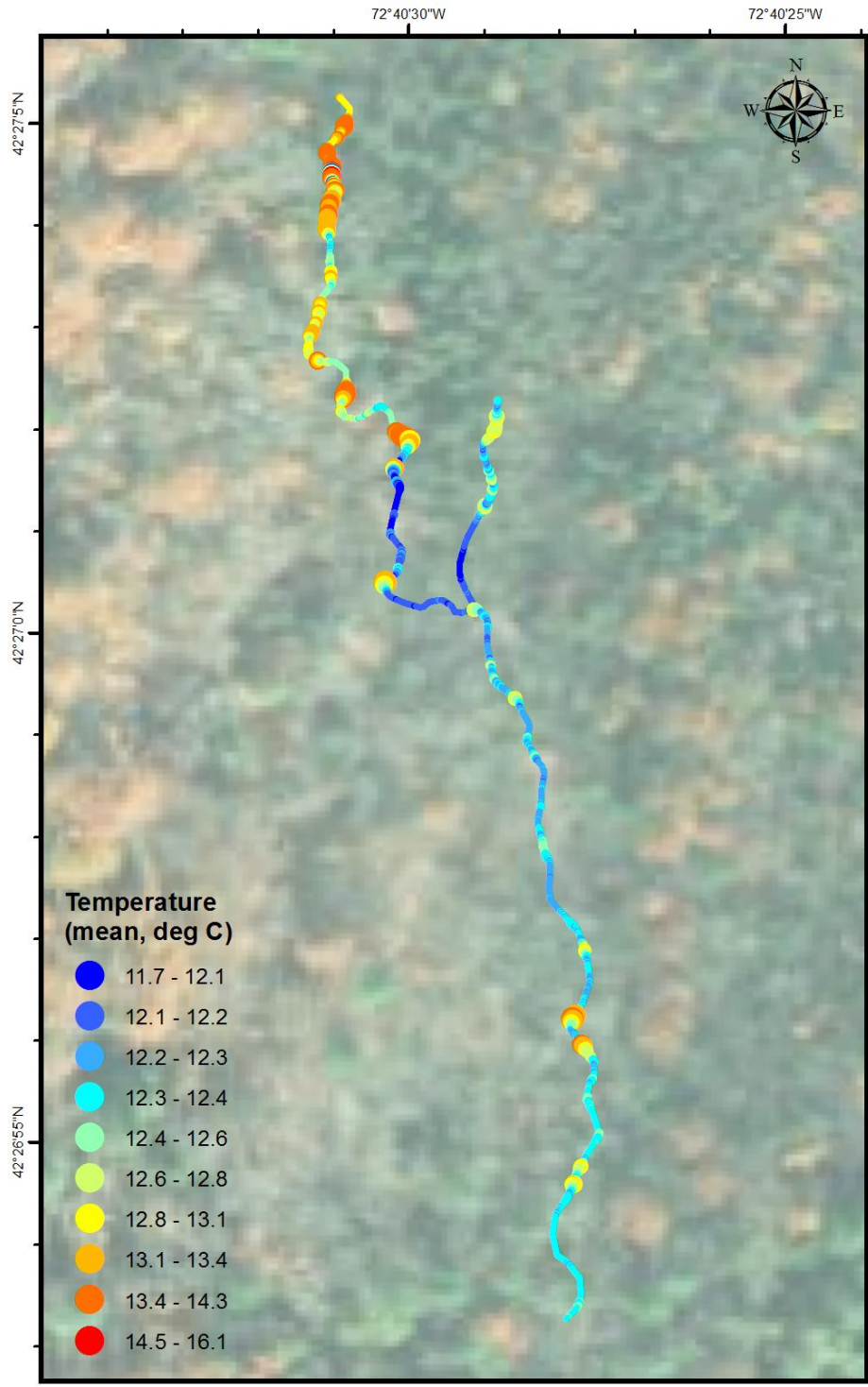


Figure 33. Mean calibrated DTS temperatures recorded at 0.25m intervals along JN brook from October 5-7. Measurement locations are colored by temperature (see legend) and scaled by standard deviation (larger dot equals a proportionally larger standard deviation).

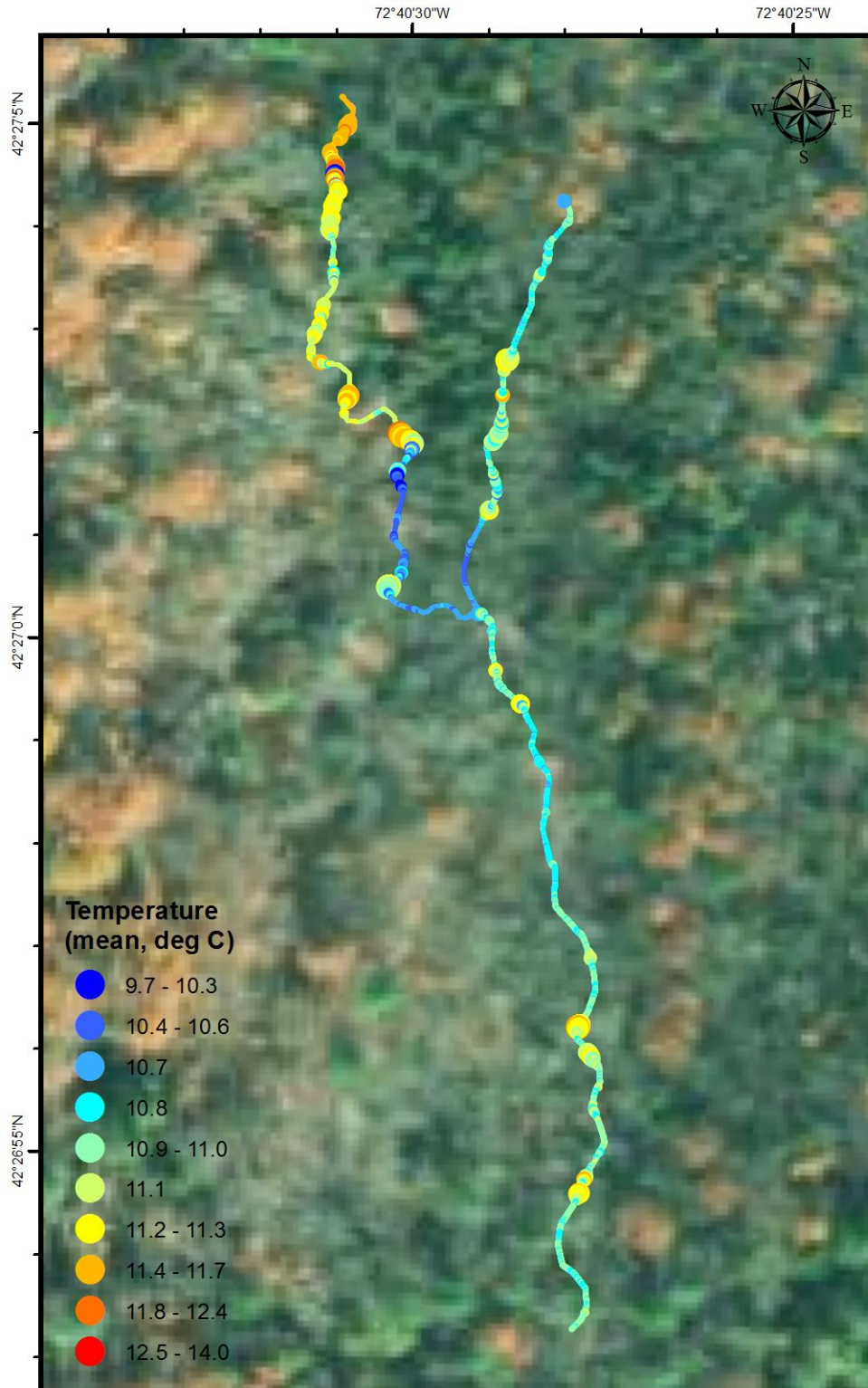


Figure 34. Mean calibrated DTS temperatures recorded at 0.25m intervals along JN brook from October 17-20. Measurement locations are colored by temperature (see legend) and scaled by standard deviation (larger dot equals a proportionally larger standard deviation).

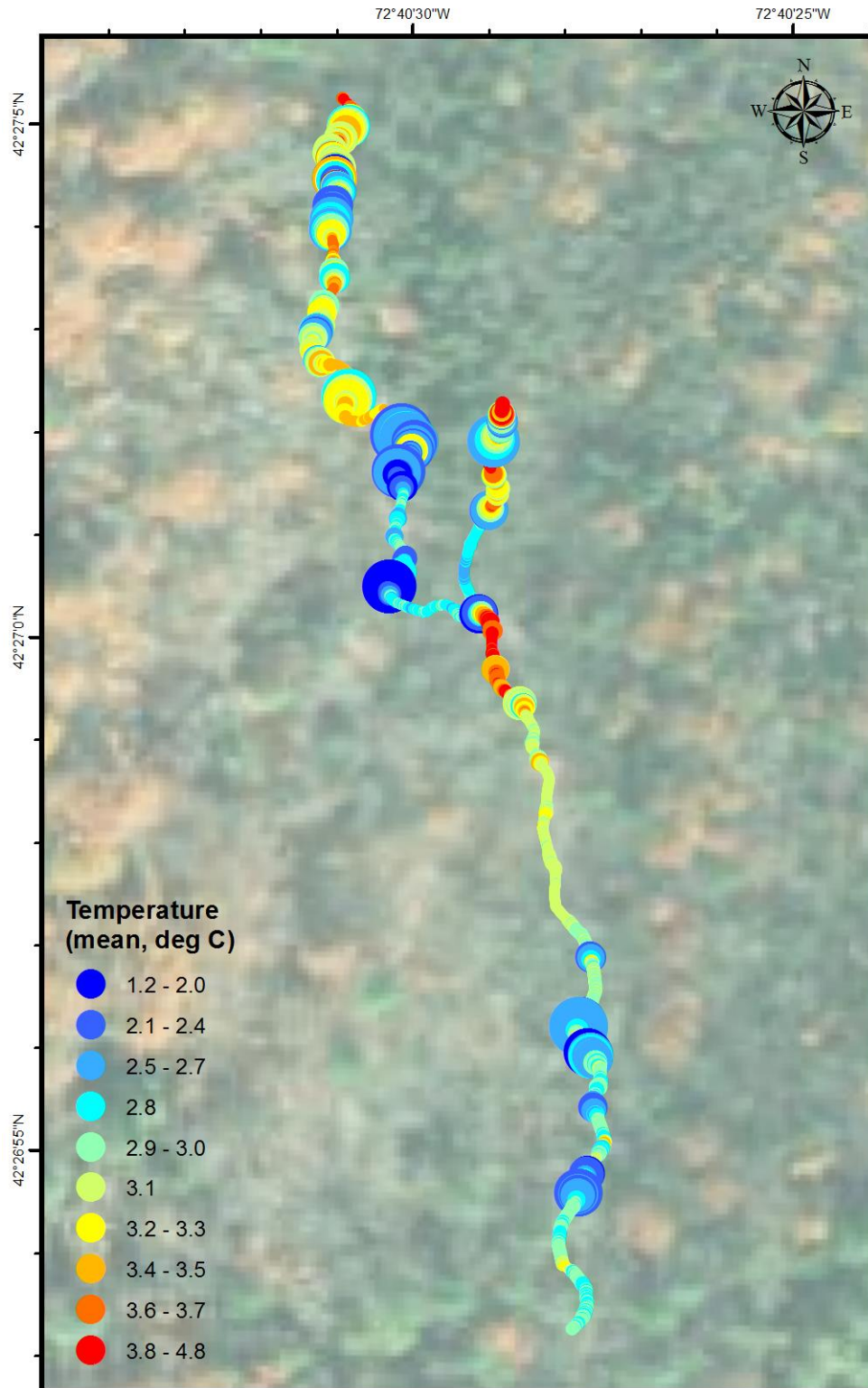


Figure 35. Mean calibrated DTS temperatures recorded at 0.25m intervals along JN brook from November 15-17. Measurement locations are colored by temperature (see legend) and scaled by standard deviation (larger dot equals a proportionally larger standard deviation).

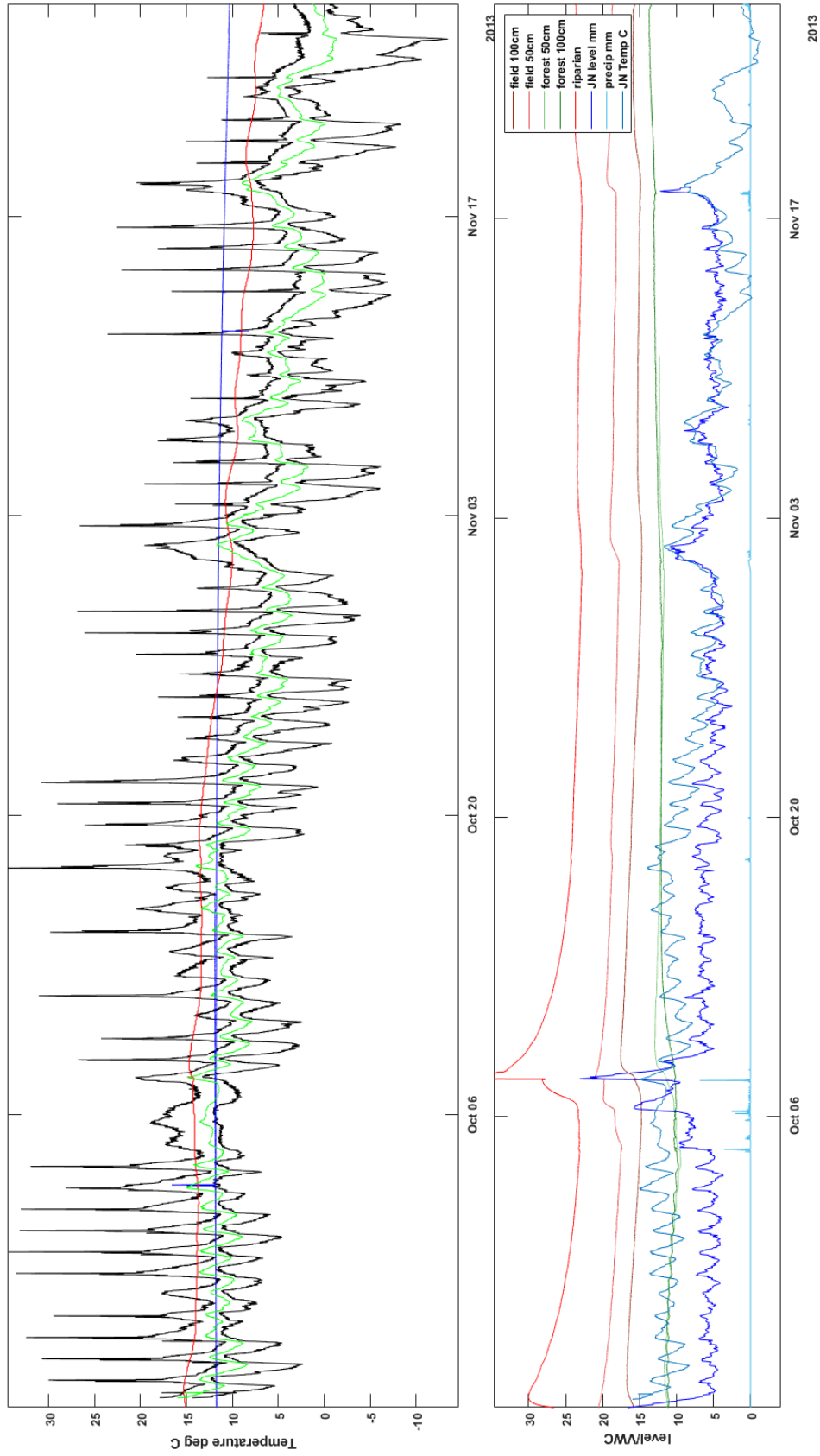


Figure 36. TOP: DTS temperature minimum (black) and maximum (green) in upstream JN over time. Blue lines indicate groundwater temperature in MFS-2. Saturated Riparian soil temperature (Red). BOTTOM: Soil moisture, precipitation, and stream stage.

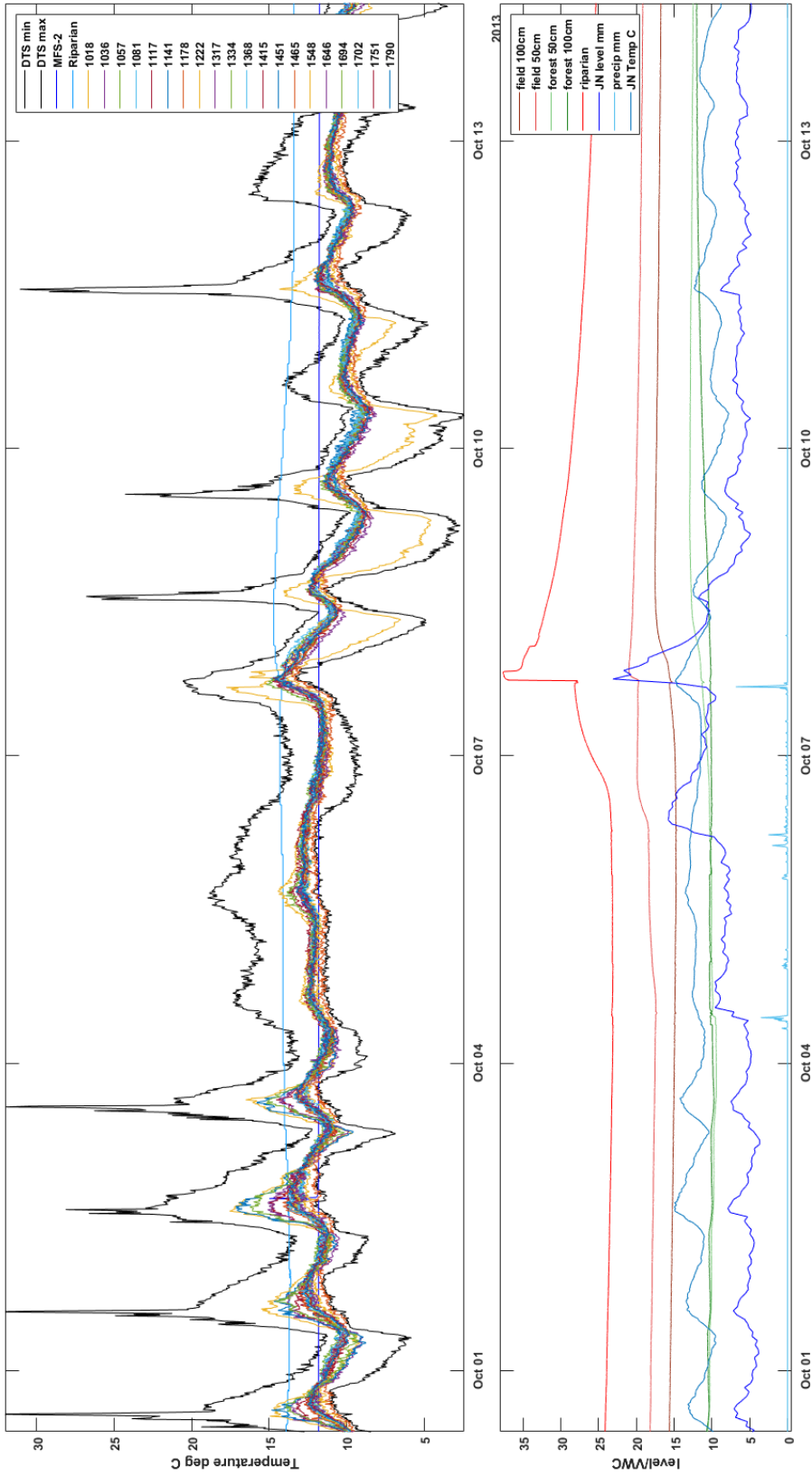


Figure 37. TOP: DTS seep locations from Figure 29 listed by cable distance, DTS temperature minimum (black), maximum (black), and mean (green) in upstream JN over time. Blue lines indicate groundwater temperature in MFS-2 and saturated riparian soil temperature is shown in red. BOTTOM: Soil moisture, precipitation, and stream stage.

CHAPTER 5

CONCLUSIONS

Observations in upstream JN from DTS temperature sensing, stable isotope sampling, and hydrometric instrumentation show interactions between soil saturation thresholds and fracture bedrock aquifers. Precipitation intensity was observed to coincide with non-linear changes in stream runoff, however threshold saturation in soil was found to be largely dependent upon antecedent soil moisture which can be intrinsically related to the saturated conductivity curve and soil type. Similarly, seep locations identified through DTS measurements showed a greater connection with groundwater temperature during non-threshold precipitation events. Threshold events activate flow through surficial soils and hydraulically-active bedrock networks which can be seen translating to the stream during high-flow events. Stream baseflow and connectivity through discrete and diffuse seep locations is largely supported by slow drainage of isotopically and thermally-mixed till aquifers. It is therefore of great interest to investigate further into the environments which are least likely to produce threshold discharge conditions and instead buffer rapid increases in soil saturation and precipitation derived runoff.

Seasonal trends in stable isotope sampling support the conceptual model of late winter and early spring recharge to fractured bedrock and the increased residence time and mixing of waters recharged into deeper till aquifers. As a result, the surficial geology and underlying streambed play a vital role in the distribution of groundwater to the stream channel. Bedrock outcrops and thin overburden provided discrete seep locations for waters derived from both bedrock fracture and till overburden, whereas alluvial sand and gravel deposits provided a thermally diffuse or dispersed input to the stream.

5.1 Study Limitations

Limitations of this study, and recommendations for future study, include the need for deployment of additional instrumentation such as soil moisture probes in a variety of riparian areas, stream piezometers, a well in the till aquifer, and upstream gaging stations. These would allow more quantitative analysis of flux into the stream and resolve the mass-balance of stable isotope measurements if coupled with more discrete isotopic sampling in upstream JN during precipitation events and at known seep locations. MFS-2 is screened across till-bedrock interface and does not represent the hydrologic characteristics of a well screened entirely in the till. Although no active fracture flowpaths were found in the bedrock in this well (Hudson, 2015), the interface of till and bedrock contained coarse gravels and could function as secondary porosity similar to a bedrock fracture. Recording changes in the canopy cover over time would help to better relate the effects of leaf drop and evapotranspiration on the behavior of seeps and threshold fluxes. In addition, placement of the DTS cable in the stream could be optimized to improve characterization of stream temperature distributions. Burying the DTS cable 1-2 inches under the stream bed would eliminate influences from shading and solar input as well as ensure submersion of the cable. However, burying the cable would negatively impact potential trout rearing habit and would be impossible where bedrock is exposed at the streambed. Prior knowledge of seep locations would also allow the cable to be judiciously placed to better monitor the exact locations at the source as opposed to the mixing zone instream.

5.2 Broader Impacts

This study place in the New England region characterized by a humid climate with strong seasonality and occasional snow cover and is transferable to hydrogeologic environments where advection of ground water is significant and recharge rates are relatively high. Maps characterizing these environments, such as compiled by Gleeson et al. (2011), suggest that these represent large portions of the US. The hydrogeologic settings of an aquifer can be categorized and projected across regional and continental scales with respect to their hydrogeologic properties, thereby enabling the relationship between water-table characteristics and patterns in groundwater-surface water interactions to larger climate trends (Gleeson et al. 2011). By focusing on how the hydrogeologic settings of aquifers relate to stream temperature distributions and the prevalence of thermal habitat for fish, this study promotes transferability to geographically similar stream catchments in New England.

Jimmy Nolan Brook and the Westbrook catchment are co-located with an on-going long-term fish movement study conducted by the Turners Falls USGS Conte Lab Fish Ecology Division. This study can be directly compared with well documented behavioral patterns of fish within the study site. Understanding the hydrogeologic controls on headwater stream habitat of JN also has direct implications for the preservation of sensitive ecological species such as the Spring Salamander and the Dwarf Wedgemussel, which live in connecting watersheds.

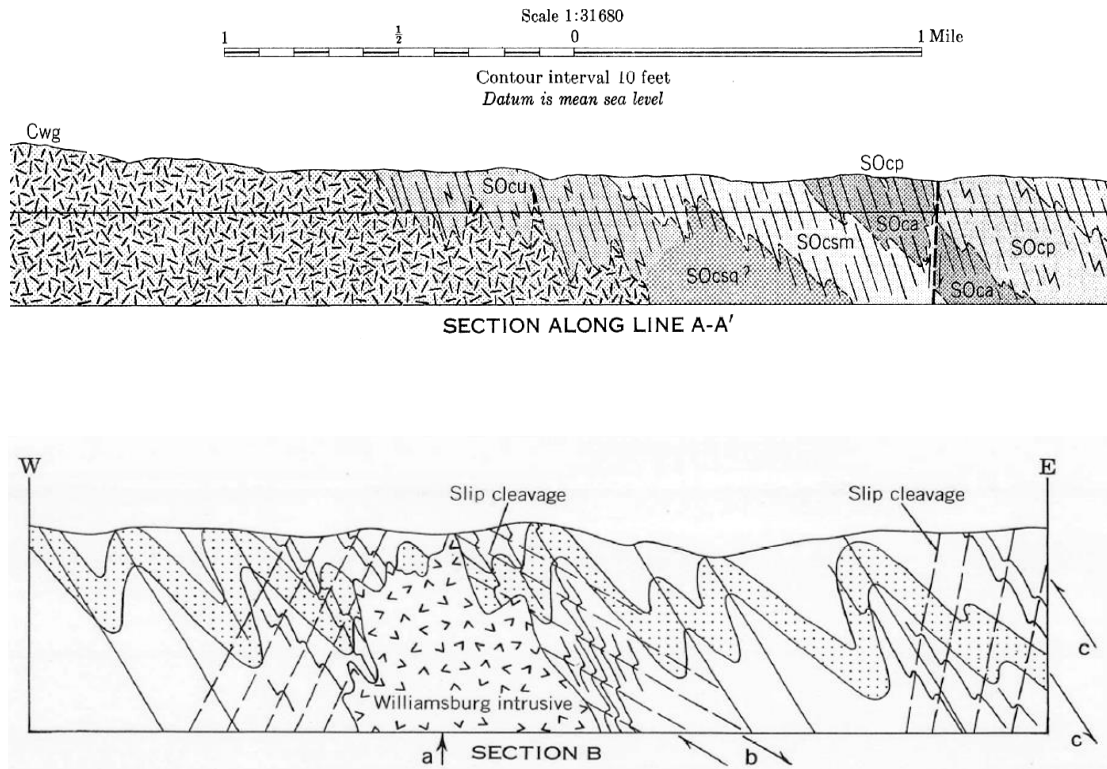
Over the coming century, summer maximum temperatures, and the number of critically warm days are predicted to increase significantly. Groundwater inflows to streams play a crucial role in mitigating the effects of these high air temperatures on

streams and creating thermal refuges for fish and this study highlights the importance of investigating the hydrogeologic heterogeneity of forested headwater catchments and how it relates to the persistence of thermal refugia. The most parsimonious conclusion from this study is that greater geologic and topographic variability appears to result in greater stream temperature variability and thermal refugia. Little has been recorded about the specifics of stream habitats predating logging and agriculture and as anadromous fish populations in New England have drastically declined or become extirpated the landscape has been that they once thrived in has been permanently changed. By examining existing trout habitat, it is the goal of this study to uncover parts of complex hydrologic framework that will allow remaining salmonid populations to survive into the future.

APPENDICES

APPENDIX A

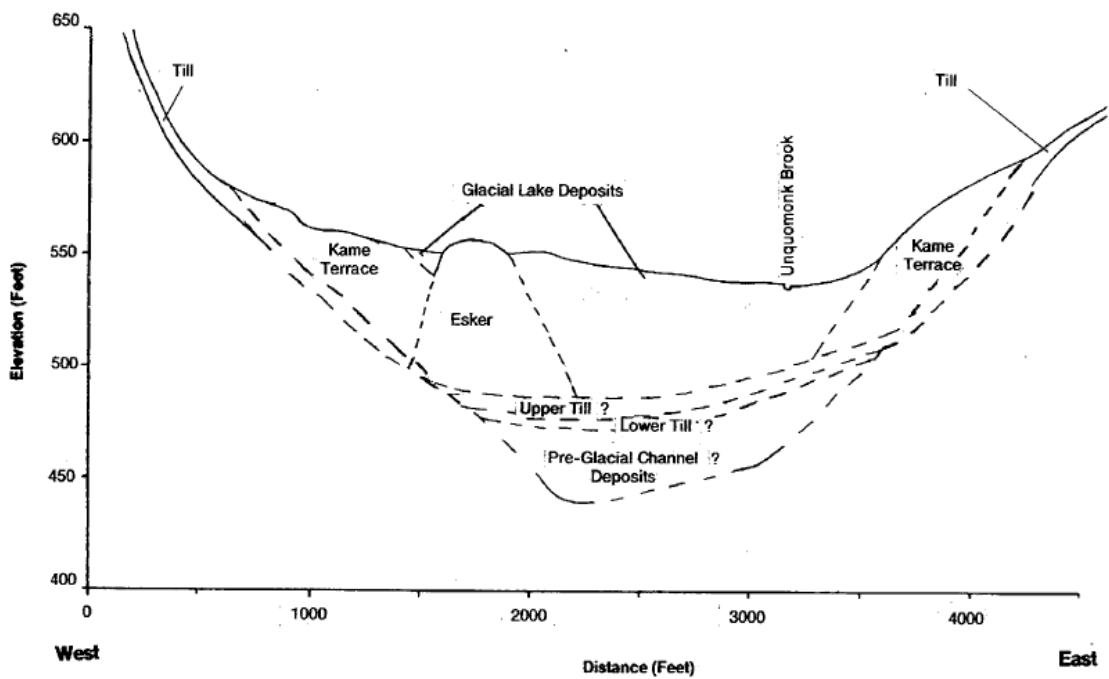
IDEALIZED STRUCTURAL GEOLOGY SECTION



Appendix A. Idealized structural geology section. Sections correspond with transects and descriptions of the structural history of the Williamsburg Quadrangle from Willard 1965.

APPENDIX B

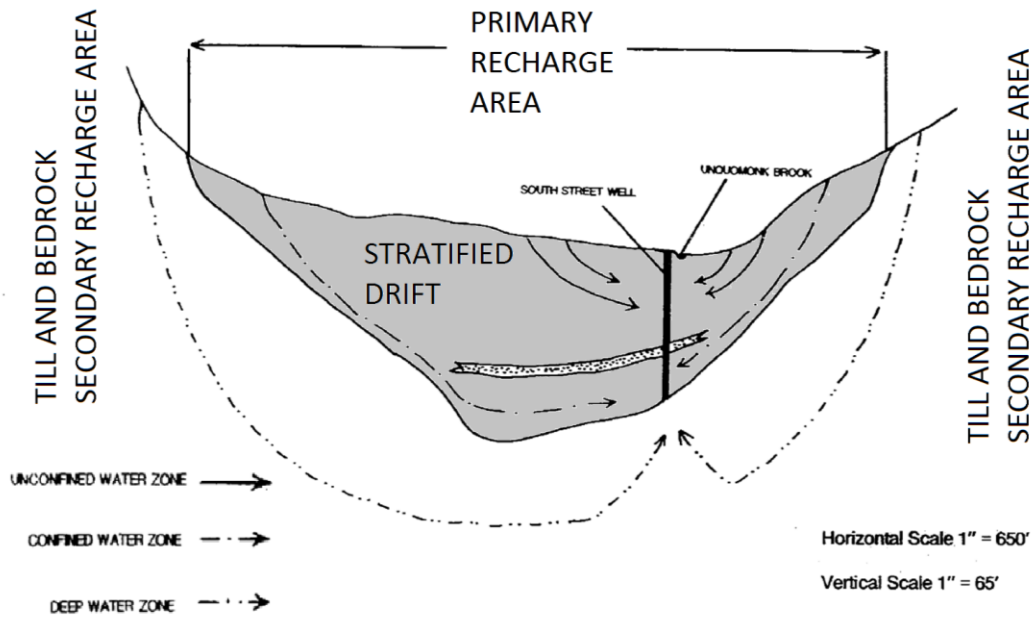
CROSS SECTION OF THE UNQUOMONK BROOK VALLEY



Cross section of the Unquom Brook valley. Conceptual geologic cross section of a stream channel in Williamsburg MA, (Storms and Motts 1987).

APPENDIX C

DIAGRAM OF GROUNDWATER FLOW PATHS



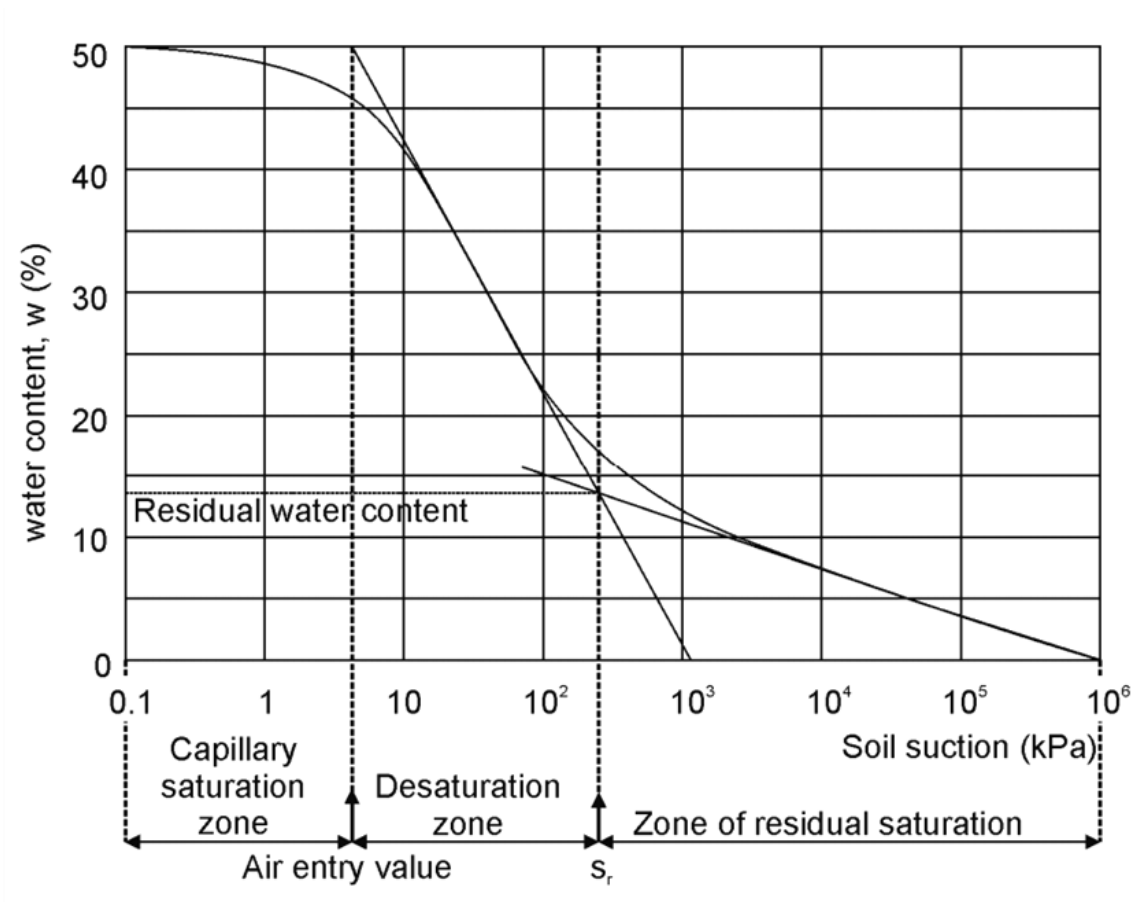
(Storms and Motts 1987)

FIGURE 4 Idealized Diagram Showing Circulation of Water in Unquom Brook Valley Aquifer.

Diagram of groundwater flow paths. Conceptualized diagram of flow in a till mantled fractured bedrock aquifer in Williamsburg Ma (Storms and Motts 1989).

APPENDIX D

SOIL WATER RETENTION CURVE



Soil water retention curve. Water contents vs. saturation zones defined by (Macek et al 2013).

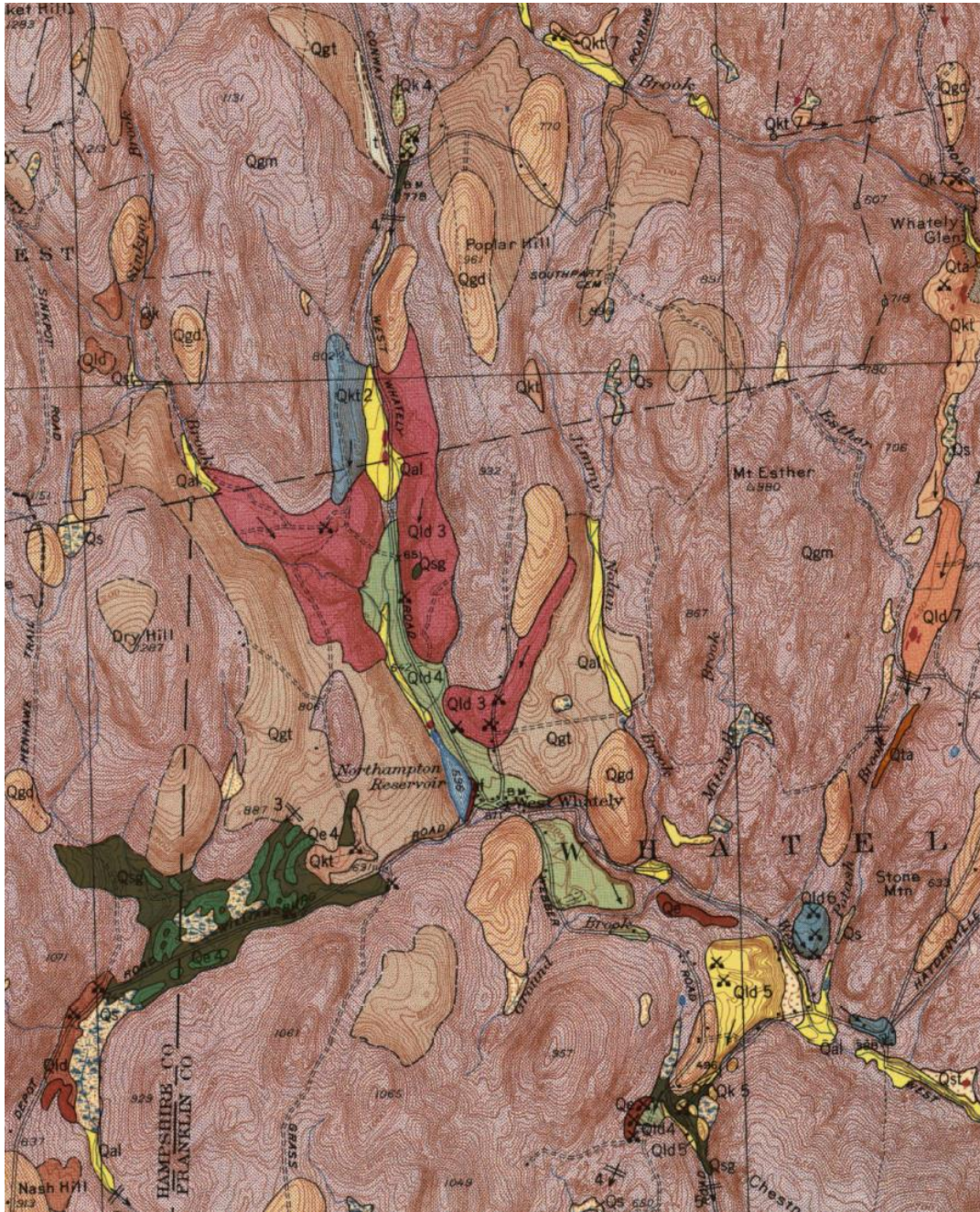
APPENDIX E

TABLE OF WATER ISOTOPE SAMPLE NAMES

Sample ID	Description
JN	Jimmy Nolan Brook at Confluence with Westbrook (downstream)
JNY	Jimmy Nolan Brook at upstream site
MB	Mitchell Brook at confluence with Westbrook (downstream)
MFS1	Fractured bedrock well
MFS2	Till overburden Well
MR	Mill river
OB	Obear brook
PLANT	Stem water from vine at MaCleish Field Station
PRE	Precipitation collector at MaCleish Field Station
RES	Northampton Reservoir outlet
SEEP	Ephemeral flow
SMC	Small creek at MaCleish Field Station
SNOW	Precipitation collector at MaCleish Field Station
SOIL	Soil lysimeters
TAP	Tap water at MaCleish Field Station
WB	West Brook River, downstream at Dudas bridge

APPENDIX F

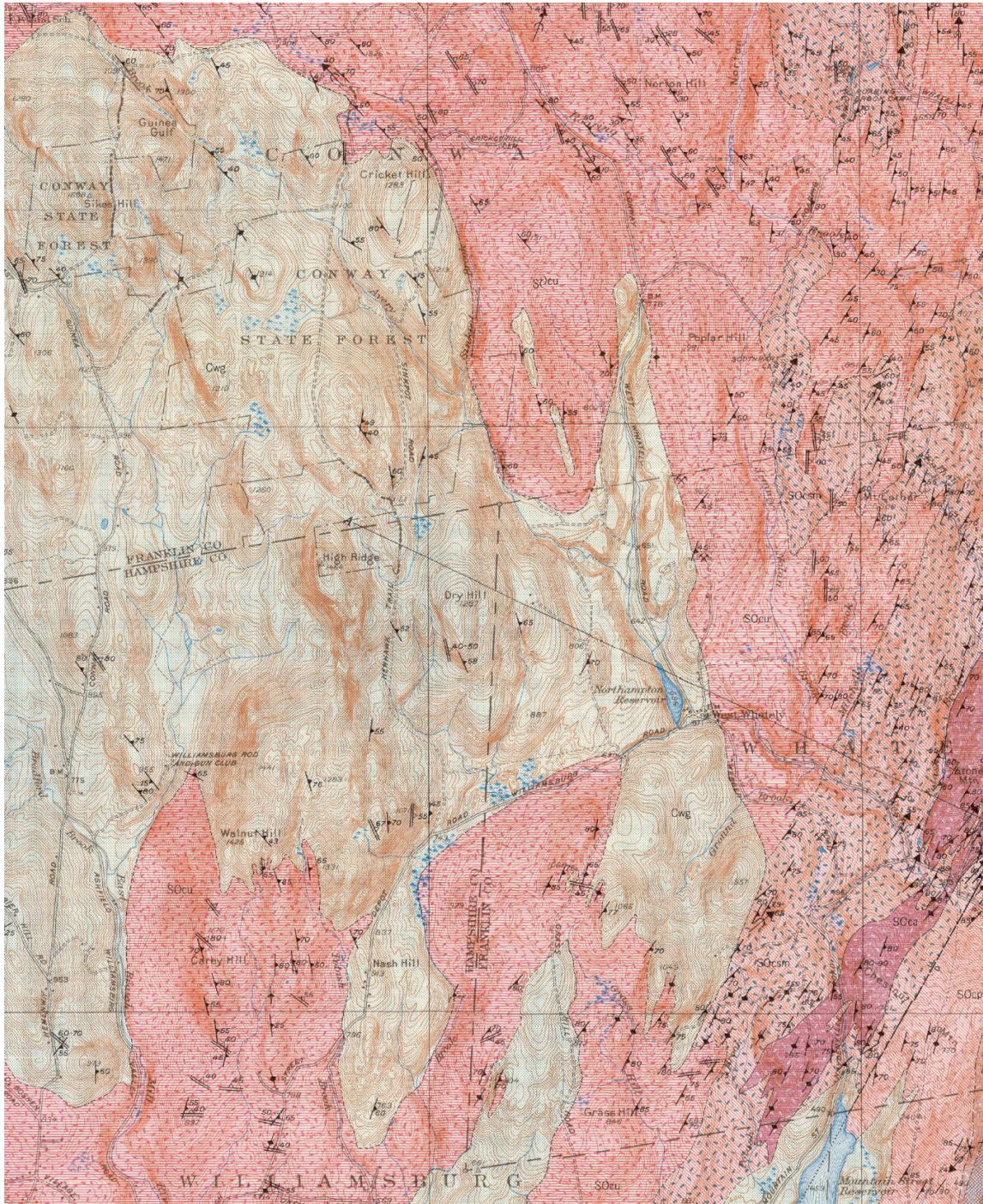
SURFICIAL GEOLOGY OF JIMMY NOLAN BROOK



Appendix F. Surficial Geology of Jimmy Nolan Brook. Image from Williamsburg Quadrangle (Seegerstrom 1955).

APPENDIX G

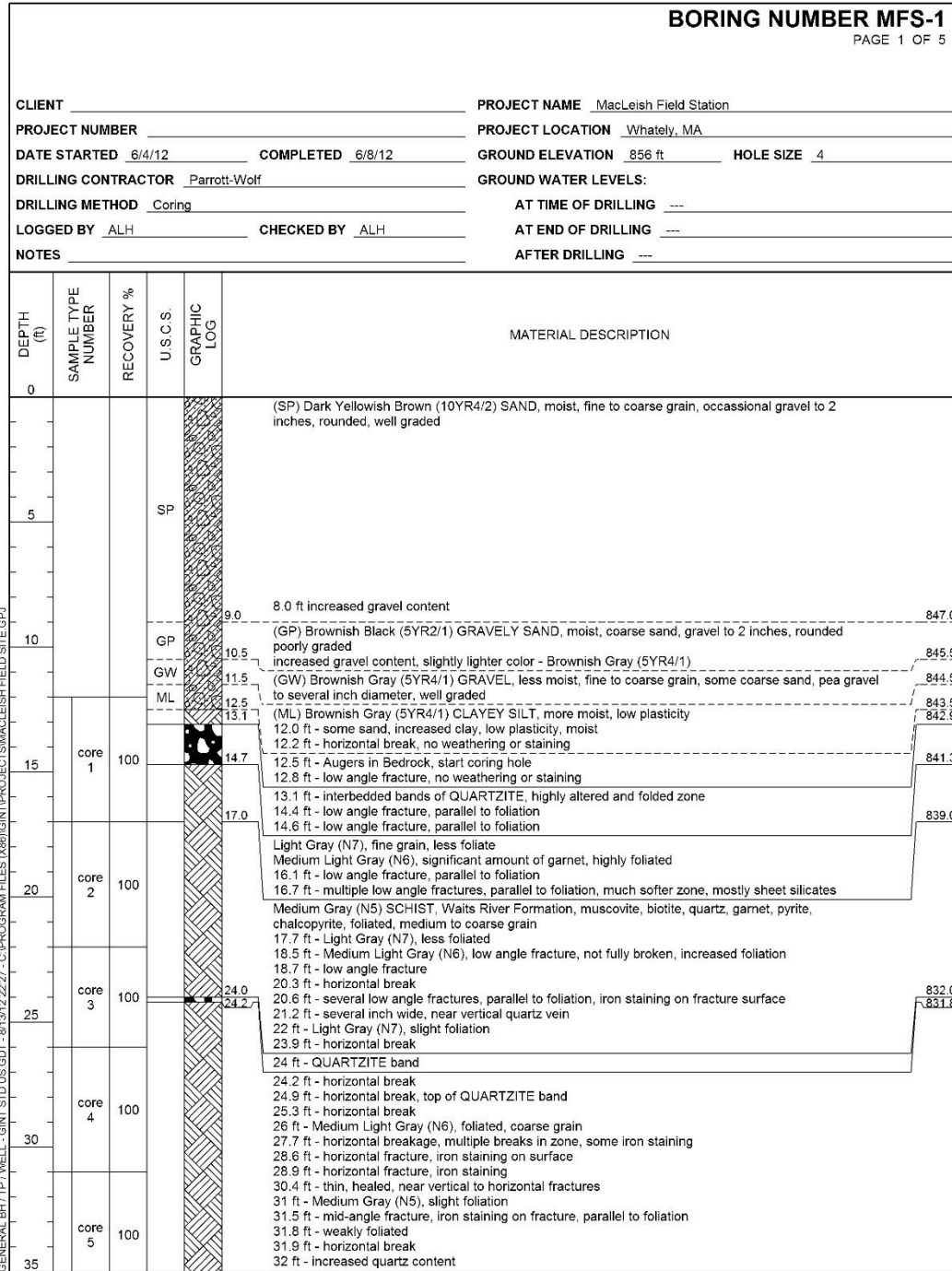
BEDROCK GEOLOGY OF THE WHATELY AREA



Appendix G. Bedrock geology of the Whately area. Image from the Williamsburg Quadrangle (Willard 1965).

APPENDIX H

CORE LOG OF FRACTURED BEDROCK WELL MFS-1.



Core log of fractured bedrock well MFS-1. Bedrock well at the MacLeish Field Station in Whately, Massachusetts.

BORING NUMBER MFS-1

PAGE 2 OF 5

CLIENT _____ PROJECT NAME MacLeish Field Station
 PROJECT NUMBER _____ PROJECT LOCATION Whately, MA

DEPTH (ft)	SAMPLE TYPE NUMBER	RECOVERY %	U.S.C.S.	GRAPHIC LOG	MATERIAL DESCRIPTION
35					
	core 6	100			32.9 ft - horizontal break 33.1 ft - foliated zone, mid-angle fracture, parallel to foliation, iron staining on fracture surface 33.4 ft - very coarse grain QUARTZITE band 33.9 ft - low angle break, parallel to foliation 34.6 ft - horizontal break 24.2 ft - horizontal break (continued) 36.4 ft - coarse grain QUARTZITE band 36.8 ft - low angle fracture 38.5 ft - coarse grain QUARTZITE band 39 ft - coarse grain QUARTZITE band, very hard (sides polished by drill) 40.5 ft - low angle broken zone, multiple fractures, more friable, soft, fine to medium grain, visible iron staining on fracture surface and in matrix 41 ft - iron staining on fracture surface 41.4 ft - mid- to high angle fracture, significant iron staining on fracture surface 41.6 ft - interbedded SCHIST and QUARTZ, thin layers 43.3 ft - mid-angle fracture
	core 7	98			
	core 8	100			47.8 ft - mid-angle fracture, parallel to foliation, muscovite along fracture surface, no weathering or staining 48.2 ft - Medium Light Gray (N6), quartz in matrix, no banding/interbedded layers 49.4 ft - mid-angle fracture, parallel to foliation 50 ft - increased grain size, less foliated 51 ft - Medium Gray (N5) SCHIST interbedded with QUARTZITE
	core 9	102			52.3 ft - low angle fracture, no weathering or staining
	core 10	100			54 ft - Light Gray (N7), less foliated, no interbedded QUARTZITE 54.2 ft - low angle fracture 56 ft - coarse grain, weakly foliated 56.6 ft - high angle fracture, cross foliation, iron staining 57.2 ft - cross cutting, near vertical thin calcite veins
	core 11	100			58.6 ft - high angle fracture, cross foliation, visible pitting/weathering on surface, iron staining 58.75 ft - horizontal break 61 ft - Medium Light Gray (N6) 61.5 ft - low angle fracture, parallel to foliation, iron staining on surface 61.6 ft - low angle fracture, parallel to foliation, iron staining on surface 61.9 ft - thin, near vertical calcite vein 63.2 ft - interbedded SCHIST and QUARTZ layers 63.3 ft - fracture parallel to foliation 64.4 ft - horizontal breakage, muscovite on surface, no weathering 65 ft - low angle fracture 65.1 ft - low angle fracture, clay minerals on surface 66 ft - Medium Gray (N5) 66.7 ft - high angle fracture, iron staining on fracture surface 66.8 ft - large quartz vein 67.3 ft - increased garnet content 67.5 ft - increased quartz content, strong foliation and folded, hard (core polished by drill) 69.2 ft - horizontal breakage
	core 12	100			70.4 ft - horizontal breakage 70.5 ft - horizontal breakage
	core 13	100			73.9 ft - mid-angle fracture, parallel to foliation, no weathering
75					

(Continued Next Page)

Appendix H (continued). Core log of fractured bedrock well MFS-1. Bedrock well at the MacLeish Field Station in Whately, Massachusetts.

BORING NUMBER MFS-1
PAGE 3 OF 5

CLIENT _____ PROJECT NAME MacLeish Field Station
PROJECT NUMBER _____ PROJECT LOCATION Whately, MA

DEPTH (ft)	SAMPLE TYPE NUMBER	RECOVERY %	U.S.C.S. GRAPHIC LOG	MATERIAL DESCRIPTION
75				24.2 ft - horizontal break (continued) 75.4 ft - horizontal breakage 75.8 ft - high angle break, no weathering, parallel to foliation
80	core 14	100		77.6 ft - low angle fracture 77.8 ft - low angle fracture, iron staining on surface 78.6 ft - horizontal breakage, muscovite and garnet
85	core 15	100		79.8 ft - horizontal breakage 80.4 ft - multiple intersecting high angle fractures, some evidence of weathering 81 ft - Medium Light Gray (N6), weakly foliated, folded 81.3 ft - horizontal breakage 81.4 ft - interbedded QUARTZITE bands 82.5 ft - broken zone (multiple low to high angle intersecting fractures) 82.8 ft - thicker bands of QUARTZITE 84 ft - horizontal breakage, muscovite on surface
90	core 16	100		85.7 ft - low angle fracture 85.9 ft - low angle fracture, increased garnet content 86.1 ft - QUARTZITE band 86.7 ft - low angle fracture 86.8 ft - QUARTZITE band 87.1 ft - QUARTZITE band, pyrite 88 ft - low angle fracture 88.75 ft - low angle fracture
91.0				89.6 ft - mid-angle fracture, cuts across foliation
91.4				90.4 ft - horizontal breakage, top of QUARTZITE vein
93.6	core 17	100		Very Light Gray (N8) QUARTZITE and Medium Dark Gray (N4) SCHIST, Waits River Formation, muscovite, biotite, pyrite, foliated 91.2 ft - low angle fracture
95.2				Medium Dark Gray (N4) SCHIST, muscovite, biotite, pyrite, foliated 91.45 ft - low angle fracture
97.4	core 18	96		92 ft - horizontal breakage 92.3 ft - top of near vertical quartz vein, foliated 93.2 ft - low angle fracture Light Gray (N7) QUARTZITE, coarse grain, pyrite 93.8 ft - horizontal breakage 94.1 ft - horizontal breakage 94.3 ft - horizontal breakage, high biotite and muscovite zone
101.0				Medium Dark Gray (N4) SCHIST, muscovite, biotite, quartz, weak foliation 95.6 ft - no foliation 96 ft - Medium Gray (N5) SCHIST, several thin, healed, high-angle fractures cutting across foliation 96.3 ft - horizontal breakage, biotite on surface 97 ft - several thin, high angle to vertical fractures 97.1 ft - low angle fracture
105	core 19	100		Very Light Gray (N8) QUARTZITE, muscovite, pyrite, coarse grain 98 ft - horizontal breakage 98.5 ft - horizontal breakage 98.6 ft - horizontal breakage 98.8 ft - horizontal breakage 99.1 ft - horizontal breakage 99.4 ft - horizontal breakage 99.6 ft - horizontal breakage 99.75 ft - horizontal breakage 100 ft - horizontal breakage 100.3 ft - horizontal breakage 100.5 ft - horizontal breakage 100.8 ft - horizontal breakage
110	core 20	94		Very Light Gray (N8) Quartz SCHIST, coarse grain, pyrite, muscovite, biotite, galena
115	core 21	100		101.3 ft - horizontal breakage 101.5 ft - horizontal breakage 101.65 ft - horizontal breakage 101.8 ft - horizontal breakage 102.05 ft - horizontal breakage





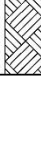
GENERAL BH / TP / WELL - GINT STD US GDT - 8/13/12 22:27 - C:\PROGRAM FILES\X86\GINT\PROJECT\SMACLEISH FIELD SITE.GPJ

(Continued Next Page)

Appendix H (continued). Core log of fractured bedrock well MFS-1. Bedrock well at the MacLeish Field Station in Whately, Massachusetts.

BORING NUMBER MFS-1
PAGE 4 OF 5

CLIENT _____ PROJECT NAME MacLeish Field Station
PROJECT NUMBER _____ PROJECT LOCATION Whately, MA

DEPTH (ft)	SAMPLE TYPE NUMBER	RECOVERY %	U.S.C.S.	GRAPHIC LOG	MATERIAL DESCRIPTION
115					
120	core 22	100			102.4 ft - horizontal breakage, stronger foliation, large amount of garnet, muscovite and biotite, folding 102.6 ft - low angle fracture 102.7 ft - low angle fracture 103.2 ft - horizontal breakage 103.5 ft - Light Gray (N7), weakly foliated 104.2 ft - horizontal breakage 104.35 ft - horizontal breakage 104.85 ft - horizontal breakage 104.9 ft - weakly foliated 105.6 ft - high angle fracture, parallel to foliation 105.75 ft - horizontal breakage 106.3 ft - low angle fracture 106.4 ft - low angle fracture 106.6 ft - low angle fracture 106.7 ft - high angle fracture, quartz on fracture surface, cuts across foliation 106.8 ft - low angle fracture
125	core 23	100			107.05 ft - mid-angle fracture, pyrite on surface, no weathering 107.4 ft - low angle fracture along foliation 107.5 ft - low angle fracture along foliation 107.7 ft - low angle fracture, very coarse grain QUARTZITE 107.85 ft - low angle fracture, pyrite on surface, weathering, iron staining 108.2 ft - horizontal fracture, very coarse grain QUARTZITE, biotite 108.4 ft - more weakly foliated/massive, calcite, pyrite, biotite, quartz, numerous thin high angle fractures
130	core 24	100			108.8 ft - near vertical fracture 110.5 ft - QUARTZITE vein Medium Gray (N5) quartz SCHIST, strongly foliated and folded, quartz, biotite, muscovite, galena, hornblende, highly fractured with high angle breaks 112 ft - bottom of high angle fractures 112.1 ft - numerous high angle, thin, healed fractures and quartz veining 112.8 ft - horizontal breakage 112.9 ft - large QUARTZITE band, very coarse grain
135	core 25	98			113 ft - horizontal breakage 113.1 ft - horizontal breakage 113.4 ft - horizontal breakage 113.6 ft - horizontal breakage 113.8 ft - horizontal breakage 114 ft - horizontal breakage 114.2 ft - low angle fracture 114.4 ft - low angle fracture and top of high angle fracture 114.7 ft - mid-angle fracture 114.85 ft - thin, healed, high angle fracture 114.9 ft - low angle fracture
140	core 26	100			Very Light Gray (N8) Quartz SCHIST, coarse grain, pyrite, muscovite, biotite, galena (continued) 115.35 ft - low angle fracture 115.5 ft - horizontal breakage, increased quartz content 115.7 ft - horizontal breakage 115.8 ft - horizontal breakage 115.9 ft - horizontal breakage 116.2 ft - horizontal breakage 116.7 ft - center of high angle fracture, cuts across foliation 116.9 ft - center of high angle fracture, cuts across foliation 117 ft - increased calcite content 117.9 ft - several small, high angle fractures, cut across foliation 118.7 ft - horizontal breakage 119 ft - low angle fracture 119.1 ft - Dark Gray (N3), increased biotite content, weaker foliation, soft, friable 119.3 ft - horizontal breakage 119.5 ft - horizontal breakage 119.8 ft - horizontal breakage 120 ft - horizontal breakage 120.1 ft - horizontal breakage 120.4 ft - possible high angle fault, visible gauge on fault surface 120.7 ft - horizontal breakage 121 ft - moderately hard, highly fractured and folded 121.4 ft - low angle fracture, pyrite mineralization on surface, no visible weathering
				141.0	
					715.0

(Continued Next Page)

Appendix H (continued). Core log of fractured bedrock well MFS-1. Bedrock well at the MacLeish Field Station in Whately, Massachusetts.

BORING NUMBER MFS-1

PAGE 5 OF 5

CLIENT _____ PROJECT NAME MacLeish Field Station
 PROJECT NUMBER _____ PROJECT LOCATION Whately, MA

DEPTH (ft)	SAMPLE TYPE NUMBER	RECOVERY %	U.S.C.S. GRAPHIC LOG	MATERIAL DESCRIPTION
				121.6 ft - multiple high angle fractures, no weathering 122.1 ft - low angle fracture 122.3 ft - low angle fracture, top of large QUARTZITE vein, very coarse grain 122.8 ft - low angle fracture Medium Gray (N5) SCHIST, pyrite, chalcocopyrite, garnet, calcite, quartz, foliated, hard, evidence of healed thin high angle fractures 123.6 ft - horizontal breakage 124.2 ft - horizontal breakage 124.8 ft - Dark Gray (N3), strong foliation 125.4 ft - low angle fracture 125.6 ft - low angle fracture 125.8 ft - low angle fracture 126.25 ft - QUARTZITE band, horizontal breakage 126.7 ft - horizontal breakage, large amount of quartzite, coarse grain 126.8 ft - Medium Gray (N5) 127 ft - several thin, near vertical fractures 129.2 ft - low angle fracture 130.1 ft - low angle fracture, quartz and silicates on surface 131.9 ft - fracture parallel to foliation 132 ft - several high angle, healed fractures 133 ft - fracture parallel to foliation 133.5 ft - two inch wide, very coarse grain QUARTZITE band, near vertical calcite healed fracture through band 133.7 ft - low angle fracture, muscovite, biotite, chalcocopyrite on surface of fracture 134 ft - low angle fracture, muscovite, biotite on fracture surface 134.3 ft - QUARTZITE band 134.5 ft - weakly foliated 135 ft - several thin healed near vertical fracture Dark Gray (N3) SCHIST, biotite, chalcocopyrite, rutile, hard, thin near vertical calcite healed fractures, several inch wide near vertical QUARTZITE band 136.3 ft - low angle fracture 136.5 ft - horizontal breakage 136.8 ft - horizontal breakage 137.4 ft - mid-angle fracture, parallel to foliation, muscovite along fracture surface, no weathering or staining 138.3 ft - low angle fracture, parallel to foliation, highly mineralized zone (pyrite and chalcocopyrite), near vertical coarse grain QUARTZITE band 138.9 ft - weakly foliated, more massive, no visible fractures 139.8 ft - very coarse grain QUARTZITE band, sulphide mineralization 140 ft - several small, high angle fractures, cut across foliation, partially to completely healed 140.5 ft - strong foliation 140.9 ft - QUARTZITE band Total Depth = 141 feet Bottom of borehole at 141.0 feet.

GENERAL BH / TP / WELL - GINT STD US.GDT - 8/13/12 22:27 - C:\PROGRAM FILES\X86\GINT\PROJECTS\MACLEISH FIELD SITE.GPJ

Appendix H (continued). Core log of fractured bedrock well MFS-1 at the MacLeish Field Station in Whately, Massachusetts.

APPENDIX I.

CORE LOG OF TILL/BEDROCK WELL MFS-2

						BORING NUMBER MFS-2		
						PAGE 1 OF 2		
CLIENT _____			PROJECT NAME <u>MacLeish Field Station</u>					
PROJECT NUMBER _____			PROJECT LOCATION <u>Whately, MA</u>					
DATE STARTED <u>6/8/12</u>		COMPLETED <u>6/12/12</u>		GROUND ELEVATION <u>845 ft</u>		HOLE SIZE <u>8</u>		
DRILLING CONTRACTOR <u>Parrott-Wolf</u>			GROUND WATER LEVELS:					
DRILLING METHOD <u>Hollow Stem Auger</u>			AT TIME OF DRILLING <u>---</u>					
LOGGED BY <u>ALH</u>			CHECKED BY <u>ALH</u>			AT END OF DRILLING <u>---</u>		
NOTES _____			AFTER DRILLING <u>---</u>					
DEPTH (ft)	SAMPLE TYPE NUMBER	RECOVERY %	BLOW COUNTS (N VALUE)	U.S.C.S.	GRAPHIC LOG	MATERIAL DESCRIPTION		
0								
	SS	63	1-2-2-2 (4)	SP-SM			(SP-SM) Dark Yellowish Brown (10YR4/2) SILTY SAND, moist, fine sand, no gravel, low plasticity	
	SS	79	3-23-20-16 (43)	SP		2.5	842.5	(SP) Dusky Brown (5YR2/2) fine SAND, moist, some fines, no gravel, nonplastic
						2.7	842.3	(SP-SM) Dark Yellowish Brown (10YR4/2) SILTY SAND, moist, fine sand, trace fine gravel
5	SS	83	5-11-21-26 (32)	SP-SM				Quartzite rock > 3 inches increased cobble content and size
	SS	75	23-33-28-25 (61)	SP-SM				cobble zone increased sand content and size, fine to medium grain, less gravel content, less fines, wet
						8.0	837.0	(ML) Dark Yellowish Brown (10YR4/2) SILT, wet, low plasticity, trace fine sand
10	SS	25	10-9-12-12 (21)	ML				
	SS	92	7-13-16-16 (29)	ML		10.0	835.0	(ML) Dark Yellowish Brown (10YR4/2) CLAYEY SILTY SAND, wet, low plasticity, fine to medium grain sand, trace gravel
						10.2	834.8	
	SS	83	19-27-37-41 (64)	SP-SM				(ML) Dark Yellowish Brown (10YR4/2) SANDY CLAYEY SILT, wet, fine sand, moderately plastic, firm, some gravel
	SS	100	28-38-40-44 (78)	SP-SM				(SP-SM) Dark Yellowish Brown (10YR4/2) SANDY GRAVELY CLAYEY SILT, wet, fine to coarse sand, moderately plastic
15	SS	94	36-48-50-3/0"	SP-SM		14.7	830.3	less sand, larger gravel, very compact, hard
						16.0	829.0	(SP-SM) Light Olive Gray (5Y5/2) SANDY SILT, moist, fine to medium sand, nonplastic, some gravel, some sand, compact, hard
						18.0	827.0	(SP-SM) Light Olive Gray (5Y5/2) SANDY SILT, wet, fine sand, nonplastic, less compact, no gravel
20	SS	83	25-24-26-28 (50)					(ML) Medium Dark Gray (N4) SILT, moist, some fine sand, nonplastic, some gravel to > 2 inches
	SS	92	20-21-27-27 (48)					
	SS	92	29-39-41-50 (80)	ML				gravel to > 4 inches
25	SS	92	23-20-43-38 (63)					
	SS	100	36-44-50/2"	SP	26.5	818.5	(SP) Dark Yellowish Brown (10YR4/2) SILTY SAND, moist, fine to coarse grain sand, some gravel, sulphide minerals	
					27.0	818.0	Total depth of augers and sampling, Air Hammer to total depth.	
30								
35								

(Continued Next Page)

Appendix I. Core log of till/bedrock well MFS-2. Monitoring well at the MacLeish Field Station in Whately, Massachusetts.

BORING NUMBER MFS-2

PAGE 2 OF 2

CLIENT _____ PROJECT NAME MacLeish Field Station
 PROJECT NUMBER _____ PROJECT LOCATION Whately, MA

DEPTH (ft)	SAMPLE TYPE NUMBER	RECOVERY %	BLOW COUNTS (N VALUE)	U.S.C.S.	GRAPHIC LOG	MATERIAL DESCRIPTION
35						
40						
45						
50						
					50.0	795.0

Total depth = 50 feet
 Bottom of borehole at 50.0 feet.

GENERAL BH / TP / WELL - GINT STD US.GDT - 8/13/12 21.D4 - C:\PROGRAM FILES (X64)\GINT\PROJECTS\MACLEISH FIELD SITE.GPJ

Appendix I (continued). Core log of till/bedrock well MFS-2. Monitoring well at the MacLeish Field Station in Whately, Massachusetts.

BIBLIOGRAPHY

- Ali, G., Oswald, C. J., Spence, C., Cammeraat, E. L. H., McGuire, K. J., Meixner, T., & Reaney, S. M. (2013). Towards a unified threshold-based hydrological theory: necessary components and recurring challenges. *Hydrological Processes*, 27(2). 313–318. doi:10.1002/hyp.9560.
- Arismendi, I., S. L. Johnson, J. B. Dunham, R. Haggerty, and D. Hockman-Wert,. (2012). The paradox of cooling streams in a warming world: Regional climate trends do not parallel variable local trends in stream temperature in the Pacific Continental United States. *Geophysical. Research. Letters*, 39: L10401.
- Bakker, M., Bartholomeus, R. P., & A., F. T. P. (2013). Groundwater recharge: processes and quantification”, 2653–2655. doi:10.1029/2011jg001693
- Becker, M. W., Georgian, T., Ambrose, H., Siniscalchi, J., & Fredrick, K. (2004). Estimating flow and flux of ground water discharge using water temperature and velocity. *Journal of Hydrology*, 296(1-4). 221–233. doi:10.1016/j.jhydrol.2004.03.025.
- Beven, K., & Germann, P. (2013). Macropores and water flow in soils revisited. *Water Resources Research*, 49(6). 3071–3092. doi:10.1002/wrcr.20156.
- Boughton, D. A., Hatch, C., & Mora, E. (2012). Identifying distinct thermal components of a creek. *Water Resources Research*, 48(9). n/a–n/a. doi:10.1029/2011WR011713.
- Buttle J.M. (1989). Soil moisture and groundwater responses to snowmelt on a drumlin sideslope, *Journal of Hydrology*, Volume 105, Issues 3–4, 28 February 1989, Pages 335-355, ISSN 0022-1694, [http://dx.doi.org/10.1016/0022-1694\(89\)90112-1](http://dx.doi.org/10.1016/0022-1694(89)90112-1).
- Cuthbert, M. O., Mackay, R., & Nimmo, J. R. (2012). Linking soil moisture balance and source-responsive models to estimate diffuse and preferential components of groundwater recharge. *Hydrology and Earth System Sciences Discussions*, 9(7). 8455–8492. doi:10.5194/hessd-9-8455-2012.
- deGroot-Hedlin, C. and Constable, S. (1990), Occam's inversion to generate smooth, two-dimensional models form magnetotelluric data. *Geophysics*, 55, 1613-1624.
- Detty, J. M., and K. J. McGuire. (2010). Topographic controls on shallow groundwater dynamics: implications of hydrologic connectivity between hillslopes and riparian zones in a till mantled catchment. *Hydrological Processes*, 24: 2222–2236.

- Garabedian, S.P., and Stone, J.R., (2004), Delineation of areas contributing water to the Dry Brook public-supply well, South Hadley, Massachusetts: U.S. Geological Survey Water-Resources Investigations Report 03-4320, 52 p.
- Gleeson, T., Marklund, L., Smith, L. and Manning, A.H. (2011). Classifying the water table at regional to continental scales. *Geophysical Research Letters*, 38, L05401.
- Genuchten M. Th Van. (1980). A closed-form for predicting the hydraulic conductivity of unsaturated soils. *Soil Science Society of America*, 44(5).891-898.
- Hatch CE, Fisher AT, Revenaugh JS, Constantz J, Ruehl C. (2006). Quantifying surface water-groundwater interactions using time series analysis of streambed thermal records: method development. *Water Resources Research* 42.
- Heeley, Richard W; Judith A Maloney; Erik Storms; (1980). Replacement of ground water supplies contaminated with pesticides in Whately and Granby, Massachusetts. National Water Well Association. Cambridge, MA : S E A Consultants.
- Hein and Stone (2014). Ice, water, and wind: a source-to-sink view of the glacial, paraglacial and coastal sediments and processes that have shaped northeastern Massachusetts neigc 2014 Hein & Stone Field Trip Guide to the lower Merrimack River Valley and Plum Island by Christopher Hein and Byron Stone. This field trip was part of the 106th meeting of the New England Intercollegiate Geological Conference (NEIGC). held at Wellesley College on October 10-13.
- Heppner, C. S., J. R. Nimmo, G. J. Folmar, W. J. Gburek, and D. W. Risser (2007). Multiple-methods investigation of recharge at a humid-region fractured rock site, Pennsylvania, USA, *Hydrogeol. J.*, 15, 915–927.
- Hudson, Amy L., "Geochemical Attributes of Hydraulically Active Fractures and Their Influence on Groundwater Quality" (2016). Doctoral Dissertations. 699.
- Johnson, S. L. (2004). Factors influencing stream temperatures in small streams: substrate effects and a shading experiment, *923(July)*. 913–923.
- Katsura, S., K. Kosugi, T. Mizutani, S. Okunaka, and T. Mizuyama. (2008). Effects of bedrock groundwater on spatial and temporal variations in soil mantle groundwater in a steep granitic headwater catchment. *Water Resources Research*, 44: W09430.
- Kelleher, C., Wagener, T., Gooseff, M., McGlynn, B., McGuire, K., & Marshall, L. (2012). Investigating controls on the thermal sensitivity of Pennsylvania streams. *Hydrological Processes*, 26(5). 771–785. doi:10.1002/hyp.8186.
- Kirchner, J. W. (2003). A double paradox in catchment hydrology and geochemistry, *Hydrol. Process.*, 10 17, 871–874, doi:10.1002/hyp.5108.

- Kirchner, J. W. (2009). Catchments as simple dynamical systems: Catchment characterization, rainfall-runoff modeling, and doing hydrology backward. *Water Resources Research*, 45(2). n/a–n/a. doi:10.1029/2008WR006912.
- Kobayashi, D., Ishii, Y., & Kodama, Y. (1999). Stream temperature, specific conductance and runoff process in mountain watersheds Abstract:, 876 (February 1998). 865–876.
- Lautz, N. T. Kranes And D. I. Siegel, (2007). Heat Tracing of Heterogeneous Hyporheic Exchange Adjacent To In-Stream Geomorphic Features *Hydrol. Process.* 24, 3074–3086.
- Lim, Kyoung Jae, Bernard A. Engel, Zhenxu Tang, Joongdae Choi, Ki-Sung Kim, Suresh Muthukrishnan, and Dibyajyoti Tripathy. (2005). Automated Web GIS Based Hydrograph Analysis Tool, WHAT. *Journal of the American Water Resources Association* 41(6):1407-1416.
- Maček, M., J. Smolar, and A. Petkovšek. (2013). "Extension of measurement range of dew-point potentiometer and evaporation method." *Proceedings of the 18th International Conference on Soil Mechanics and Geotechnical Engineering, Paris 2013.*
- McDonnell, J. J., Sivapalan, M., Vaché, K., Dunn, S., Grant, G., Haggerty, R., Hinz, C., et al. (2007). Moving beyond heterogeneity and process complexity: A new vision for watershed hydrology. *Water Resources Research*, 43(7). n/a–n/a. doi:10.1029/2006WR005467.
- Mirus, B. B., & Nimmo, J. R. (2013). Balancing practicality and hydrologic realism: A parsimonious approach for simulating rapid groundwater recharge via unsaturated-zone preferential flow. *Water Resources Research*, 49(3). 1458–1465. doi:10.1002/wrcr.20141.
- Morrill, J., R. Bales, and M. Conklin. (2005). Estimating Stream Temperature from Air Temperature: Implications for Future Water Quality. *Journal of Environmental Engineering*, 131: 139–146.
- Nathan S., Boutt, D.F., and S. B. Mabee, (2006). Prototype Three-Dimensional Geologic Model of the Marlborough Quadrangle, Massachusetts: 3-D Modeling on a Shoestring, 2006 Geological Society of America Annual Meeting, Philadelphia, PA, October.
- Nimmo, John R. (2010). Theory for Source-Responsive and Free-Surface Film Modeling of Unsaturated Flow. *Vadose Zone J.*9: 295–306.

- Palacky, G. J., (1988). Resistivity characteristics of geologic targets, in *Investigations in Geophysics vol. 3: Electromagnetic methods in applied geophysics-theory*, vol. 1, edited by M. N. Nabighian, Soc. Expl. Geophys., 53–129.
- Rodhe, A., & Bockgård, N. (2006). Groundwater recharge in a hard rock aquifer: A conceptual model including surface-loading effects. *Journal of Hydrology*, 330(3-4). 389–401. doi:10.1016/j.jhydrol.2006.03.032.
- Salve, R., Rempe, D. M., & Dietrich, W. E. (2012). Rain, rock moisture dynamics, and the rapid response of perched groundwater in weathered, fractured argillite underlying a steep hillslope. *Water Resources Research*, 48(11). n/a–n/a. doi:10.1029/2012WR012583.
- Segerstrom., (1955). Williamsburg Geologic Quadrangle. United States Geological Survey.
- Segerstrom, K. (1955). Surficial Geology of the Williamsburg Quadrangle, Massachusetts. US Department of the Interior, US Geological Survey.
- Stone, J.R., and DiGiacomo-Cohen, M.L., comps. (2010). Surficial geologic map of the Heath-Northfield-Southwick- Hampden 24-quadrangle area in the Connecticut Valley region, west-central Massachusetts: U.S. Geological Survey. Open-File Report 2006-1260-G.
- Stone, B.D., Stone, J.R., Masterson, J.P., and O’Leary, D.W. (2004). Integrating 3-D facies analysis of glacial aquifer systems with ground-water flow models: Examples from New England and the Great Lake region, USA. Workshop Extended Abstracts submitted for Geological Models For Groundwater Flow Modeling, May 15, 2004, 49th annual Meeting Geological Association of Canada, Mineralogical Association of Canada, St. Catherines, Ontario, Canada.
- Storms, Erik, and Motts, Ward S. (1987). Hydrogeologic investigation of Williamsburg, MA. Proceeding of the fourth annual Eastern Regional Ground Water Conference, 4: Dublin, National Water Well Association, p. 467-490.
- Torgersen, C.E., J.L. Ebersole, and D. M. Keenan. (2012). Primer for Identifying Cold-Water Refuges to Protect and Restore Thermal Diversity in Riverine Landscapes. EPA 910-C-12-001 U.S. Environmental Protection Agency, Seattle, Washington, USA.
- Whately OSRP. Open Space and Recreation Plan. Section 4 – Environmental Inventory and Analysis 4-16.
- Webb, David M. Hannah, R. Dan Moore, Lee E. Brown⁴ And Franz Nobilis. (2008). Recent Advances In Stream And River Temperature Research, *Hydrol. Process.* 22, 902–918.

- Webb, B. W., & Zhang, Y. (1997). Webb - Spatial and temporal variability in the components of the river heat budget. *Hydrological Processes*.
- Westhoff, M. C., Savenije, H. H. G., Luxemburg, W. M. J., Stelling, G. S., van de Giesen, N. C., Selker, J. S., Uhlenbrook, S. (2007). A distributed stream temperature model using high resolution temperature observations. *Hydrology and Earth System Sciences Discussions*, 4(1). 125–149. doi:10.5194/hessd-4-125-2007.
- Xu, C. L., Letcher, B. H., & Nislow, K. H. (2010). Size-dependent survival of brook trout *Salvelinus fontinalis* in summer: effects of water temperature and stream flow. *Journal of fish biology*, 76(10). 2342–69. doi:10.1111/j.1095-8649.2010.02619.
- Yu, Xinbao and Yu, Xiong. (2006). "Time Domain Reflectometry Tests of Multilayered Soils", Proc. TDR 2006, Purdue University, West Lafayette, USA, Sept. 2006, Paper ID 3, 16 p., <https://engineering.purdue.edu/TDR/Papers>.